

UNIVERSITÀ della CALABRIA
Facoltà di Ingegneria
Dipartimento di Meccanica

Scuola di Dottorato “Pitagora” in Scienze Ingegneristiche
Dottorato di Ricerca in Ingegneria Meccanica XXII Ciclo

SETTORE SCIENTIFICO DISCIPLINARE: ING-IND/16

Tesi di Dottorato

Methodologies to enhance performances in sheet metal
forming processes

Coordinatore
Prof. Sergio Rizzuti

Supervisore
Prof. Luigino Filice

Candidato
Ing. Giuseppe Leonardo Manco

Dissertazione finale sottomessa per ottenere il titolo di Dottore di Ricerca in Ingegneria Meccanica
Anno Accademico 2008/2009

UNIVERSITY OF CALABRIA

FACULTY OF ENGINEERING

DEPARTMENT OF MECHANICAL ENGINEERING

PhD Thesis

*METHODOLOGIES TO ENHANCE PERFORMANCES IN
SHEET METAL FORMING PROCESSES*

Supervisors

PROF. LUIGINO FILICE

Dr. GIUSEPPINA AMBROGIO

Candidate

GIUSEPPE LEONARDO MANCO

Coordinator

PROF. SERGIO RIZZUTI

RESEARCH FIELD ING-IND/16 - ACADEMIC YEAR 2009 – 2010

The work detailed in this thesis is the result of my engagements as a PhD researcher at the Mechanical Department at University of Calabria, as Research Assistant at the “Institute for Manufacturing” (IfM) at University of Cambridge (April-June 2008) and at “Institut für Bildsamer Formgebung” (IBF) at RWTH Aachen University (July 2008- January 2009).

University of Calabria



A mia madre e a mio padre

Contents

Preface

List of figures	ix
------------------------	----

List of table	xv
----------------------	----

Introduction

1.1	Warm formability	2
1.2	Incremental forming processes	3
	1.2.1 Single Point Incremental Forming (SPIF)	4
	1.2.2 Two Point Incremental Forming (TPIF)	4
	1.2.3 Kinematic Incremental Sheet Forming (KISF)	6
	1.2.4 The market for incremental forming processes	6
1.3	Scope of this thesis	8

Experimental Equipment, Cad/Cam System And Measurement System

2.1	Introduction and scope of this chapter	10
2.2	Equipment for Incremental Forming	10
	2.2.1 The CNC Machine	11
	2.2.2 The AMINO DLNC-RB forming machine	12
2.3	The Idraulic press	12
2.4	Measurement equipments	13
	2.4.1 Force Measurements	13
	2.4.2 Strain Measurements	15
	2.4.3 Thinning Measurements	17
	2.4.4 Accuracy Measurements	17

2.6 CAD/CAM system	19
Warm Formability and Warm Deep Drawing of Magnesium Alloys	
3.1 Introduction and scope of this chapter	20
3.2 State of the art in warm forming of magnesium alloys	21
3.2.1 Concluding on the state	22
3.3 Material and formability tests	22
3.4 Warm deep drawing experiments	23
3.4.1 Equipment design	24
3.5 Numerical analysis	27
3.5.1 Discussion of the results	28
3.5.2 Conclusion on the numerical study of warm forming	29
3.6 A statistical analysis of the process parameters	29
3.6.1 Plan of experiment	29
3.6.2 The analysis of variance	32
3.6.3 Discussion of the Results	33
3.6.4 Conclusions on the influence of process parameter	34
Study on AISF Formability	
4.1 Introduction and scope of this chapter	36
4.2 Forming limit diagrams in AISF	37
4.2.1 Conclusions on the state of the art	40
4.3 Single slope analysis	42
4.3.1 Experimental campaign	43
4.3.2 Statistical analysis	44
4.3.3 Model validation	47
4.3.4 Concluding on single slope formability analysis	50
4.4 Double slope formability analysis	51
4.4.1 Deep geometries: formability analysis	51
4.4.2 Consideration on the single slope prediction procedure	53
4.4.3 Experimental campaign	54
4.4.4 Numerical analysis	56
4.4.5 Concluding on double slope formability analysis	58
4.5 Multi slope formability analysis	59
4.5.1 Multislope IF process	59

4.5.2 Experimental campaign	60
4.5.3 Statistical analysis	63
4.5.4 Conclusions on multislope analysis	66
4.6 Thinning analysis in AISF processes	66
4.6.1 AISF process evidences	66
4.6.2 Experimental campaign	67
4.6.3 Statistical analysis of the results	71
4.6.4 Concluding on thinning in AISF	74
Study on AISF accuracy	
5.1 Introduction and scope of this chapter	75
5.2 State of the art on the accuracy and springback compensation	75
5.2.1 Discussion of the state of the art.	77
5.3 A study on the accuracy in Incremental Forming process	78
5.3.1 Geometrical considerations on springback	78
5.3.2 Experimental investigation	80
5.3.3 Discussion of the results	82
5.3.4 Conclusions on the experimental measure of part accuracy	84
5.4 Numerical capability to predict the springback	85
5.4.1 Numerical capability	86
5.4.2 Numerical analysis	88
5.4.3 Discussion of the results	89
5.4.4 Conclusions on numerical capability	91
5.5 A novel approach: the back-drawing strategy	91
5.5.1 Back drawing: the Experimental Campaign	93
5.5.2 Conclusion on the back-drawing strategy	98
Strategies to control the thickness distribution in SPIF: by changing the tool trajectory	
6.1 Introduction and scope of this chapter	100
6.2 Formability and thickness distribution	100
6.3 Tool path optimization	102
6.4 Experimental evidences	104
6.5 Numerical simulation	107
6.6 Conclusion on the proposed strategy to optimize the thickness distribution	109

Warm Incremental Forming and Hybrid Incremental Forming	
7.1 Introduction and scope of this chapter	110
7.2 Warm Incremental Forming	111
7.2.1 Experimental evidences and preliminary investigations	111
7.2.2 The experimental equipment	112
7.2.3 Fracture evidences	113
7.2.4 Plan of the experiments and main results	114
7.2.5 Conclusions on the Warm Incremental Forming process	119
7.3 Hybrid Incremental Forming Process	119
7.3.1 Process Investigation: the experimental set-up	122
7.3.2 Experimental test	123
7.3.3 Forming of a hemisphere	123
7.3.4 Process modelling	125
7.3.5 CAX developments	127
7.3.6 Summary and outlook on the proposed hybrid process	127
Summary and outlooks	129
References	130

List of figures

Figure 1.1	The HCP structure and the slip planes of magnesium alloys	3
Figure 1.2	Single point incremental sheet forming SPIF	4
Figure 1.3	Two-point incremental sheet forming—TPIF.	5
Figure 1.4	Kinematic incremental sheet forming using two forming tools—KISF.	6
Figure 1.5	Trends in the car industry: increasing variety of models and variants, decreasing lifetime	7
Figure 2.1	Basic apparatus for SPIF at University of Calabria	11
Figure 2.2	The hydraulic press machine Instron 1206	12
Figure 2.3	The SPIF equipment for forces measurement on CNC machine	14
Figure 2.4	The utilised data acquisition system on the CNC machine	14
Figure 2.5	Set-up for on line force measurements	15
Figure 2.6	Typical set-up of on-line optical deformation measurements for AISF	16
Figure 2.7	The laser triangulation principle	17
Figure 2.8	The laser based scanning system set-up	18
Figure 2.9	Measurement of the sheet thickness and bulge height from digitized surfaces	19
Figure 3.1	Equipments utilised for material characterization.	23
Figure 3.2	Working Limit Diagram of AZ31 at the limits of the investigated range.	23
Figure 3.3	Equipment used for warm deep drawing tests.	25
Figure 3.4	Equipment for deep drawing tests mounted on the testing machine.	25
Figure 3.5	LDR results for AZ31 at 250°C.	26
Figure 3.6	Experiments carried out with a LDR= 2.63: sound (a), with wrinkling (b) and broken parts (c).	26

Figure 3.7	The numerical model.	27
Figure 3.8	Numerical results for components: sound (a), with wrinkles (b) and broken (c).	28
Figure 3.9	Numerical and experimental temperature on the sample.	28
Figure 3.10	Specimens obtained at 200°C.	31
Figure 3.11	Specimens obtained at 250°C.	31
Figure 3.12	Specimens obtained at 300°C.	31
Figure 3.13	Wrinkled and broken components.	32
Figure 3.14	Normal probability plot for the proposed model	33
Figure 3.15	LDR value depending on temperature and punch speed.	34
Figure 4.1	Illustration of the “incremental bulging test”, with modified z-pitch compared to Iseki’s original proposal	38
Figure 4.2	Comparison of different experimental and theoretical ([SR75]) necking and fracture limit curves for commercially pure aluminium	42
Figure 4.3	The investigated experimental plane.	44
Figure 4.4	Dp/s values for experiments carried out for $\alpha = \alpha_{max}$	46
Figure 4.5	Normal Probability Plot and Prediction Capability for the investigated analysis	46
Figure 4.6	Comparison between the predicted height and the obtained one during the validation tests.	47
Figure 4.7	Thickness distribution with $\alpha_1 = 65^\circ$ and $\alpha_2 = 70^\circ$	48
Figure 4.8	Experimental-Numerical comparisons for $\alpha_1 = 65^\circ$	49
Figure 4.9	Experimental-Numerical comparisons for $\alpha_1 = 70^\circ$	49
Figure 4.10	Experimental-Numerical comparison for $\alpha_1 = 75^\circ$	50
Figure 4.11	Thickness distribution along the transverse profile	51
Figure 4.12	Normal Force and Thickness distribution along the transverse section ($D_p = 12\text{mm}$, $p = 0.5\text{mm}$, $\alpha = 70^\circ$)	52

Figure 4.13	Sketch of geometrical parameters	54
Figure 4.14	Sound component obtained with $\alpha_1=65^\circ$ and $\alpha_2=70^\circ$	55
Figure 4.15	Comparison between experimental and analytical results	58
Figure 4.16	The investigated multislope shape	60
Figure 4.17	Experimental equipment and component	61
Figure 4.18	Comparison between expected final height (H_f) and measured one (H_{exp}). Test are reported in their actual order (randomized)	62
Figure 4.19	Marginal posterior probabilities for factors A-K, Box-Meyer analysis	64
Figure 4.20	Normal plot of effects, projected 23 design in factors A, B, D	65
Figure 4.21	Typical thickness distribution in AISF process	67
Figure 4.22	The investigated experimental plane	68
Figure 4.23	Thickness distribution at the varying of the initial sheet thickness ($a=70^\circ$, $D_p=15\text{mm}$, $p=0.65\text{mm}$)	69
Figure 4.24	Thickness distribution at the varying of the wall inclination angle ($s=1.5\text{mm}$, $D_p=15\text{mm}$, $p=0.65\text{mm}$)	70
Figure 4.25	Thickness distribution at the varying of the tool diameter ($s=1.5\text{mm}$, $a=70^\circ$, $p=0.65\text{mm}$)	70
Figure 4.26	Thickness distribution at the varying of the tool depth step ($s=1.5\text{mm}$, $a=70^\circ$, $D_p=15\text{mm}$)	71
Figure 4.27	Normal Probability Plot	73
Figure 4.28	Prediction Capability Diagram	73
Figure 5.1	Illustration of the correlation algorithm proposed in [Jun03] for the improvement of the geometric accuracy	76
Figure 5.2	The investigated geometries	79
Figure 5.3	Results of the intermediate and final step in the manufacturing of the free-form component	81
Figure 5.4	Virtual models after the manufacturing phase and after the sheet trimming	82

Figure 5.5	Comparisons between the CAD model and the manufactured one at the end of the SPIF process and between the last and trimmed product for AA 5754 – H22	83
Figure 5.6	Numerically measured total displacement at the punch removal	87
Figure 5.7	Comparisons between the measured final geometry of the part and both the explicit and the implicit formulation results	87
Figure 5.8	Total displacement after the trimming for DC04	89
Figure 5.9	Error distribution for the tests carried out on AA 1050-O and on DC04	90
Figure 5.10	The two steps of the Back-Drawing Incremental Forming	93
Figure 5.11	Error trend vs. incremental forming repetitions ($p=1\text{mm}$, $s=1\text{mm}$)	93
Figure 5.12	Whole field diverting on DC04 Steel (Depth step $p=0.3\text{mm}$; thickness $s=1\text{mm}$)	95
Figure 5.13	Whole field diverting on DC04 Steel (Depth step $p=0.3\text{mm}$; thickness $s=2\text{mm}$)	95
Figure 5.14	Whole field diverting on DC04 Steel (Depth step $p=1\text{mm}$; thickness $s=1\text{mm}$)	96
Figure 5.15	Whole field diverting on DC04 Steel (Depth step $p=1\text{mm}$; thickness $s=2\text{mm}$)	96
Figure 5.16	Whole field diverting on AA1050-O Aluminium Alloy (Depth step $p=0.3\text{mm}$; thickness $s=1\text{mm}$)	97
Figure 5.17	Whole field diverting on AA1050-O Aluminium Alloy (Depth step $p=0.3\text{mm}$; thickness $s=2\text{mm}$)	97
Figure 5.18	Whole field diverting on AA1050-O Aluminium Alloy (Depth step $p=1\text{mm}$; thickness $s=1\text{mm}$)	98
Figure 5.19	Whole field diverting on AA1050-O Aluminium Alloy (Depth step $p=1\text{mm}$; thickness $s=2\text{mm}$)	98
Figure 6.1	Punch force and thickness distribution obtainable in SPIF process	102
Figure 6.2	Details of the investigated tool paths	103
Figure 6.3	Experimental profile	104
Figure 6.4	Thickness distributions for the investigated tool trajectories and wall	105

	inclination angle $\alpha = 60^\circ$	
Figure 6.5	Thickness distributions for the investigated tool trajectories and wall inclination angle $\alpha = 70^\circ$	105
Figure 6.6	Possible defect in Incremental Slope trajectory	107
Figure 6.7	Possible loss of accuracy using Decremental Slope	107
Figure 6.8	Comparison between experimental and numerical thickness distributions, $\alpha = 60^\circ$	108
Figure 6.9	Comparison between experimental and numerical thickness distributions, $\alpha = 70^\circ$	109
Figure 7.1	Strains at failure at different temperatures	112
Figure 7.2	The experimental equipment	113
Figure 7.3	A sound specimen ($\alpha = 50^\circ$)	113
Figure 7.4	Material failure due to oxidation	114
Figure 7.5	Forming load vs. tool depth step trend	116
Figure 7.6	Forming load vs. tool diameter	116
Figure 7.7	Forming load vs. temperature trend	116
Figure 7.8	FLD0 at 200°C (mean value and standard deviation)	117
Figure 7.9	FLD0 at 250°C (mean value and standard deviation)	117
Figure 7.10	FLD0 at 300°C (mean value and standard deviation)	118
Figure 7.11	Principle of the process combination	121
Figure 7.12	The experimental set up	122
Figure 7.13	Comparison of thickness reduction induced by AISF and stretch forming	124
Figure 7.14	Comparison of AISF and SF+AISF for a spherical cap with a groove	124
Figure 7.15	Comparison of thickness for pure AISF and AISF+SF	125
Figure 7.16	Comparison of FEA and experiments for SF+AISF	126

Figure 7.17	Comparison of FEA and experiments for AISF	126
Figure 7.18	CAX process chain	127

List of table

Table 3.1	Range of the investigated parameters	24
Table 3.2	Factors investigated in the experimental campaign	30
Table 3.3	Output of the experimental campaign	30
Table 3.4	ANOVA Results	32
Table 3.5	Performance indexes	33
Table 4.1	Extreme Value of the Experimental Plane	44
Table 4.2	Influence of input variables and their interactions on H_{\max}	45
Table 4.3	Validation tests	47
Table 4.4	Investigated wall inclination angles	55
Table 4.5	Outputs for model highlighted in equation	56
Table 4.6	Outputs for model highlighted in equation	56
Table 4.7	Investigated factors and their levels	61
Table 4.8	The 12-run Plackett-Burman design for factors A-K, and the responses obtained	62
Table 4.9	The projected 2^3 design (in standard order) and the data for factors A,B, D	65
Table 4.10	Extreme Value of the Experimental Plane	69
Table 4.11	Model definition	71
Table 4.12	ANOVA results	72
Table 5.1	Materials chemical compositions (% of mass)	80
Table 5.2	Geometrical discrepancies evaluated between the CAD model and the manufactured component	84
Table 5.3	Geometrical discrepancies evaluated between the manufactured and trimmed component	84
Table 5.4	Explicit and implicit error distribution	88
Table 5.5	Numerical model suitability measured by the comparison with the	90

	real product at the end of the manufacturing step (Step 1)	
Table 5.6	Numerical model suitability measured by the comparison with the real product at the end of the trimming (Step 2)	91
Table 5.7	Error for IF and BIF processes for DC04 and AA1050-O, for changing process conditions	94
Table 6.1	Smallest thickness measured at the varying of the tool path	106
Table 7.1	Failure conditions at room temperature	112
Table 7.2	Ranges of the experimental plan	114
Table 7.3	Experimental results at 200°C	115
Table 7.4	Experimental results at 300°C	115
Table 7.5	Influence of input variables on FLD_0	118

Introduction

The sheet metal forming is a wide domain in which the traditional processes showed their drawbacks in the last decades. This is mainly due to the change of industrial scenario and to the customer requirements that are moving to more exigent specifics. Nowadays the product complexity is increased for the new aesthetical trends and for the high level of technology provided in the final product. Moreover, the “Green House” effect and the Kyoto protocol pushed the researchers all over the world to study the production taking into account the global sustainability. This fact induced the firms and the research to focalize their attention on new process solutions and on new materials.

Considering the new materials in the last decade it is clearly discernible a wide trend focused on the “light alloys” characterized by an high ratio strength versus density. In fact in term of pollution reduction a suitable way to obtain that is surely the weight reduction politics. Moreover, from a manufacturing point of view, the “light alloys” introduced some new criticism due to the lack of knowledge in particular in the sheet metal forming processes. In fact, it is usual to produce some components in light alloy by casting or forging processes but in the sheet metal domain the not fully understood material behaviour is the main drawbacks which border a wide and easy industrial application. In detail, the light alloys, due to their microstructure, show poor attitude to be deformed at room temperature but this aspect is improved increasing the process temperature. It is worth to observe that the introduction of temperature as a process parameter increase the process complexity and so the research efforts up to now were not able to fill the gap of knowledge and further resources have to be invested in this field.

Considering the possibility to satisfy the market requirements by process innovation, in the last years some interesting solutions were proposed. In particular, with the aim to increase the process flexibility according to the high product customization trend, in the last years, the

incremental forming processes showed their potentiality. In fact, nowadays many research team in industries or in academy focus their attention on this class of processes. Moreover, up to now, due to the not fully understood process mechanic the incremental forming process shows some relevant drawbacks with a strong impact on the industrial applicability. In fact, the lack of knowledge affects the process control and so the part feasibility in term of formability, failure prediction, shape accuracy or thickness uniformity. Starting from these considerations it is clear that more efforts have to be concentrated on the process knowledge in order to enhance the global process performance.

In this thesis, with the aim to fill a part of the aforementioned lacks of knowledge an investigation on both the strategies is presented. More in detail, the possibility to enhance the process performances adopting new material is investigated by studying the application of a light alloy (Mg alloy) in a traditional deep drawing process while the process performances enhancement by new processes application is analysed with regard to the Asymmetric Incremental Forming process.

In the next section an overview on the state of art introduce the “warm formability” of magnesium alloys and the family of incremental forming processes.

1.1 Warm formability

Magnesium alloys is one of the lightest metals that can be employed for structural use. In the past, the demand for this alloys as a structural material was not high because of its less availability commercially as well as limited manufacturing methods. In recent years, the die casting of magnesium alloy has been prevailing in the making of parts in the automotive industry [ETP+98, MKM97] and such items as the covers of notebook computers as well as cellular phones. However, this process is not ideal in making thin-walled magnesium structures because an excessive amount of waste material can result. A potential solution would be to resort to the sheet forming process. It is commonly recognized that magnesium possesses poor formability at room temperature because of its hexagonal close-packed structure [TYH99, TFH98]. The HCP structure, in which dislocation movement is restricted only in the basal plane, makes magnesium alloys very difficult to deform at room temperature [SEC+06, FES+07]. As a matter of fact, HCP metals does not have enough independent slip systems to deform without extensive occurrence of twinning. The formability of Mg alloys can be increased by deforming at high temperatures [SEC+06, FES+07].

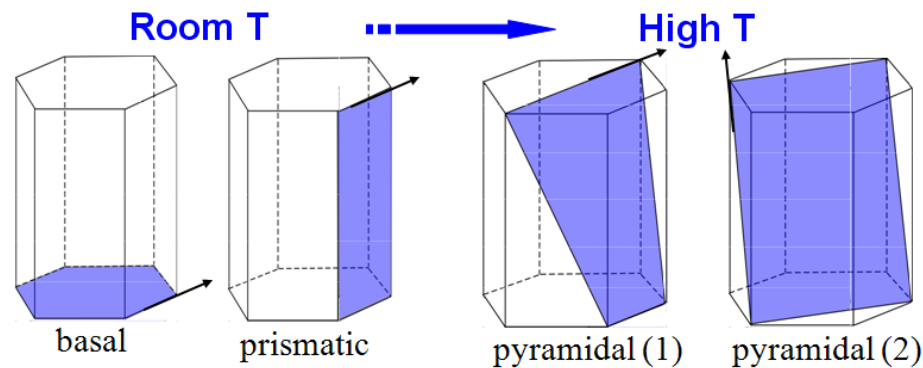


Figure 1.1: The HCP structure and the slip planes of magnesium alloys

As well known, temperatures above 200°C cause additional slip systems to become activated, thus conferring to these alloys an acceptable ductility; unfortunately, forming operations in the high temperature regime result in high costs. This observation is presently driving an additional effort to overcome the forming problems experienced by the most used wrought Mg alloy, the AZ31, by forming in warm conditions, i.e. by deforming between 200 and 300°C.

Further details are reported in the chapter 3.

1.2 Incremental forming processes

Several names are currently in use for this process, e.g. “incremental sheet forming—ISF” [KP03], “sheet incremental forming—SIF” [GCA05], or “kinematical incremental sheet forming—KISF” [Jad04]. Sometimes, the process is also referred to as “dieless incremental forming” [Mat01]. In a recent paper, Jeswiet et al. [JMH⁺05] put forward the following name and definition, which are used in this thesis:

In this work as stated before, the definition of Jeswiet is adopted in which:

“Asymmetric Incremental Sheet Forming (AISF) is a process which:

- 1. is a sheet metal forming process,*
- 2. has a solid, small-sized forming tool,*
- 3. does not have large, dedicated dies,*
- 4. has a forming tool which is in continuous contact with sheet metal,*
- 5. has a tool that moves under control, in three dimensional space,*
- 6. can produce asymmetric sheet metal shapes.”*

It is worth to mention that although the first idea of this process was described and patented by Leszak in 1967 at that period the CNC controllers were not available so the industries and the researcher focused their attention on AISF is from the 1990s.

AISF present the following typologies:

1.2.1 Single Point Incremental Forming (SPIF)

The characteristic feature of SPIF is that a part is shaped by the action of a CNC controlled forming tool that has a single-point contact with the sheet metal. The blank is clamped in a blank holder that remains at a constant height (see Fig. 1.2). This process variant is truly “dieless” if no support tool is used [LGB01]. In most cases, however, a dedicated rig or backplate is used to create a defined transition between the flange and the actual part. Both variations of the SPIF process are displayed in Fig. 1.2. Early work on this process variant was done e.g. by Matsubara [Mat94], Jeswiet et al. [JH01], Leach et al. [LGB01] and Filice et al. [FFM01]. It is worth mentioning that there is no single-point contact when a backplate is used. Nevertheless, the acronym “SPIF” is well-established and shall henceforth be used in this work for the process variations shown in Figure 1.2.

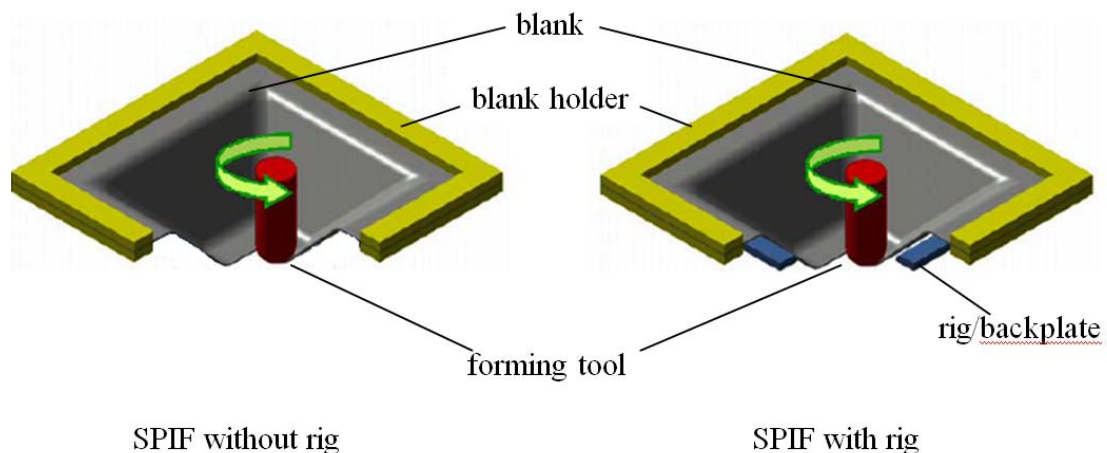


Figure 1.2: Single point incremental sheet forming SPIF

1.2.2 Two Point Incremental Forming (TPIF)

TPIF was introduced by Matsubara [Mat94] to meet the need for quick, inexpensive production of low volume asymmetric sheet metal parts. With the TPIF process, the metal blank moves vertically on bearings which move on blank holder posts, along the z-axis, as the forming tool pushes into the sheet metal. This process has two points where the sheet metal is pressed, simultaneously, hence it is called Two Point Incremental Forming (TPIF) in order to

differentiate it from Single Point Incremental Forming (SPIF) which has just one point at which force is applied. The point, where plastic deformation occurs, is directly under the forming tool. When it is used in a CNC mill, it is mounted in the spindle. The forming tool pushes down on the sheet metal, causing plastic deformation at a point, during its trajectory, which is the outline of the shape being manufactured. In TPIF, one tool presses into the sheet and the other acts as a partial die. Because of the partial die, TPIF is not truly dieless, although it is often called that. The TPIF apparatus, shown in Figure 1.3, consists of an apparatus, which clamps the sheet metal (blankholder), and allows for downward movement with the tool-path increments in the z-axis direction.

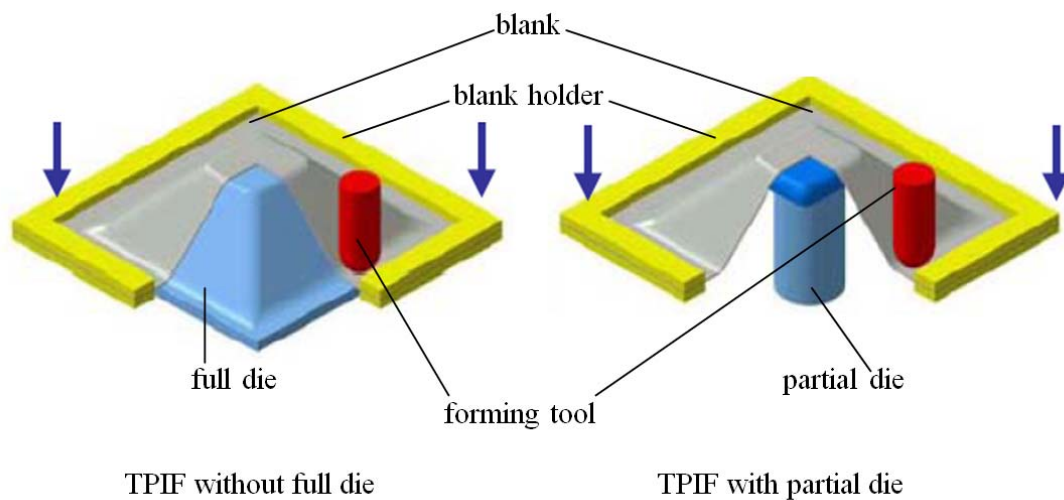


Figure 1.3: Two-point incremental sheet forming—TPIF.

The centre of the blank is supported with a stationary post (a partial die) and a clamped perimeter (blankholder) that moves down as deformation of the sheet progresses. To prevent twisting of the shape about the partial die there is a support plate under the blank. The partial die can be replaced by a shape that acts as a full die over which the sheet is formed incrementally by the single point. Generally, the forming tool, utilised in TPIF, is a steel rod with a smooth, hemispherical tip. The motion of this tool is controlled through CNC programming of a series of incremental contours. Shear forming theory can be applied even in this case: in fact, the experimental work shows measured thickness matches thickness calculated with the sine law, for cones formed with various wall angles [Mat94]. Because the flange material remains undeformed, the wall thickness can be easily calculated by the sine law, assuming a volume constancy.

1.2.3 Kinematic Incremental Sheet Forming (KISF)

In this new development two forming tools are used (one on either side of the blank), which are actuated simultaneously. It is illustrated in Fig. 1.4. This process variant is a truly dieless sheet metal forming process. It offers additional flexibility over the SPIF process. It was first described in a Japanese patent [SYN+97]. Currently, the biggest challenge in the development of KISF seems to be the definition and synchronisation of the tool paths of the master and slave tool [MSDZ07, MZB+07, JGHK03].

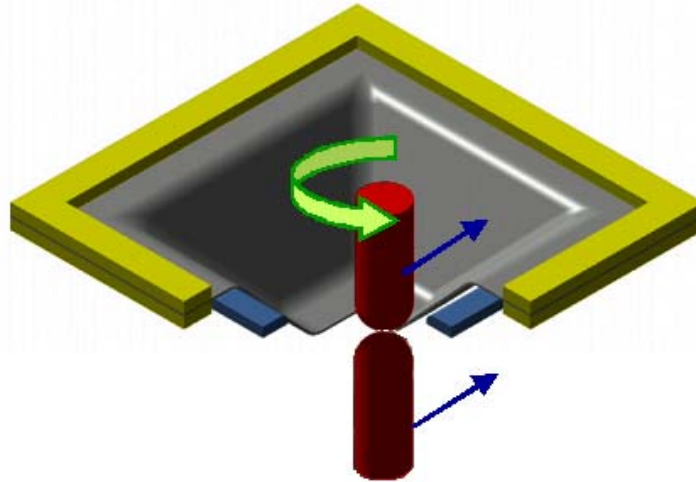


Figure 1.4: Kinematic incremental sheet forming using two forming tools—KISF.

1.2.4 The market for incremental forming processes

Due to its intrinsic characteristics the AISF process cannot replace the conventional processes, like deep drawing, for mass production but it can be applied in the small batch production. For sake of clarity a short overview onto the actual market and on its perspectives and trends is reported. The small batch production market is a part of the traditional market involving the niche production, but also in the traditional applications like automotive industries a deeper analysis can show more potential application field for AISF process. In fact, considering the automotive field, the prototyping or the production of highly customized car, like ambulance, limousine, funerary vehicle or more the restoration of veteran or vintage car can be considered as a niche production.

Furthermore as shown in Figure 1.5, there is a clear trend towards shortening the life cycle of a car design. At the same time, the number of car types and variants increases, while the number of car platforms decreases.

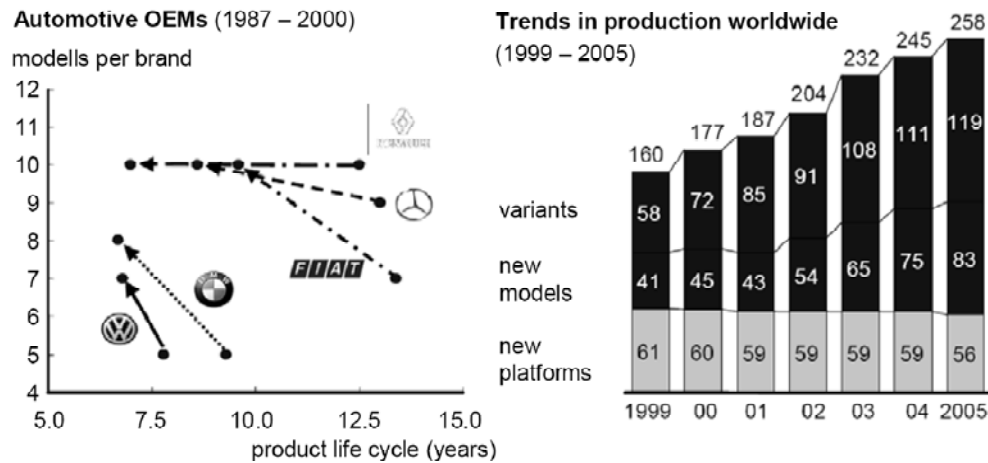


Figure 1.5: Trends in the car industry: increasing variety of models and variants, decreasing lifetime [N.N06].

As detailed by Neugebauer in [NKBG07], the car industry in Germany employed approximately 766,000 people in 2005, representing 13.2% of the total industrial workforce.

Since 2003, one third of the total R&D investments in Germany has stemmed from the German automobile industry. This makes the car industry a key player in the economy. With stalling global production and sales figures, it is forecast that the trend towards batch size reduction will continue, especially in the premium car segment, which is stated to be of great importance to German car manufacturers. This example of the German car industry blends well into a general trend towards individualized production in high-wage countries. Tseng et al. [TJ01] define mass customization as “producing goods and services to meet individual customer’s needs with near mass production efficiency”. Besides producing individualised products from scratch, AISF offers a way to customize mass products, e.g. to produce cars with an individual design based on series cars [BMW].

New market perspectives. AISF offers a number of favourable features that might open new markets. One salient feature is that—within the process limits—complicated, almost arbitrarily shaped free-form surfaces can be manufactured. This includes parts that cannot be manufactured by deep-drawing, like the design examples shown by Matsubara [Mat01]. Thus, AISF enables potential applications in architecture and design, domestic appliances, etc. The Italian company MONTES was reported to manufacture up to 20 pieces of design furniture per month by AISF [Rod06]. An advantage of AISF over deep-drawing is that forming forces do not increase when the size of the part increases since the plastic deformation is induced locally. This might open the possibility to use AISF for very large sheet metal parts, e.g. in the

aerospace industry or in civil engineering/architecture. Other potential applications are the replacement of rapid prototyping parts that are currently made of non-metallic materials [Rod06], the rapid manufacturing of dies (e.g. for injection-moulding, the production of composite materials, etc.) [ABRM06] and the repair or replacement of damaged or out-dated sheet metal parts.

Moreover there are some industrial field, like aerospace industries, in which the market is traditionally determined by large parts in relatively small batch size.

1.3 Scope of this thesis

Despite almost 15 years of development and research on incremental forming processes the limits are not overcome and moreover the not fully understood process mechanic border their industrial applications although the noticeable advantages recognizable from a literature review.

On the other hands new materials showing a high formability introduce, in turn, some criticisms, mainly related to the higher costs and sometimes to the lower workability. In fact, the light alloys can show interesting features since the cost is not prohibitive and there is already some technical knowledge available on their workability which permits feasible applications. In fact, some components in automotive and transportation industry are already produced in Magnesium alloys.

Within this framework, the present work of research is carried out with the aim to perform reliable strategies to enhance the formability controlling the process and thinking to new possibility to overcome the process drawbacks which afflict the extensive application of the aforementioned manufacturing approaches.

This work starts with a short overview on the warm formability and on the incremental forming processes. After that, in the chapter 2 all the standard equipments used in this thesis are presented and the systems and the methods of measurements are discussed.

In the chapter 3 the experimental and numerical investigations on the warm deep drawing of magnesium alloys are reported and a statistical model to predict the formability is presented.

Incremental sheet forming processes are discussed in the chapter 4, 5 and 6.

In particular an analysis of formability and of its indicator is presented in chapter 4, in which some statistical and empirical models are derived and a numerical analysis is showed in order to build a reliable predictive FE model. On the other hand, new formability indicators are introduced and discussed starting from simple geometries analysis and finishing with more complex parts. However in chapter 5, some studies on part geometry are presented with the aim to understand the springback influence at the end of the process and after the trimming operation and so to ensure a process suitability in term of accuracy. Furthermore a new approach to overcome the geometrical part deviation based on iterative approach is presented.

In chapter 6 a study on thinning behaviour is carried out with the aim to propose new strategies to overcome the excessive thinning and to obtain a more homogeneous thickness.

Finally, in the chapter 7 the possibility to enhance the global process performances and to extend the range of industrial application by building new processes is examined. In fact, a merging between the work carried out for the magnesium alloys and for the Incremental Forming process is reported and a novel process namely Warm Incremental Forming is developed and presented. In addition, with the aim to overcome some process limits another new process is build and introduced namely Hybrid Incremental Sheet Forming obtained combining the stretch forming process with the Incremental Forming.

At the end, in the appendices chapters an overview on the statistical methods used in this thesis is reported.

Experimental Equipment, Cad/Cam System And Measurement System

2.1 Introduction and scope of this chapter

In this chapter, an overview of the equipment and the measurement system used in this thesis is reported.

It is worth to mention that for some experiments the equipment were developed from scratch at the machine workshop of the Mechanical Department of Calabria, at the Institute for Metal Forming (IBF) of RWTH Aachen University and at the Institute of Manufacturing (IFM) of the Cambridge University. For these developed and built equipments a deep discussion about their concept and their application is reported in the proper sections.

2.2 Equipment for Incremental Forming

Generally, all CNC-controlled three-axis machines are suitable to perform the Single Point Incremental Forming. High speeds, large working volumes and sufficient stiffness are favourable. Milling machines are available in different designs, which differ in working volume, maximum feed rate, maximum load, stiffness and cost prices. These are machines, which can be used for Incremental Forming but they can be used for other machining processes, hence they are multi-purpose. One manufacturer makes a specially designed machine that is dedicated to incremental forming only, even if it is less flexible according to the criteria set out by Schmoekel [Sch92]. A list of the types of machines available to do incremental forming is:

- CNC milling machines;
- Purpose built machines;
- Robots;
- Stewart platforms and Hexapods.

Moreover in this thesis all the experiments were carried out with the CNC milling machine or with the AMINO technology , concerning the work carried out at the IBF of Aachen.

2.2.1 The CNC Machine

It has been shown that there is a wide diversity in the type of machine that can be used to achieve Asymmetric Single Point Incremental forming. A manufacturer can choose between dedicated machines or flexible machines as envisaged by Schmoekel [Sch92]. The last possibility has been taken into account during the development of the research at the Mechanical Department of the University of Calabria, either for inexpensiveness reasons that to pursue more flexibility and facility to be adopted by small and medium enterprises which characterise the productive context of our country.

In detail, the set-up of AISF process at the University of Calabria is characterised by four basic elements(Figure 1.9):

- a sheet metal blank,
- a blankholder,
- a single point forming tool, and
- CNC motion,

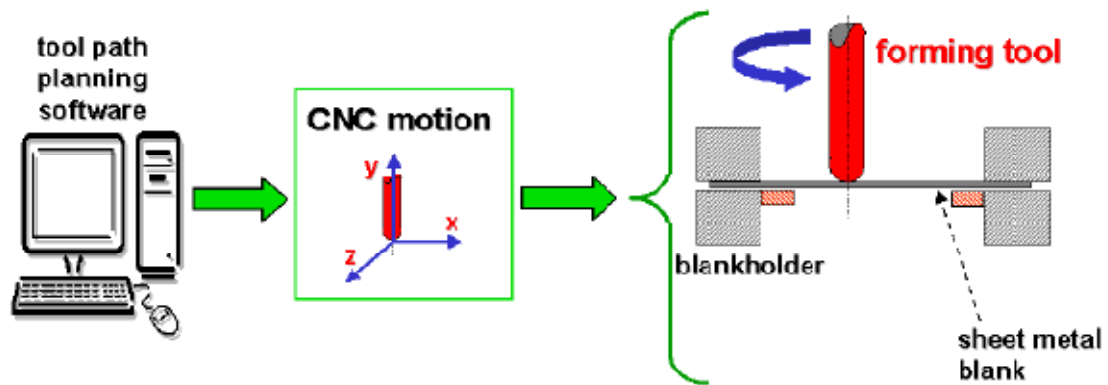


Figure 2.1 – Basic apparatus for SPIF at University of Calabria

The CNC milling machines used in this thesis are an old CNC Olivetti milling machine and a modern MAZAK “work center” multipurpose.

2.2.2 The AMINO DLNC-RB forming machine

The experiments made at the Institute of Metal Forming IBF –RWTH Aachen University were carried out on a 3-axis CNC machine, built specifically for AISF: the AMINO DLNC-RB forming machine(Fig. 2.1).

The machine is equipped with a CNC control of type FANUC® model 16i. It has a maximum workspace of $500 \times 500 \times 250$ mm³ and can exert maximum forces of 1.5 kN in vertical direction and 0.5 kN in the x and y direction. The maximum feed rate in x and y direction is 30 m/min. In practise, the average feed rate will be lower: due to the limited workspace, the machine cannot accelerate to maximum speed and maintain it over a long distance. During two-point incremental forming (TPIF), the sheet is clamped in a blank holder. Four guideways constrain the blank holder to perform only motions in vertical direction. The blank holder motions can be controlled by means of two pneumatic cylinders. When the machine is used for SPIF, the blank holder is kept at constant height.

2.3 The Idraulic press

The Instron 1276 hydraulic press machine was used in this thesis to carry out the deep drawing experiments. In particular this testing machine can provide 1000kN of load cell and it is controlled by MTS pc.



Figure 2.2: The hydraulic press machine Instron 1206

Obviously, for the deep drawing experiments a proper set-up was designed and built but for all the details see section 3.4.

2.4 Measurement equipments

Measurement systems for the on-line and off-line analysis of force, strain, geometry accuracy were used several times in this thesis e.g. to determine the forming limit diagram or to validate the finite element models.

In this paragraph an overview of the used systems is reported

2.4.1 Force Measurements

The force measurement can give important information concerning the force requirements for a given manufacturing process. In particular, these information can be used to avoid machine overload and to build suitable process models. Moreover another important application of force measurement can be the FE model validation.

Concerning the deep-drawing experiments the force measurement system is well assessed and normally consist in a load cell placed in the mechanical, hydraulic or pneumatic press. In this work the load measurement for the deep-drawing experiments were carried out by the internal load cells of the 1276 testing machine used.

Regarding the AISF process since the process is relatively new some different approaches to measure the process load are recognizable in literature.

State of the art in force measurement in AISF

Different approaches were proposed in literature for on-line measurement off process loads, the main difference between these system is due to the sensor positioning. In fact, Jeswiet et al [JMH⁺05] proposed a system based on a Weathstone bridge of strain gauges mounted on the tool, Bambach [Bam08] used a piezoelectric sensor mounted on the tools; while Filice et al [FAM06] and Ambrogio et al [AFM06] used a piezoelectric sensor mounted below the clamping frame. Moreover to remark the importance of force measurements it is worth to say that an approach of failure prevision, based on force trend control has been proposed by Ambrogio et al [AFM06].

The used equipments

In this work the load measurement has been carried out following the methods proposed by Bambach [Bam03] and Filice [FAM06]. In particular, the latter has been implemented on a CNC milling machine mounting the piezoelectric system on the machine frame. The system is system in fig.2.3,2.4.



Figure 2.3 – The SPIF equipment for forces measurement on CNC machine

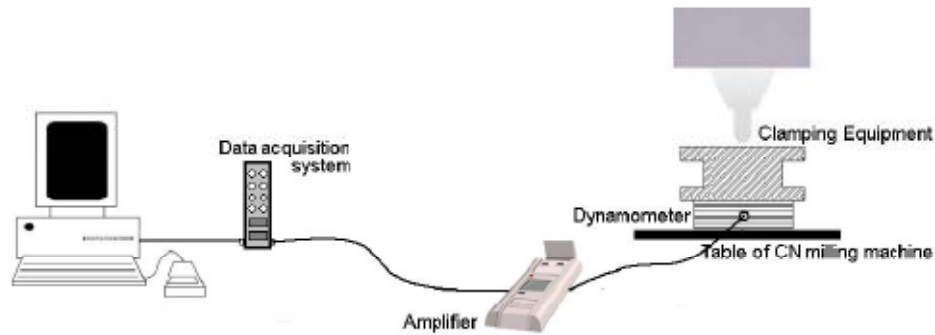


Figure 2.4 – the utilised data acquisition system on the CNC machine

The vertical force exchanged between the punch and the sheet, FZ , was measured all over the process and any twisting effect was neutralised by the high global stiffness of the equipment. Of course, taking into account the current inclination of the lateral surface of the formed part, both the normal (FN) and the tangential force (FT) may be easily calculated. In fact:

$$FN = FZ \cos \alpha \text{ and } FT = FZ \sin \alpha \quad (2.1)$$

Moreover it is worth to mention that for the experiments carried out with the MAZAK CNC machine the load measurement has been done also with the MAZAK load control. This control allows the user to avoid the machine overload but can be used to read the process forces.

During the experiment carried out at IBF- RWTH the process loads were measured mounting a piezoelectric sensor on the punch as showed in figure 2.5. In particular, force measurements were realised by mounting a piezoelectric sensor between the sleeve and the collet of the forming head (Figure. 2.5). The sensor records the three force components that the tool experiences during forming. In order to correlate results from FEA and experiments, the same spatial synchronisation as in the case of the optical measurements was applied. The relation of the measured values and the position of the forming head can be established using the same break points—e.g. prior to every vertical step-down—as in the temporal synchronisation of the optical measurements.

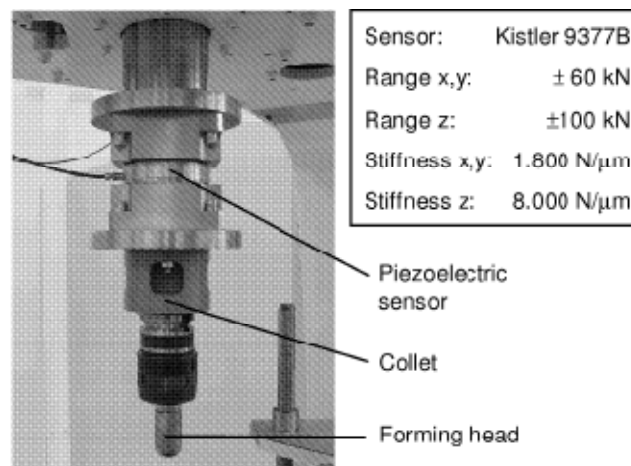


Figure 2.5 : Set-up for on line force measurements

2.4.2 Strain Measurements

The strain analysis can be executed in two different way: on-line and off-line. The more diffused are surely the off-line strain measurement this is due to the simplicity and for economical motivation. The concept of off-line strain measurement consist of a confront between a segment on the part measured before and after the deformation. This measurement can be executed by printing a grid circle on the part surface and measuring with a optical device the final dimension of the circles.

In the experiments carried out at the Mechanical Department of University of Calabria the aforementioned methods has been used. In particular the optical measurement of the deformed grid of circle was measured by a Leica optical stereo zoom.

For all the measurements carried out at the IBF of RWTH – Aachen University the optical measurement system provided by GOM was used. In particular for the on line strain measurements carried out for incremental forming processes or for material characterization, the ARAMIS system was used. For the off-line strain measurement the ARGUS system was used.

On-line strain measurements

Stereo vision systems like ARAMIS® are widely used to record displacement and strain fields on-line during sheet metal forming, e.g. to determine forming limit diagrams [Gal05]. In order to trace the movements of material points under deformation, a stochastic black-and-white spray pattern is applied to the sheet's surface prior to forming. "Material points" are defined as patches or facets on the pattern which are identified during all recorded load stages through their individual greyscale distribution. As a primary variable, the stereo vision system computes the 3D displacements of all material points. Deformation measures can be obtained from the displacement fields in a straightforward manner.

Optical deformation measurement was used by Bambach et al. [BHJ03] to analyze early stages of the forming of a pyramidal part by SPIF. The typical set-up is shown in Figure.2.6. Two CCD cameras are placed under the blank holder, focusing on the area of interest on the sheet. Prior to starting the measurements, a calibration procedure is carried out. In order to avoid decalibration during the set-up phase of the experiment, the calibration procedure was always performed in-situ after the camera system had been firmly mounted on the x-y-table.

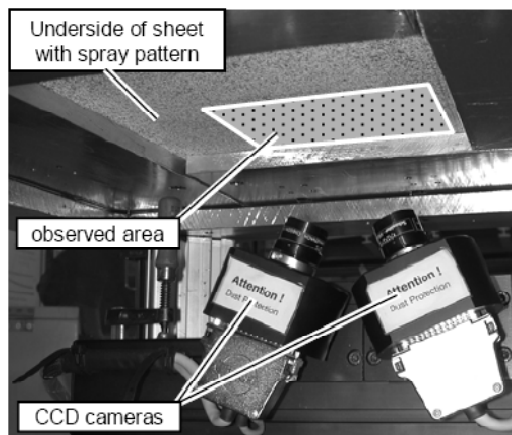


Figure 2.6 Typical set-up of on-line optical deformation measurements for AISF

Off-line strain measurements

In order to measure strains for a complete part, the GOM ARGUS® system is used. Strain measurements are based on a grid of circular dots that are etched on the sheet metal blank prior to forming. These dots follow the deformation of the part during forming. In the deformation analysis, the grid is recorded by a CCD camera. Once the centres of all dots are found, a deformed “mesh” can be computed that represents the geometry of the part. Principal surface stretches are computed from the local deformation of the points. It should be mentioned that through thickness shear can affect the accuracy of thickness estimates that are computed from the surface strains.

2.4.3 Thinning Measurements

The thinning measurements were carried out by traditional contact methods or optical device as Leica stereo zoom or more with ATOS system. The latter system is discussed in the next paragraphs.

2.4.4 Accuracy Measurements

Laser scanner measurements system

To evaluate the geometrical accuracy, the whole field of discrepancies was rebuilt utilising a proper contactless “reverse engineering technique”. In particular, a Minolta Vivid 300 laser scanning systems has been used. This system is able to rebuild the product geometry by laser triangulation principle [VMC97] (see Figure 2.7).

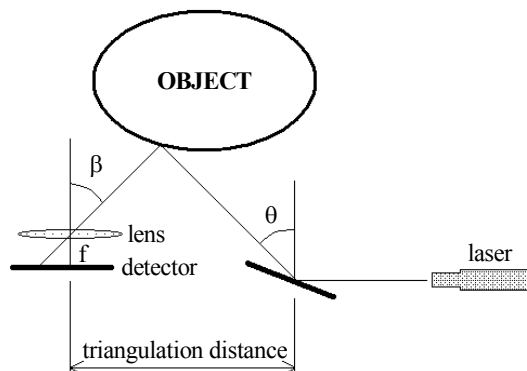


Figure 2.7: The laser triangulation principle

This technique is based on a laser source which irradiates a body by a reflected beam. The diffused light is then revealed by a CCD sensor, placed at a known distance from the laser

source. Subsequently, starting from the obtained CCD image, the spatial coordinates of some surface points may be calculated. The utilised set-up consists of the described scanning system and a rotating support on which the deformed workpiece can be univocally placed. In this way any problem due to the repositioning of the sample is avoided (Figure 2.8).

The sheet surface has been accurately matt by using a proper painting since some metals (for instance Aluminium) show a very high reflectance.



Figure 2.8: The laser based scanning system set-up

Once the sample position optimisation has been performed and the acquisition parameters have been chosen, the virtual comparison has been executed in Rapid Forms 2006® software. This tool automatically allows to apply an optimised procedure which minimizes the positioning error between two surfaces. Naturally, the right positioning was ensured also by some remarkable points (“Markers”), traced on the measured surface, that are discernible on each cloud. In this way, it is possible to reproduce the whole field discrepancies map of the two surfaces.

The discrepancies calculation is defined by the following indicator:

$$- \quad (2.2)$$

$$(2.3)$$

and by σ , the standard deviation.

GOM ATOS measurement system

The GOM ATOS® system was used for two purposes: to digitize formed sheet metal parts and to measure the thickness of parts nondestructively. Digitizing is based on the triangulation

principle: different fringe patterns are projected on the object to be digitized and recorded by two cameras. 3D coordinates for each camera pixel are then obtained using certain transformation equations. Depending on the camera resolution, point clouds of up to 4 million surface points can be obtained. Further information and references are available in [RRT00]. Digitizing yields experimental reference values of the geometry of parts after forming. This information can be used for a comparison with finite element calculations to assess the prediction of springback, or to analyze the geometrical accuracy of formed parts.

The sheet thickness is determined by digitizing both the inner and outer surface of a part. This is accomplished by placing reference points around the part that can be seen by the cameras when both the upper and lower surface are digitized. After the measurement procedure, two sets of measured points are given, representing both the inner and outer surface.

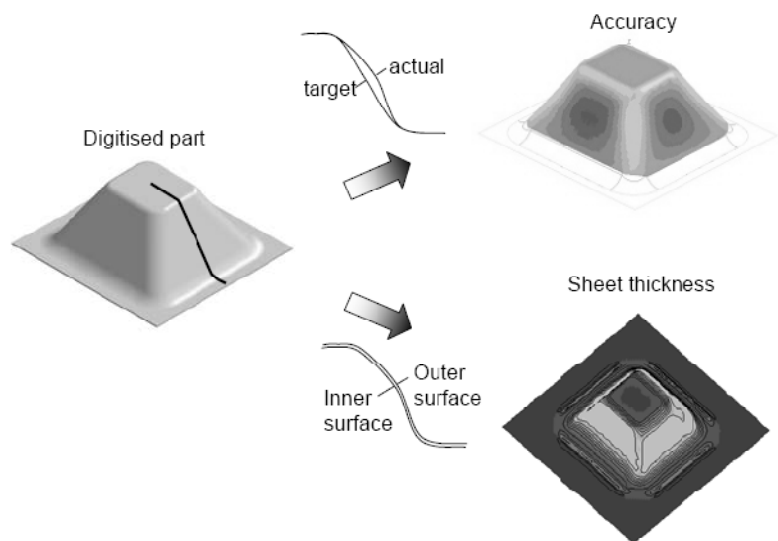


Figure 2.9: Measurement of the sheet thickness and bulge height from digitized surfaces

Given that both surfaces were recorded in the same coordinate system, we can determine their distance everywhere on the part and thus obtain full-scale information about the sheet thickness distribution. Similarly, the distance between a digitized part and its reference geometry can be evaluated to analyze bulges that occur due to springback .

2.6 CAD/CAM system

Warm Formability and Warm Deep Drawing of Magnesium Alloys

3.1 Introduction and scope of this chapter

According to the new keywords which are influencing the approach to the industrial problems in the last years, energy saving is probably one of the most relevant since it is clear that the energetic resources are limited and, in the next time, they will constitute a strategic problem all over the world. For this reason, industry is changing its strategies and the use of the lightweight materials become a key-factor for instance when mobile structures are designed, such as automobiles. Magnesium alloys are well known to the engineers but their workability at room temperature is very low. For this reason, warm forming processes were developed and introduced.

In this framework, the present investigation aims to adjust a combined numerical–experimental procedure to design and optimise warm deep drawing operations of magnesium alloys. Unlike an industrial stamping process, in which the products are very complex, the deep drawing is characterised by simple geometries but by severe conditions in terms of strain levels that involve serious problems of necking and wrinkling. Moreover, the present study allows to derive an analytical model able to predict limit drawing ratio (LDR) at varying the process parameters that is related to the formability of sheet metal. Furthermore the present chapter is focused on an experimental campaign executed by using a proper DOE approach. The highlighted statistical methodology, in fact, allows to definitively establish which parameters are significant on the output results, thanks to ANOVA application.

Finally, a warm deep drawing process on a magnesium alloy was taken into account with the aim to set-up a simulative environment based on the FE formulation able to analyse the process well predicting both the fracture and the wrinkles insurgence.

3.2 State of the art in warm forming of magnesium alloys

In the last years, manufacturing industry is changing its strategies since new impellent demands appeared instead of the traditional requirements based on the cost saving, high productivity and quality. As a matter of fact, nowadays a higher attention is focused on the satisfaction of environmental and energy saving needs, together to other issues related to the sustainability engineering. Among the numerous solutions aimed to approach this new goal, the development of technologies based on the use of lightweight materials, such as magnesium alloys, is strongly increasing, in particular in the automobile structures, because great advantages can be obtained reducing the body inertia.

On the other hand, magnesium alloys present some drawbacks that reduce the using suitability. Their HCP structure, in which dislocation movement is restricted only in the basal plane, makes magnesium alloys very difficult to deform at room temperature [SEC+06, FES+07]. As a matter of fact, HCP metals does not have enough independent slip systems to deform without extensive occurrence of twinning. The formability of Mg alloys can be increased by deforming at high temperatures [SEC+06, FES+07]. As well known, temperatures above 200°C cause additional slip systems to become activated, thus conferring to these alloys an acceptable ductility; unfortunately, forming operations in the high temperature regime result in high costs. This observation is presently driving an additional effort to overcome the forming problems experienced by the most used wrought Mg alloy, the AZ31, by forming in warm conditions, i.e. by deforming between 200 and 300°C.

For this reason, new technologies were developed and the use of non-room temperature seems to be a suitable approach.

In this study a warm deep drawing process of magnesium alloys was investigated in order to implement the above strategy. This introduces a further complexity in the analysis since formability window strongly depends on different parameters [CH03, KOR+01]. Sheet metal forming operations are so diverse in type, extent and rate that it is difficult to provide an accurate evaluation of formability suitable for all process conditions. The knowledge of material properties and the careful analysis of the various types of straining conditions occurring in sheet forming operations are necessary in determining the probability of successful production and in developing the most efficient processing route.

As far as the deep drawing process is concerned, it is critically affected by the occurrence of forming failures such as the wrinkling, necking or fracture.

A currently used methodology to predict such defects is based on the Finite Element Method (FEM), an effective and time saving approach whose effectiveness is strongly related to the accurate knowledge of input data, such as constitutive equations, friction conditions, forming limit curves (FLCs), wrinkling limit curves (WLCs), etc. [ZYW06]. Of course, these curves must be available as input for the numerical simulation: a proper set of tests was developed in order to experimentally build the FLCs and WLCs varying the test temperature.

3.2.1 Concluding on the state of art and the aim of this chapter

In this framework, the present investigation aims to adjust a combined numerical–experimental procedure to design warm deep drawing operations of magnesium alloys.

A wide base of knowledge was developed and utilised in the subsequent numerical analysis, aimed to describe the phenomena involved in the forming process in different conditions.

The finite element simulation was performed taking into account the thermal phenomena and all the experimental cases were accurately simulated.

As a result, it is possible to state that numerical simulation well describes the investigated process, notwithstanding its complexity due to the thermal dependent material characteristics. This is possible, with the modern numerical codes, only running a staggered simulation able to calculate the mechanical step using the explicit integration and the thermal diffusion implementing an implicit approach. In fact, a pure isothermal simulation is not suitable in such a process since the thermal gradient in the equipment and especially in the workpiece is responsible of the final performance. In fact, the material characteristics strongly depend on the actual temperature. All these aspects are accurately discussed in the next sections.

3.3 Material and formability tests

The material investigated was AZ31 magnesium alloy supplied in form of 1 mm thick sheets. The formability of AZ31 was evaluated by performing Nakazima-based tests, in the temperature range varying from 200 to 300°C, using an equipment consisting of a die, a blank-holder and a hemispherical punch (Figure 3.1a). Details about formability tests are reported in [ABF+07].

The wrinkles behaviour was investigated by means of the wedge test, in the temperature range varying from 200 to 300°C, with an equipment (Figure 3.1b) that allows the drawing of trapezoidal specimens [ABF+07].

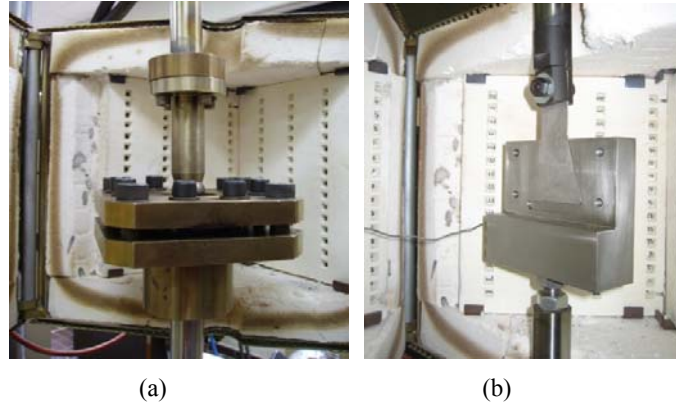


Figure 3.1. Equipments utilised for material characterization.

The forming limit curves (FLCs) and wrinkling limit curves (WLCs) obtained are shown in Figure 3.2 [ABF+07]. It was observed that an increase in temperature allows an enlargement of the safe region within FLCs and WLCs.

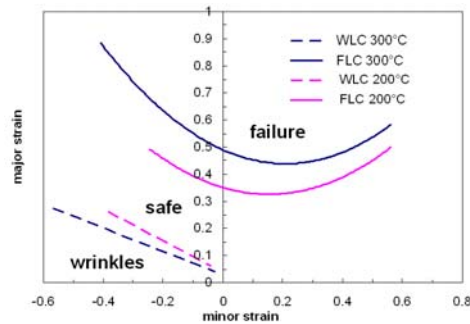


Figure 3.2. Working Limit Diagram of AZ31 at the limits of the investigated range.

Both FLCs and WLCs were implemented into a Finite Element environment in order to predict if the calculated strain distribution could lead to the forming of sound components or if the occurrence of material breaking as well as wrinkles becomes possible.

3.4 Warm deep drawing experiments

The aim of the experimental campaign was the obtaining of consistent data on the limiting drawing ratio (LDR) allowable in the warm deep drawing of AZ31 magnesium alloy and on other phenomena such as wrinkles and temperature dependence.

In a preliminary analysis, aimed to obtain the LDR, temperature was kept constant at 250°C.

Also the initial blankholder pressure (BHP) is a relevant process parameter and it was initially imposed equal to 1% of the actual material flow stress (σ_0) at the forming temperature.

Once the LDR was defined, further experiments were scheduled and carried out in order to verify the effect of temperature and BHP on the manufactured specimens. The range of analysis is reported in the Table 3.1.

Parameters	Lowest	Highest
T [°C]	200	300
BHP [MPa]	0.2% σ_0	1% σ_0

Table 3.1. Range of the investigated parameters.

A proper equipment was designed and manufactured at the University of Calabria. The aim of the experimental campaign was the obtaining of consistent data on the limiting drawing ratio (LDR) allowable in the warm deep drawing of AZ31 magnesium alloy and on other phenomena such as wrinkles and temperature dependence. In order to simplify the analysis the experiments set was executed on 1mm thick sheet and varying the other process parameters.

3.4.1 Equipment Design.

In order to well perform the experimental tests on the warm deep drawing (WDD) process, a proper equipment was designed and developed.

A double heating system, with a heater band placed on the perimeter of the die and four 1.5 kW cartridge heaters directly placed inside the blankholder, was used (Figures 3.3 and 3.4). Both the heating systems were driven by proper PID controllers in order to ensure temperature stability during the tests.

An accurate temperature control was obtained using three different thermocouples: two of them were used for the controller feedback, whilst the third one was placed directly in contact with the sheet in order to measure the actual testing temperature.

The punch diameter was equal to 38 mm whilst the die diameter was 40.5 mm. The punch and die rounds were 5 mm and 6 mm, respectively. An electro-hydraulic Instron 1276 testing machine with a load capacity equal to 1MN was used. A proper cooling system was designed in order to avoid the heat transfer to the machine elements.

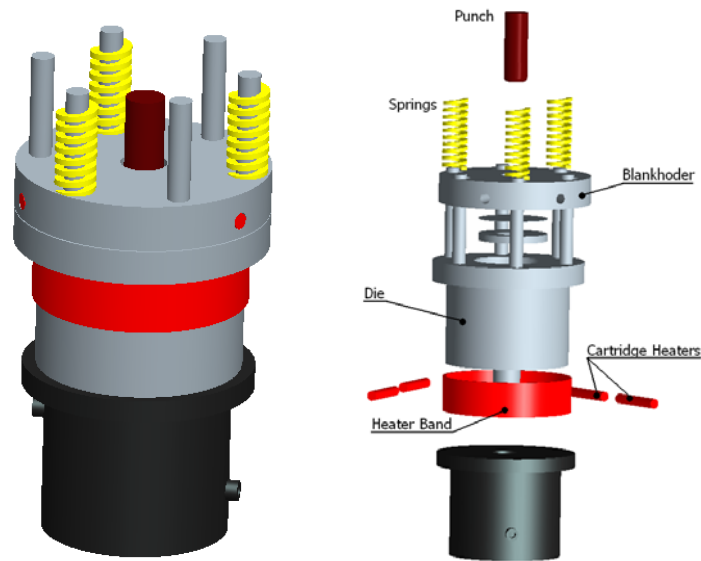


Figure. 3.3: Equipment used for warm deep drawing tests.

Figure 3.4 shows the deep drawing equipment mounted on the testing machine. The blankholder pressure was applied by means of three high performance springs with a stiffness equal to 400 N/mm. In all the tests, the target temperature was kept constant for 10 minutes before running in order to ensure the initial isothermal condition.

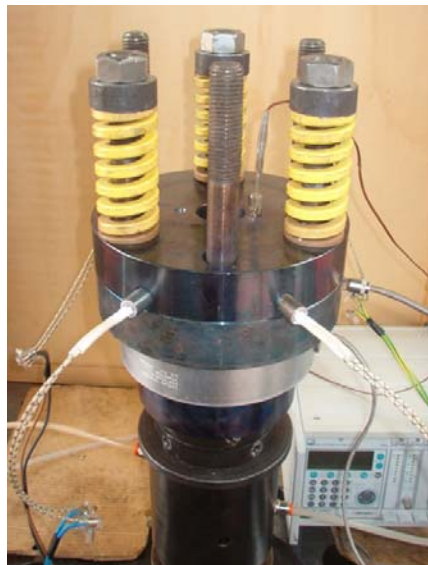


Figure 3.4: Equipment for deep drawing tests mounted on the testing machine.

Temperature could change during the process due to the contact with cold parts, the conversion into heat of the deformation energy and the increase in the BHP value. The latter, in particular, improves the thermal exchange between blankholder and specimen. In this study, the first problem was minimized by keeping the equipment as close as to the test temperature, the second phenomenon was reduced using a very low punch speed. On the other hand, the effect of the BHP was revealed during the tests, even if its impact on the temperature increase was limited to about 10°C.

However, the prediction of the temperature changes and the related material characteristic represent the most interesting reason for which the thermo-mechanical simulation of this kind of processes is suitable.

Figure 3.5 shows different specimens obtained varying the drawing ratio.

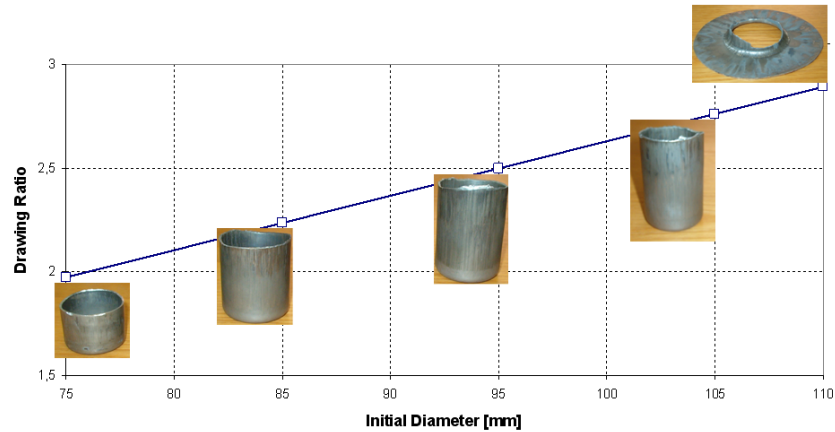


Figure 3.5: LDR results for AZ31 at 250°C.



Figure 3.6: Experiments carried out with a LDR= 2.63: sound (a), with wrinkling (b) and broken parts (c).

Figure 3.6 shows some of more interesting experimental results obtained for a fixed DR equal to 2.63. More in detail, the sound product was obtained working at 250°C and with a BHP equal to 1% σ_0 (Figure 3.6a) whilst a sample in which the wrinkles occurred, in the same

geometrical and thermal conditions, was obtained with a BHP value of $0.2\% \sigma_0$ (Figure 3.6b); finally, Figure 3.6c shows a broken part obtained with a temperature of 200°C .

3.5 Numerical analysis

An important aspect of the research on warm deep drawing is the development of a design environment able to simulate the actual complexity of the real warm deep drawing process of AZ31 magnesium alloy.

In this analysis, a commercial FE code, which implements the explicit formulation, based on the dynamic equations, was used. The main difficulties occurring when this approach is adopted, in terms of kinetic energy, mass tuning, speed tuning, in order to have obtain quick and reliable solutions, have been well investigated in literature [AF04]. On the other hand, it is widely recognized that explicit simulation of sheet metal forming processes is assessed only using isothermal conditions, whilst heavier problems occur when simulating thermal phenomena, such as those taking place in the actual processes where thermal gradients could occur on the workpiece [YMN+04]. This can affect the simulation effectiveness since materials such as magnesium alloys are very sensitive to temperature changes. For the above mentioned reasons, the analysis was run by a staggered simulation consisting of an explicit mechanical step followed by an implicit pure thermal step. Figure 3.7 shows the numerical model used at the beginning of the simulation.

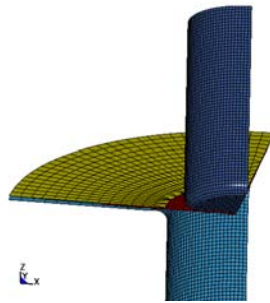


Figure 3.7: The numerical model.

Such explicit-implicit combined approach, even if produces an increase in the computation time, leads to a more realistic simulation of the experiments. The wrinkle and fracture insurgence was predicted by implementing the FLCs and WLCs, obtained at different temperatures (Figure 3.2), into the FE code. This allows to design the warm deep drawing process ensuring that the strain distribution falls within the safe region included between WLC and FLC at the test temperature. To this purpose, Figure 3.8 shows the ability of the FE code in predicting wrinkles and fracture insurgence.

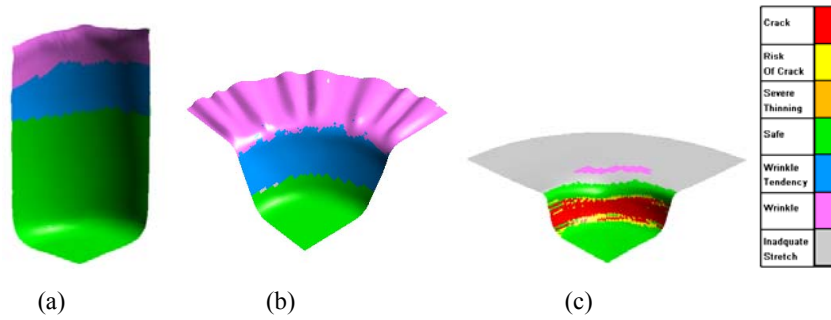


Figure 3.8: Numerical results for components: sound (a), with wrinkles (b) and broken (c).

3.5.1 Discussion of the results

For sake of shortness, some relevant experimental cases were compared with numerical predictions in the following analysis.

In fact, this work tends to propose a robust methodology that can be of course extended to other parameters if required in the industrial applications. For instance, sheet thickness and severe induced thermal gradient can be considered in further researches.

However, in the most relevant investigated cases it is possible to observe a good capability of the “customized” simulator predicting the process issues.

In particular, the sound component, experimentally obtained for $DR=2.63$, $BHP=1\%\sigma_0$ and $T_0=250^\circ\text{C}$, is well predicted (Figure 3.8a); at the same time, wrinkles can be detected by analysis numerical results corresponding to $DR=2.63$, $BHP=0.2\%\sigma_0$ and $T_0=250^\circ\text{C}$ (Figure 3.8b); finally, a broken part is numerically predicted in the case characterized by $DR=2.63$, $BHP=1\%\sigma_0$ and $T_0=200^\circ\text{C}$, as shown in the Figures 3.8c. As above introduced, the sheet temperature slightly changed in the investigated cases, however, the temperature revealed by the thermocouple shows a good agreement with the simulation (Figure 3.9).

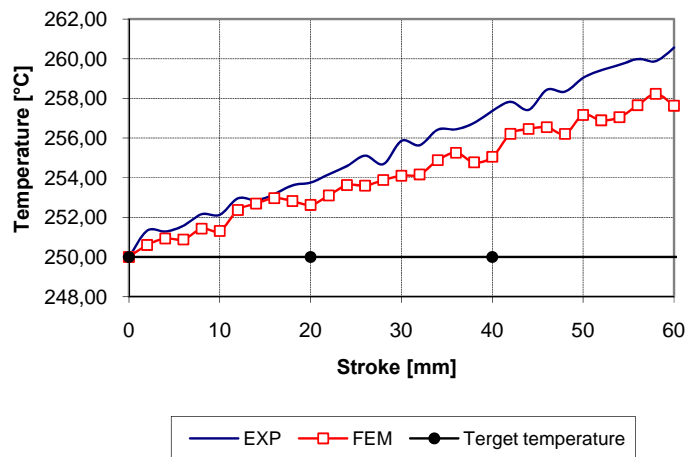


Figure 3.9. Numerical and experimental temperature on the sample.

3.5.2 Conclusion on the numerical study of warm forming

Warm processes of magnesium alloys surely represent the most effective way in order to obtain industrially suitable components due to its low formability at room temperature.

In this study the set-up of an effective design environment based on the use of Finite Element formulation was discussed, taking into account a reference process (deep drawing) and the results of a wide experimental analysis.

As a conclusion, it is possible to state that numerical analysis of not-room temperature processes on magnesium alloy requires a coupled thermo-mechanical simulation. In fact, the material characteristic is strictly related to the punctual temperature that has to be accurately calculated. In fact, both the wrinkles occurrence and the material damage strictly depend on the strain history and the material temperature. Thus, as here demonstrated, a proper numerical simulation can support the analyst to design a manufacturing process remaining in the working window and, finally, obtaining sound parts.

3.6 A statistical analysis of the process parameters influence on LDR

3.6.1 Plan of the experiments.

First of all, a preliminary analysis, aimed to obtain the LDR, was performed for a fixed temperature of 250°C.

A particular attention was paid to fix the blankholder pressure (BHP) value. In fact, the initial blankholder pressure is a relevant process parameter that can affect the final result. For this reason, the preliminary set of experiments was carried out by changing the initial BHP in the range [0.5% - 1,2%] of the actual material flow stress (σ_0) at the forming temperature.

This factor is directly responsible of the wrinkling insurgence as well as early fracture in the specimen. According to that, this preliminary analysis was considered necessary to optimise the BHP in order to obtain sound components. As a result, a value of about 1% of the actual flow stress represents the best trade-off between wrinkles insurgence and failure approaching [ZM98, KS00, CCY+04]. Actually, the above value could be optimised as function of the initial diameter and temperature but, for sake of simplicity, it was kept constant all over the tests. To simplify the analysis and to reduce the number of experiments, all the tests were performed on sheets characterised by a thickness of 1 mm. The utilized material was an AZ31B Magnesium alloy. On the contrary, the study was focalised on the sensitivity analysis of the tool velocity (mm/sec) and sheet temperature (°C). According to the data available from literature review on the same blank material AZ31-B [FES+07, ABF+07,

ABB+08], it was considered strategic to design a preliminary factorial experimental plane, 2^k , where the two factors are exactly the ones above highlighted while the highest and lowest levels were fixed according to their significance (Table 3.2).

Table 3.2. Factors investigated in the experimental campaign.

Factors	Lowest	Highest
v [mm/sec]	0.1	1
T [°C]	200	300

Each case of the factorial plane was repeated varying the blank dimension in order to find the Limit Drawing Ratio (LDR) for fixed process conditions.

Furthermore, it is well known from the literature review that the considered Magnesium alloy AZ31 is characterised by a not linear behaviour between 200°C and 300° [AFM+07, ZYW06] from the formability point of view. For this reason, it was considered strategic to repeat the same tests at 250°C.

At the same time, in order to obtain more reliable experimental data, every test was repeated three times. The cases which belong to the Factorial Plane were analysed by using an ANOVA analysis.

On the other hand, taking into account the LDR factor as the main output of the experimental campaign, it is possible to synthesise the optimal conditions depending on process temperature and punch speed in the next Table 3.3.

Table 3.3. Output of the experimental campaign.

T [°C]	v [mm/sec]	D₀ [mm]	LDR
200	0.1	90	2.37
	1	80	2.11
250	0.1	90	2.37
	1	105	2.76
300	0.1	85	2.24
	1	100	2.63

In the following figures, the sound components at the LDR condition, varying the testing temperature (Figures 3.10-3.11-3.12), and some defected components (Figure 3.13) are shown.

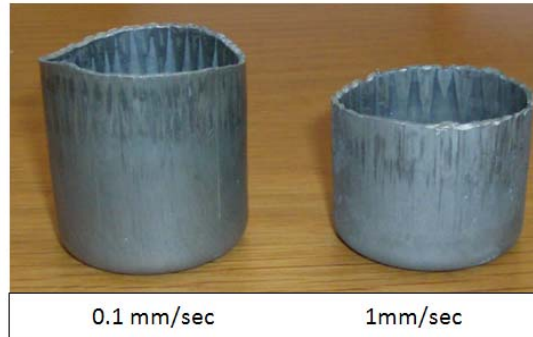


Figure 3.10: Specimens obtained at 200°C.

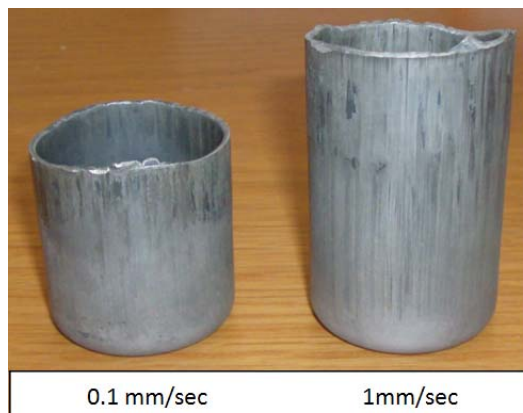


Figure 3.11: Specimens obtained at 250°C.

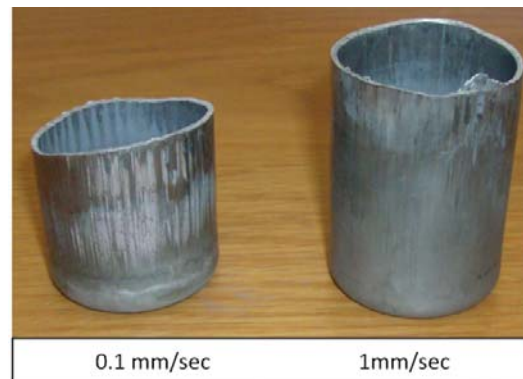


Figure 3.12: Specimens obtained at 300°C.



Figure 3.13: Wrinkled and broken components.

3.6.2 The Analysis of Variance.

The experimental results were analyzed by ANOVA in order to highlight the effects of the single independent factors and their interactions on the dependent one (see Table 3.4). Focalsing the ANOVA methodology only on the highest and lowest highlighted values, it selected exactly a factorial model to describe the results.

Table 3.4. ANOVA Results.

Factors	p - value	Influence on LDR
V	0.0031	High
T	0.0017	High
v*T	< 0.0001	High

Values of “*Prob > F*” (p-value) less than 0.05 indicate that the model terms are significant. In this analysis, it results that both velocity and temperature are important on the output measures, but their interaction is particularly relevant on the final result.

At the same time, the Predicted R-squared of 0.9942 is in reasonable agreement with the Adjusted R-squared of 0.9974 (see Table 3.5), such as the Adequate Precision higher than 4 highlighted the model suitability to be used for navigate in the design phase, since the signal to the noise ratio is adequate low (Table 3.5).

Table 3.5. Performance indexes.

R-Squared	0.9985
Adj R-Squared	0.9974
Pred R-Squared	0.9942
Adeq Precision	58.890

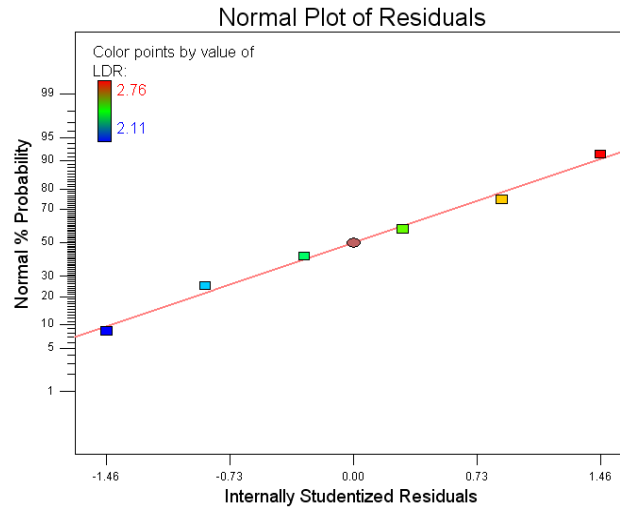


Figure 3.14: Normal probability plot for the proposed model

3.6.3 Discussion of the Results

Figure 3.15 summarises some results of the experimental tests in terms of obtained LDR in the different conditions. In particular, having a look at the figure, it is possible to observe that several phenomena occur as it will briefly discussed.

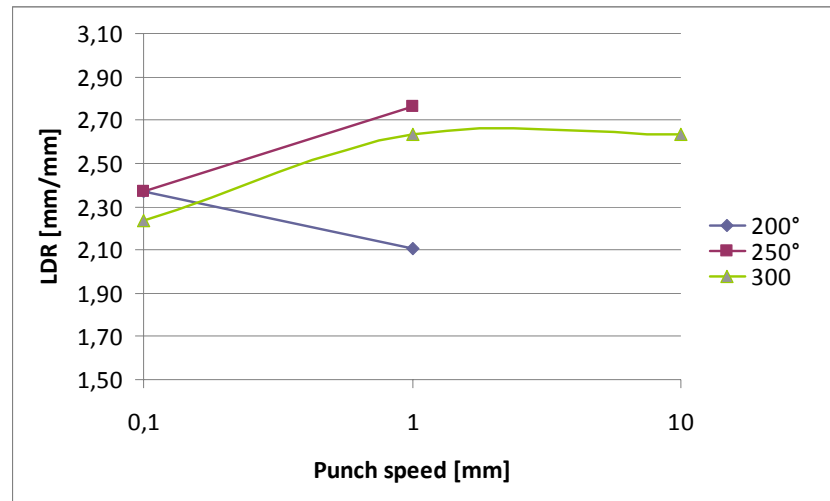


Figure 3.15: LDR value depending on temperature and punch speed.

First of all, according to other researchers, it is possible to see that the formability presents a peak at 250°C [ZYW06]. This is true at all the investigated punch speeds.

However, the dependence of formability on punch speed strongly depends on temperature.

More in detail, at 200°C an increase in the punch speed leads to a decrease in formability due to the strain hardening and twinning effects. A different behaviour is observed at higher temperatures where the LDR value increases by increasing punch speed. Such behaviour can be attributed to the activation of new slip systems and the occurrence of dynamic recrystallisation. They contrast the strain hardening and twinning effects, due to the increase of punch speed, leading to an improvement of formability. The slightly lower LDR values at 300°C, irrespective of punch speed, could be attributed to the relatively low values of the strain rate sensitivity exhibited by the studied alloy (about 0.1 at 300°C) that are not able to compensate the decreasing in the strain hardening coefficient (about 0.2 at 300°C) with increasing temperature.

3.6.4 Conclusions on the influence of process parameter

An experimental campaign to investigate the role of both temperature and punch speed in warm deep drawing of AZ31 Magnesium alloy was presented in this analysis.

A peak of formability at 250°C is showed for the above material, according to already published researches.

At the same time, low punch speeds are not suitable for temperature over the recrystallization threshold (about 240°C for this material). However, the beneficial effect tends to reduce when punch speed increases too much.

As a conclusion, the optimal WDD process design is not very easy for AZ31B sheets. Thus, relevant efforts are required to build a more robust and wide base of knowledge (for example investigating other thicknesses) to help the designer in performing reliable processes.

Study on AISF Formability

4.1 Introduction and scope of this chapter

Formability is a relevant issue in AISF and so in Single Point Incremental Forming (SPIF) process since it is one of the main point of strength together to the possibility to avoid any dedicated die. Several researches agree that, depending on working material and process parameters, in SPIF operations there is a threshold slope of the wall that cannot be overcome without material breaking. If deep Incremental Forming is taken into account, despite the previous statement it is possible to demonstrate that, when the threshold angle is imposed, there is a relation between the actual workpiece depth and the material breaking approaching. In this chapter, the latter relationship is investigated and formally derived by using a proper statistical regression.

The formability of sheet metal forming processes is usually considered with conventional diagrams named forming limit diagrams. Nowadays it is universally recognized that these diagrams are a reliable instrument for sheet metal processes design. Anyhow, because of they were developed properly for stamping processes and normally applied to all the other sheet metal processes. This consideration allow to understand the need of a deeper knowledge on AISF formability in general and on the forming limit diagram for AISF also.

In this chapter, after a short overview of the state of the art on AISF formability, by analysis of forming limit diagrams and models, an experimental and numerical analysis of the AISF formability is reported. In particular, starting from the conclusions on the state of the art (section 4.2 and 4.2.1) and from the meaningless of the standard formability indicator some new models are presented.

In details, due to the not fully FLD_0 significance two new formability indicators are proposed. The first one is the maximum feasible depth that is surely more useful from an industrial point of view for sake of easiness. More in detail, due to the fact that the formability

is strongly affected by the wall slope value, the analysis is carried out starting from an easy shape characterized by a single slope wall angle in order to verify the results for a double slope and to generalize for a multi slope conditions. For these motivation the first part of this chapter is divided in the following sections:

- Formability analysis of single slope deep geometries
- Formability analysis of double slope deep geometries
- Formability analysis of multi slope deep geometries

The second formability indicator proposed and analyzed is the thinning; in details with the aim to predict the thinning as a function of the process parameters, a statistical model is presented in section 4.6.

4.2 Forming limit diagrams in AISF

A number of tests have been devised up to now to record the limit strains in AISF:

Iseki [Ise00] proposed an “Incremental Bulging Test” (IBT) to determine the forming limits in AISF. The test can be explained as a combination of movements in the x-y plane and along the z-axis. In the plane, the path consists either of a parallel or perpendicular strokes of the tool. In [Ise00], the ratio n_y/n_x is introduced as a measure of the number of strokes along the x- and y-axis. Setting $n_y = 0$ is equal to an IBT test with straight to-and-fro motions of the forming tool as shown in Figure 4.1 (Unlike proposed in [Ise00], the step-down motion in Figure 4.1 is performed continuously here, in order to avoid force peaks and that the corners are overly loaded by the sharp step-down in the corners.) By varying this ratio different final strains can be obtained. Along the z-direction, a stepdown d_z that is purely oriented along the z-direction is performed. In [Ise00], an empirical formula for the FLC found in AISF is given

$$\varepsilon_1 + \beta \varepsilon_2 = \varepsilon_{pB}, \quad (4.1)$$

where β and ε_{pB} are material constants. Iseki remarks that

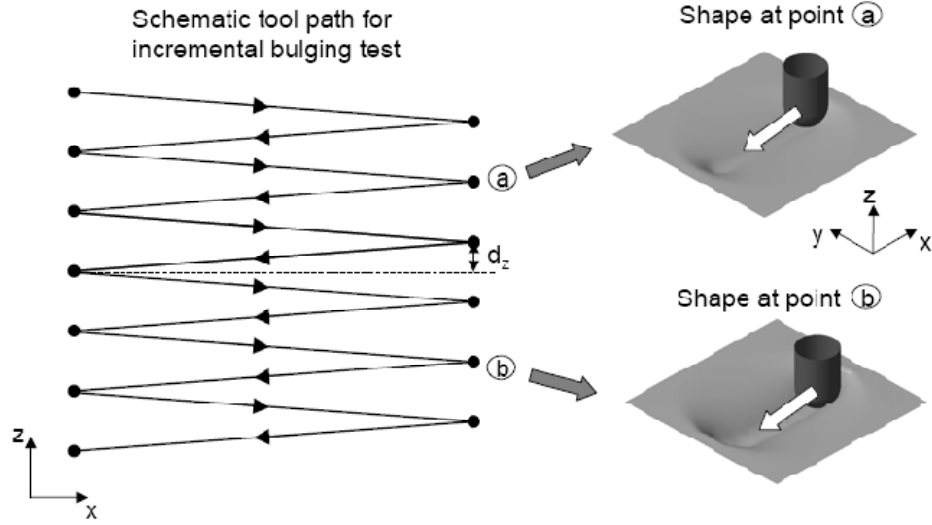


Figure 4.1: Illustration of the “incremental bulging test”, with modified z-pitch compared to Iseki’s original proposal.

- based on the measurements, the strain paths are assumed to be approximately linear,
- the value ε_{pB} depends on the tool pitch,
- the value β varies between 1-2 in the experiments,
- the “classical” forming limits by Swift [Swi52], Støren & Rice [SR75] etc. cannot represent the behaviour of sheet metal in AISF.

The experiments detailed in [Ise00] were conducted for aluminium, brass and stainless steel. It is worth mentioning that a value of $\beta = 1$ in Eq. (4.1) corresponds to a material failure at constant thickness strain for all strain states. Since volume constancy implies that

$$\varepsilon_1 + \varepsilon_2 + \varepsilon_3 = 0, \quad (4.2)$$

the constant ε_{pB} in Eq. (4.1) corresponds to the thickness strain ε_3 . This strain can be related to the draw angle φ using the sine law, which yields

$$\varepsilon_{pB} = -\varepsilon_3 = -\ln\left(\frac{t}{t_0}\right) = -\ln(\sin \varphi)$$

$$t_0 = -\ln(\sin \varphi). \quad (4.3)$$

Filice *et al.* [FFM02] devised a biaxial stretching test similar to the incremental bulging test proposed by Iseki, and a second test shape, which is a conical shape obtained by a spiral tool path. It was found that an “FLC” can be given as

$$\varepsilon_1 = -1.040\varepsilon_2 + 108.2\% \quad (4.4)$$

showing again that the FLC is represented by a characteristic thickness strain at fracture. Given that such a strain exists, the analysis of the FLC can be reduced to finding the maximum achievable strain under plane strain conditions. This point, called FLD_0 would mark the axis intercept with the ordinate for an FLC with a constant slope of -1. By means of the sine law, the FLD_0 is sometimes related to the maximum draw angle, ϕ , that can be found by continuously increasing the wall angle of e.g. a conical shape until the sheet fails [JMH+05].

Additional work regarding the forming limits in AISF was done by Kim and Park and Shim and Park [KP02, SP01], who used several test shapes with a polyhedral contour. The findings regarding the shape of the forming limit curve agree with the results stated by the authors cited before. Additionally, it was concluded that the FLC depends on friction and plastic anisotropy of the sheet metal. The forming limits were found to increase with decreasing vertical pitch. Furthermore, it was shown that the forming limits are higher along the transverse direction when small tools are used, while the opposite holds for the rolling direction.

Jeswiet and Young [JY05] carried out experiments on two aluminium alloys using axisymmetric shapes (cone, hyperbola, dome), a square pyramidal frustum and a flower shape to create different states of strain. The maximum achievable draw angle ϕ_{max} was analysed, which was considered identical to the FLD_0 value. An empirical expression relating the maximum draw angle and the sheet thickness was reported,

$$\phi_{max} = \kappa t_0 + \beta, \quad (4.5)$$

where $\kappa = 8.5 \text{ deg/mm}$, $\beta = 60.7$ for 3003-0 aluminium, and $\kappa = 3.3 \text{ degrees/mm}$, $\beta = 58.3$ for 5754-0 aluminium. A linear relationship between minor and major strains was found, which is in conformance with the findings of the other authors mentioned previously. In an attempt to correlate the forming limits with material properties, Micari [Mic04] used a response surface model to identify the material parameters with the largest influence on the FLD_0 . The following expression was obtained:

$$FLD_0 = 8.64 - 36.2n - 0.00798K + 0.373R - 0.104A\% + 0.0301K \cdot n + 0.607n \cdot A\%. \quad (4.6)$$

K and n are the coefficients of the Ludwik-Hollomon description of the flow stress, $\sigma_V = K\varepsilon^n$, A is the reduction in area upon rupture in a tensile test, and R is the r-value. From Eq. (4.6) it can be seen that the hardening exponent n has a dominant influence on the FLD_0 value. A Box-Behnken model was introduced by Jeswiet *et al.* [HJ07] to determine response surfaces for the maximum draw angle as a function of material type, thickness, geometry, tool radius and step-down.

Another empirical model for the occurrence of fracture in AISF was given by Strano *et al.* [SCR04]. Based on an experimental investigation of 230 parts, a formula for the probability of fracture P_s of an AA1050-O sheet was derived:

$$\ln\left(\frac{P_s}{1-P_s}\right) = 11.125 + 6.722\varepsilon_t - 22.46f_z^* \quad (4.7)$$

Here, ε_t is the thickness strain, and f_z^* is a “corrected” feed rate that takes into account the curvature of the part.

The work cited so far gives no explanation for the extended forming limits in AISF. An attempt to explain the dependence of the forming limits on the process parameters was made by Bambach *et al.* [BHJ03]. Using the Gurson model for ductile fracture, the increase of attainable strains with decreasing tool diameter and increasing vertical step-down were predicted in a qualitative way. It was found that the action of the tool superimposes hydrostatic pressure, which might be a qualitative explanation for the high forming limits. The presence of negative pressure stresses was also reported by Ambrogio *et al.* [AFFM04]. Allwood *et al.* [AST07] put forward the idea that the increased forming limits in AISF are due to through-thickness shear. By taking into account shear in the Marciniak-Kuczynski (M-K) analysis, it is shown that the presence of through-thickness shear can increase the necking limits considerably. In addition, Allwood *et al.* point out that the principal axes of deformation should rotate during AISF. Consequently, principal surface stretches are found on the surface of parts made using AISF rather than strains that are representative for the through-thickness behaviour. The increase in necking limits and the presence of shear were shown with an incremental forming process called “paddle forming”, which uses a rotating paddle to deform sheet metal. With this process, a considerable amount of through-thickness shear was created. Hadoush *et al.* [HBH07] attribute the large attainable strains in AISF to cyclic bending. Using a finite element model of a strip that is stretched, and, at the same time, undergoes cyclic bending (imposed by a set of three rolls), it is shown that the deformation can remain stable up to strains that are considerably bigger than in uniaxial tension. Van Bael *et al.* [BEH+07, EHB+07] investigated the forming limits in SPIF with a Marciniak-Kuczynski model, taking into account the serrated strain paths that are characteristic for AISF. Their model allowed for the prediction of increased strains to failure but the predicted necking strains were smaller than those observed in experiments.

4.2.1 Conclusions on the state of the art

From the literature cited so far, the following facts shall be stressed:

- All cited authors agree that the forming limits found in AISF are a straight line of negative slope in the stretching region and that the forming limits are considerably higher than those obtained in conventional Nakajima tests. However, there is no agreed-on standard for the forming limit tests or the evaluation procedures to record an FLC for AISF. None of the cited authors verifies that the prerequisites for the determination of an FLC are met in their tests. As a consequence, FLD0 values and maximum draw angles can only provide rough guidelines to the designer.

- Despite the fact that an FLD is not an appropriate tool to measure the forming limits in AISF, it is interesting that large strains can be found in AISF. It was stated according to Pearce [PP74], that any curve between the necking and fracture limit curve can be obtained depending on the gauge length used. The necking limit curve typically rises, the fracture limit curve drops with increasing biaxiality. This suggests that the measured strains cited in the literature might either reproduce the fracture limit curve, a known property, or represent a new phenomenon. Hence, it is not precisely defined what is meant by an FLC for AISF in the literature. Figure 4.2 shows a comparison of measured and modelled curves for the FLCN and the FLCF along with the FLC for AISF found by Micari (Eq. 4.6). It is remarkable that the FLC for AISF obtained by Micari falls in-between the experimental and theoretical FLCs for necking and fracture, which is in agreement with the arguments given above and stresses the need for a proper definition of the term “forming limits” in the context of AISF.

- The nature of the forming limits in AISF is not yet comprehensively understood. Allwood et al. [AST07] attribute the large attainable strains in AISF to shear, Hadoush et al. [HBH07] to cyclic bending, Bambach et al. [BHJ03] to pressure stresses superimposed by the tool, van Bael et al. [BEH+07] to the non-linear strain paths and Kitazawa [KOS03] treats the limit strains using a model for low cycle fatigue.

As Marcianiak points out, there are a number of influencing factors that determine the onset of necking and fracture. It is unlikely that the large strains can be attributed to just one phenomenon alone. To understand the forming limits in AISF it seems necessary to understand the interplay of process mechanics and material behaviour.

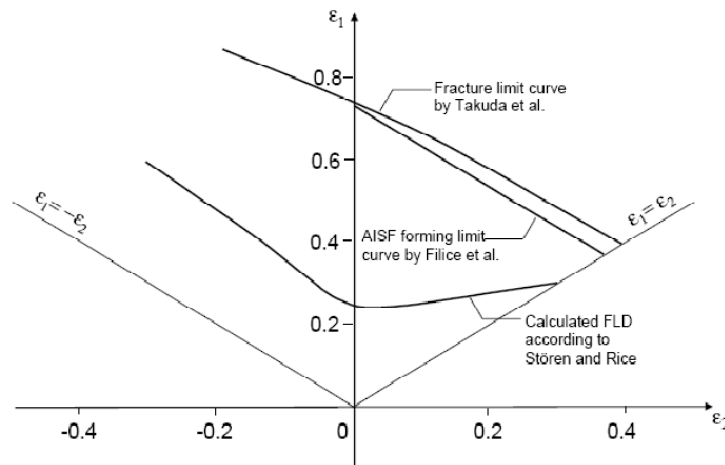


Figure: 4.2 Comparison of different experimental and theoretical ([SR75]) necking and fracture limit curves for commercially pure aluminium

A model for the forming limits in AISF should explain the experimentally observed dependencies of the forming limits on the process parameters, predominantly on the tool diameter and the vertical pitch value. In consequence, it can be stated that:

- FLCs cannot be applied to AISF,
- appropriate tests and evaluation procedures to determine the forming limits in AISF should be defined,
- the evaluation should clearly distinguish between necking and rupture,
- models for the formability prediction are needed.

4.3 Single slope analysis

Usually FLD_0 point is used in Incremental Forming to define the formability; sometimes it is defined more simply from a geometrical point of view, by means of the maximum wall inclination angle α_{max} . However, some applications have shown that slope angles, higher than the critical one, can be safely obtained specially when complex geometry, characterized by a variable slope wall, has to be manufactured [ADF+05]. The latter, for instance, are usually characterized by different slopes, sometimes higher than the critical one, with a depth associated to each slope usually low. In this case, also vertical walls can be manufactured imposing a depth of few millimeters since the low sheet stiffness and the punch radius induce

a transient behaviour that avoids the severe thinning which theoretically corresponds to the imposed slope [AFS+06].

In other words, a different behaviour can be observed with respect to the common pieces, so that the simple knowledge of the α_{\max} value results not adequate for the design of the manufacturing step in the above specified conditions.

For this reasons, it is easy to image that a correlation between the critical slope angle and the workpiece depth could be established, for given material and process parameters. In other words, when the critical angle is adopted, it is reasonable to think that material damage occurs only after a certain depth.

An experimental campaign was carry out in order to acquire consistent data related to the discussed issue. Subsequently, a statistical analysis was carried out, obtaining a formal law able to predict which is the allowable depth when the critical slope angle is reached or overcome, varying the other process parameters.

4.3.1 Experimental campaign

Starting from the available base of knowledge on the considered process, a set of experiments was properly designed and executed in order to deeply analyze the role played by the process parameters correlation with respect to the component soundness.

According to the formability limit for the utilized material, namely an Aluminium Alloy 1050-O, some tests were done varying those process parameters which directly influence the formability, such as the tool diameter (D_p), the tool depth step (p), the wall inclination angle (α) and, finally, the sheet thickness (s). Naturally, others variables, like the tool speed rotation or the tool feed rate, were kept constant to reduce the problem complexity and because they have not a significant influence on the material breaking [AFF+03]. A frustum of cone, having a major base diameter (D_0) equal to 80 mm, was chosen as specimen shape for the whole experimental campaign and, as consequence, each experiment was carried out up to reach the material breaking or, vice versa, a final height equal to the major base dimension. In this way, for the experiments which led to breaking, the final height reached by the product at the necking conditions (H_{\max}) was measured.

All the experiments were performed on a 3-axis CNC milling machine, equipped with a clamping device and a baking plate to ensure the sheet locking. An emulsion of mineral oils was utilized to lubricate the interface between the punch and the sheet.

4.3.2 Statistical analysis

The experiments were analyzed following the Response Surface Methodology. In this way, as above introduced, four independent factors were considered, while the dependent one was derived by the measure of the component final height. In Table 4.1 the lowest and the highest values for the investigated range are displayed. Since the analysis was executed at the formability limit, the lowest wall inclination angle was fixed equal to the critical slope for the investigated material, i.e. 70° , with the aim to better specify the influence of the other parameters with respect to the maximum achievable height [AFF+03].

Each experiment was firstly designed belonging to a CCD face centered plane in order to reduce the number of tests; subsequently, during the analysis, the plane was reduced neglecting the experiments which allowed a sound component. Furthermore, an external bound to generalize the analytical model applicability (Figure 4.3) also when maximum depth is allowed was introduced.

TABLE 4.1. Extreme Value of the Experimental Plane.

Parameters	Lowest Value	Highest Value
Wall Inclination Angle (α)	70°	80°
Tool Diameter (D_p)	12mm	18mm
Tool Depth Step (p)	0.3mm	1mm
Sheet Thickness (s)	1mm	2mm

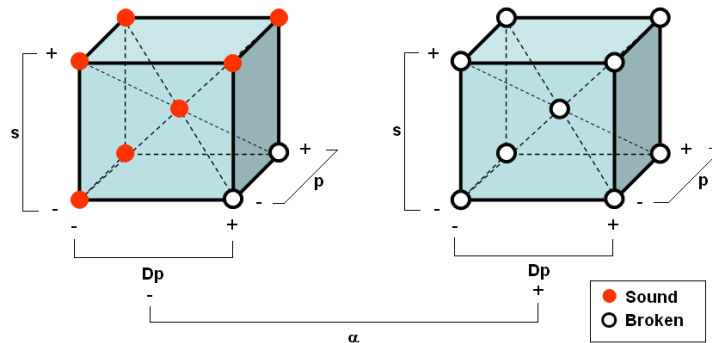


Figure 4.3: The investigated experimental plane.

The experimental results were analyzed by the ANOVA in order to highlight the effects of the single independent factors and their interactions on the dependent one (see Table 4.2).

TABLE 4.2. Influence of input variables and their interactions on H_{\max} .

		Factors						
		α	D_p	P	S	αD_p	αp	α^*s
Influence on H_{\max}		High	High	High	High	Medium	Medium	Medium
		α^2	D_p^2	p^2	s^2	D_p^*p	D_p^*s	P^*s
		No	Low	No	No	No	No	No

As it can be easily observed, the first order factors are the most significant when determining the product final height. This confirms the results recognizable from the state of the art [JMH⁺05]. On the other hand, only the interaction between the wall inclination angle and the other process parameters is partially significant to influence the output value, confirming again the relevant role played by the former parameter on formability in Incremental Forming process.

ANOVA methodology allowed also to identify a quadratic model as the most suitable solution to describe the investigated phenomenon and to predict the maximum achievable height. As above introduced, a bound was defined to identify the not critical conditions which allow to obtain deep component, with a final height equal to its major base. In fact, as it is already known, the slope angle equal to the critical one, namely $\alpha_{\max}=70^\circ$ for the AA 1050–O, represents a threshold value which divides the super safe conditions ($\alpha < \alpha_{\max}$) and the unsafe ones ($\alpha \geq \alpha_{\max}$). At the same time, observing only those experiments which led to sound product, it is easy to understand that a strong influence is played by the tool diameter and the sheet thickness; more in detail, the material formability, in terms of achieved depth, decreases increasing the tool diameter D_p and reducing the sheet thickness s . This result can be easily explained considering that the same portion of material repeatedly undergoes to the punch action, determining a sort of material removal by wear. In this way, it can be assessed that formability is proportional to the tool diameter and inversely proportional to the sheet thickness, so that the ratio D_p/s can be proposed to classify the safe and unsafe cases for $\alpha=70^\circ$. More in detail, if D_p/s is higher than a critical value K^* or $\alpha > \alpha_{\max}$, the achievable specimen height can be predicted according to the following equation (4.8):

$$H_{\max} = 130.93 - 12.61D_p + 54.56p - 0.89\alpha + 45.64s + 0.068D_p \cdot \alpha - 0.62p \cdot \alpha - 0.488\alpha \cdot s + 0.254D_p^2 \quad (4.8)$$

On the contrary, safe configurations, which corresponds to slope angle lower than α_{max} or equal to α_{max} but characterized by a ratio $D_p/s < K^*$, can be manufactured up to maximum investigated depth ($H_{max} = 100\% \cdot D_0$). Due to the number of experiments carried out, it was not possible to fix an exact value for the K^* -factor. However, an uncertainty region, ($13 \leq K^* \leq 18$), divides safe and un-safe conditions.

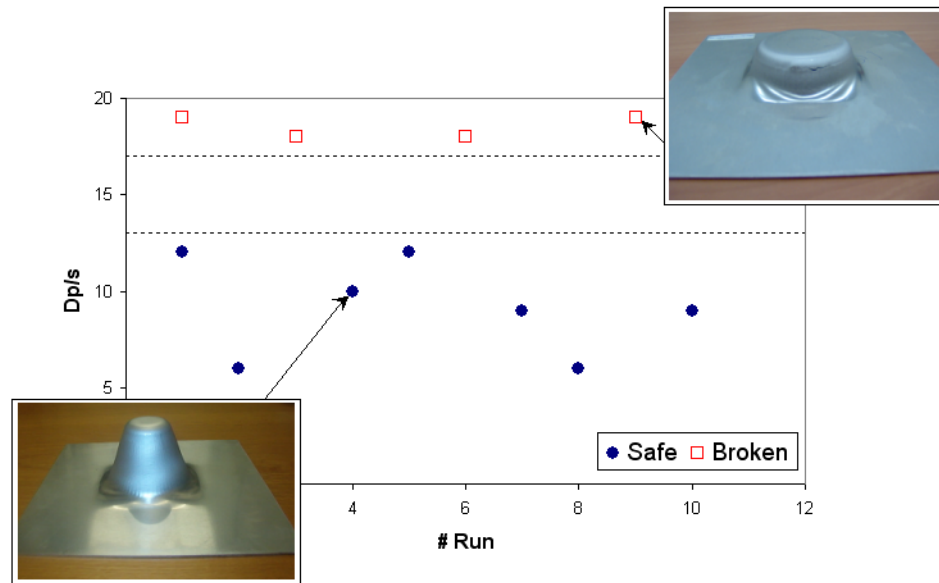


Figure 4.4: D_p/s values for experiments carried out for $\alpha = \alpha_{max}$.

Naturally, the model suitability was firstly statistically evaluated taking into account some performance indexes, such as the $R^2 = 98\%$, the $R^2_{corr} = 96\%$, the $R^2_{Pred} = 89\%$, rather than the Normal Probability Plot and the Prediction Capability Diagram (see Figure 4.5).

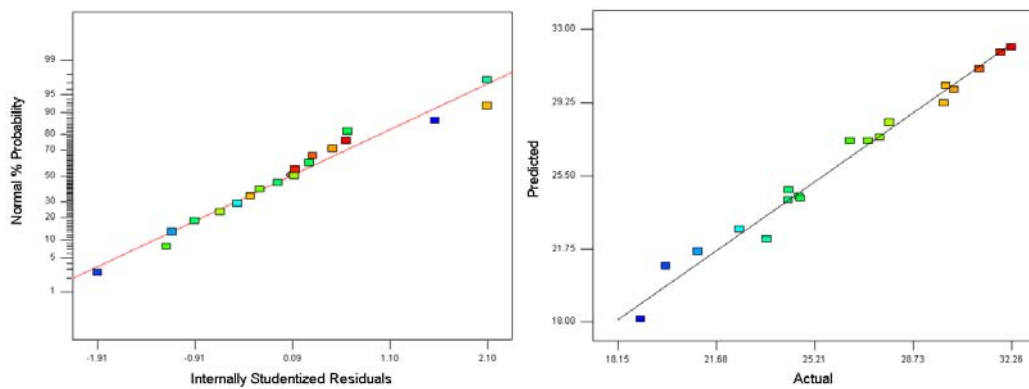


Figure 4.5. Normal Probability Plot and Prediction Capability for the investigated analysis .

4.3.3 Model validation

The analytical model was finally assessed executing tests characterized by three new parameters configurations. For sake of simplicity the geometry was always the same. Only critical conditions were considered during this phase ($\alpha \geq \alpha_{max}$) and, according to the model prediction, the experiments were properly designed to reach the material breaking condition or the fixed upper-bound ($H_{max} = 100\% \cdot D_0$). The analyzed cases and the comparison between the experimentally obtained depth and the predicted one are shown in the next Figure 4.6 and Table 4.3.

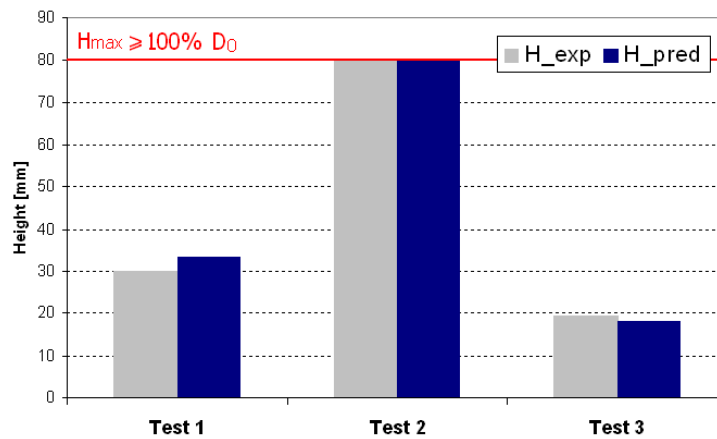


Figure 4.6: Comparison between the predicted height and the obtained one during the validation tests.

TABLE 4.3. Validation tests.

	D_p [mm]	p [mm]	α [°]	s [mm]	H_{exp} [mm]	H_{Pred} [mm]
Test 1	12	1	77	2	30	33.2
Test 2	15	0.5	70	1.5	80	80
Test 3	18	0.5	90	1.5	19.5	18.2

A suitable model behaviour was observed both in the prediction of safe conditions than in the unsafe ones, thus confirming the model capability to be used as design tool when slope angle, higher than the critical one for a specific material, has to be manufactured.

4.3.4 Concluding on single slope formability analysis

In this paragraphs, a simple model to relate the maximum component depth and the process parameters when the critical slope angle in incremental forming process is overcome was proposed and tested.

In particular, it supplies good results when single slope geometries are manufactured by Incremental Forming. However, it was stated that it is not correct to define a critical slope angle for given material and process parameters; on the contrary, there are some conditions in which a certain depth is obtainable even if the critical slope is overcome.

The applicability of this logic is very important in the practice because real parts are usually characterised by several slopes, but for a limited depth. Thus, it is possible to think that a robust design has to take into account the investigated phenomenon in order to allow the possibility to extend the process applicability also to geometries having punctual severe wall slopes.

Naturally, further investigations are required to definitively asses and complete the highlighted model. First of all, the variability due to a more complex geometry and the material influence have to be investigated and introduced into the analysis.

4.4 Double slope formability analysis

4.4.1 Deep geometries: formability analysis

It is a common opinion that SPIF process is strongly characterised by a localised deformation mechanics, which makes easier the material behaviour but at the same time determines a not uniform thickness distribution on the final product [AFG+05a], as highlighted in Figure 4.11. The process mechanics can be better understood looking simultaneously at the punch normal force and sheet thickness (Figure 4.12). It is well known that the SPIF process is characterised by a transient time which corresponds to the first loops executed by the punch movement.

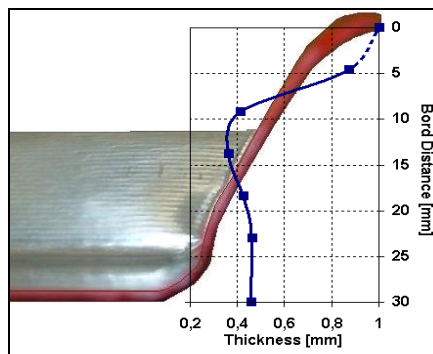


Figure 4.11: Thickness distribution along the transverse profile.

The typical distribution, measured for severe but not dangerous values of the wall inclination angle, shows a polynomial trend for the normal force and a corresponding decreasing thickness [FAM06] (Figure 4.12).

During the first loops, in fact, a more accentuate thinning occurs and, consequently, there is a reduction of the punch force. In addition the bending component plays a limited role in the complex deformation mechanics, since no rigid movements are easily allowed. Furthermore, due to the contact between the punch and the sheet, a certain removal of sheet material occurs, in particular for high α values. In this case, in fact, according to the imposed path, the punch works several times the same region, determining sheet wear. Although a lubricant is used and the punch rotates, friction and wear cannot be avoided, as demonstrated by the observation of some powder of the sheet material in the lubricant. Of course this phenomenon is exalted when low strength materials are formed. Commercially pure Aluminium Alloy, utilised for these tests, shows this kind of behaviour.

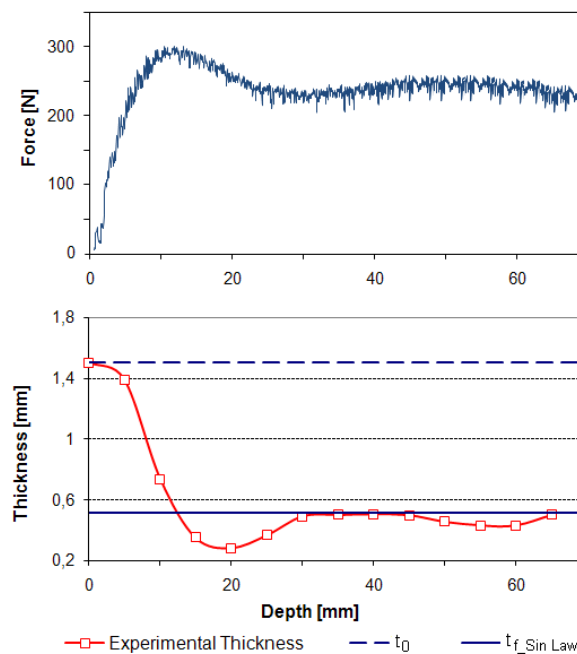


Figure 4.12: Normal Force and Thickness distribution along the transverse section
($D_p=12\text{mm}$, $p=0.5\text{mm}$, $\alpha=70^\circ$).

After this first stage, the process tends to become stationary and then the punch force reaches again a steady state value. Therefore process conditions are severe, but not enough to determine material failure. Since Incremental Forming is characterized by localized deformation, keeping constant the process parameters thinning remains a local effect, and the thin section does not influence material integrity during the process.

At the same time, while the force reaches the stationary condition soon, the thickness distribution approaches the one predicted by the well known Sine Law [KN99] only when manufacturing deep products.

All these considerations lead to conclude that only an analysis on deep geometry components allows to well asses the formability analysis and to completely determine the critical value for the slope angle. According to the last remarks, in fact, it is possible to state that the critical wall inclination angle is the larger base angle, that can be safely manufactured for deep geometry. On the contrary, when a “fleet” component has to be manufactured, slope angle higher than the critical one can be obtained without any problem [Fil06]. Therefore, to fully understand that, a combined study between part height and imposed wall inclination angle has to be executed.

To do that and to formalize the results in an analytical law, an experimental campaign was performed according to a proper statistical design of the experiments (DOE).

4.4.2 Consideration on the single slope prediction procedure

At the end of the single slope analysis, an analytical law able to predict the maximum product height for a frustum of cone geometry was derived and validated, thus obtaining a suitable control procedure to classify the process feasibility with respect to safe ($\alpha < \alpha_{max}$) and unsafe conditions ($\alpha \geq \alpha_{max}$). In particular, observing only those experiments which led to sound products, it is easy to understand that a strong influence is due to the tool diameter and the sheet thickness; more in detail, the material formability, in terms of achieved depth, is proportional to the tool diameter and inversely proportional to the sheet thickness, so that the ratio D_p/s was proposed to divide the safe and unsafe results for a slope angle equal to the critical one $\alpha_{max}=70^\circ$.

Concluding, the predictive procedure can be so synthesized:

$$\text{IF } [\alpha > \alpha_{max} \text{ OR } (\alpha = \alpha_{max} \text{ AND } D_p/s \geq K^*)]$$

THEN

$$H_{max} = 130.63 - 12.61D_p + 54.56p - 0.89\alpha + 45.64s + 0.068D_p \cdot \alpha - 0.62p \cdot \alpha - 0.488\alpha \cdot s + 0.254D_p^2 \quad (4.9)$$

$$\text{ELSE } H_{max} = 100\% \cdot D_0$$

where K^* is the threshold value between sound and broken component in critical conditions and D_0 is the initial major diameter. In the study, H_{\max} was chosen equal to D_0 .

Starting by these results a new experimental investigation was designed in order to enlarge the proposed approach and well asses the control procedure when more complex geometries have to be manufactured.

4.4.3 Experimental campaign

With the double aim to well asses the analytical model (4.9) applicability and to better understand as the formability limit changes varying the product shape, a more general experimental campaign was designed. It is quite obvious that introducing new degrees of freedom in the geometry the problem complexity increase. Actually, the analysis complexity increases since the maximum reachable height is not simply influenced by the process parameters or by the material properties. On the contrary, the transverse section changes or the partial slopes of the wall angle play a relevant role on the final results. With this perspective, the problem related to predict the maximum product depth could become NP-hard, since higher number of factors increase the problem dimension, thus increasing the solution time. To reduce the problem complexity, some factors were fixed and neglected from the analysis. To do that, firstly, it was decided to keep constant the process parameters during the whole experimental campaign; more in detail:

- Punch diameter (D_p) was fixed equal to 12 mm;
- Tool depth step (p) was fixed equal to 1 mm;
- Sheet thickness (s) equal to 1 mm was utilised.

Starting by these conditions, the same material was used again for the experiments, in order to manufacture a frustum of cone geometry characterised by a double curvature along the transverse section. According to the major base diameter (D_0), the maximum design height to reach (H_f) was fixed equal to 70 mm. Vice versa, two different slopes were imposed to the first $H_1=20$ mm and the last $H_2=50$ mm (Figure 4.13).

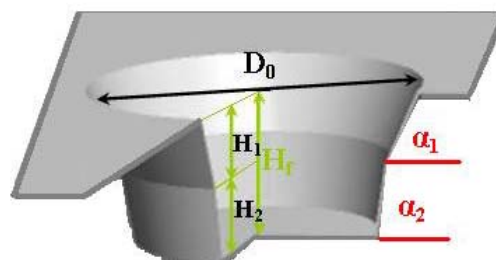


Figure 4.13: Sketch of geometrical parameters.

In order to well explore the problem both safe and unsafe wall inclination angle were taken into account for α_1 and α_2 values shown in the next table 4.4.

Table 4.4. Investigated wall inclination angles.

α_1	55°	60°	65°	70°	75°
α_2	60°	65°	70°	75°	80°

Actually, besides some factors were kept constant, the variability introduced by the combinations between the two imposed angles made the problem too much complex to be reduced. The DOE analysis and the Response Surface Methodology were again applied, by using an orthogonal plane, characterised by the full combination between the above specified factors, putting aside from certain safe and unsafe conditions. Each test was repeated three times in order to obtain a higher robustness. The chosen range for the slope angles was enlarged with the aim to fully understand how process mechanics evolves, and if it is really possible to consider only the portion of material which locally undergoes to plastic deformation.

In figure 4.14, an experimental results is proposed to show a sound component at the imposed maximum depth.

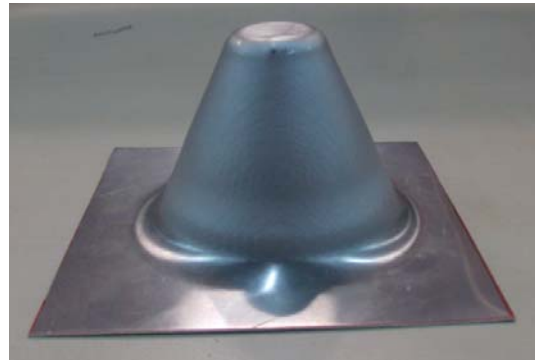


Figure 4.14: Sound component obtained with $\alpha_1=65^\circ$ and $\alpha_2=70^\circ$.

First of all, the comparison between the experimental results, in terms of final height, and the same predicted by using the specified algorithm (2) was executed. Actually, the experimental campaign highlighted that increasing the shape complexity the equation (2) loses consistency. Anyway, this is not novelty, since it was derived for single slope angle.

By examining the results it can be easily observed that the final depth of the second part of the geometry H_{2_exp} resulted always lower than the one predicted for a single slope manufacturing.

Thus, the former loops play a significant role on the second ones in spite of the particular process mechanics.

To better justify the influence of the first step (H_1), the ANOVA method was applied to the set of data experimentally obtained by double slope components. To do that, the influence of the slope angles α_1 and α_2 was considered such main factor on the response final height, H_f .

Furthermore, the final thickness of the workpiece at the end of the step 1 (after depth H_1) was introduced, as additional factor, in the analysis. Concluding, the experiments were separately treated according to Equations (4.10) and (4.11):

$$H_f = f(\alpha_1, \alpha_2) \quad (4.10)$$

$$H_f = f(\alpha_1, t_1, \alpha_2) \quad (4.11)$$

Naturally, for sake of clearness, both the experimental conditions were assessed and finally compared with respect to some statistical performance indexes. All the ANOVA results are in the next tables.

Table 4.5. Outputs for model highlighted in equation (4.10).

Factors	p-value	Significance
α_1	< 0.0001	High
α_2	0.0046	Medium
$\alpha_1 \cdot \alpha_2$	0.7846	No
α_1^2	0.0007	High
α_2^2	0.8112	No
R-squared		0.93
Adj R-squared		0.91
Pred R-squared		0.87
Adeq precision		21.99

Table 4.6. Outputs for model highlighted in equation (4.11).

Factors	p-value	Significance
α_1	< 0.0001	High
t_1	< 0.0001	High

α_2	< 0.0001	High
$\alpha_1 \cdot t_1$	0.0002	High
$\alpha_1 \cdot \alpha_2$	0.0542	Low
$\alpha_2 \cdot t_1$	0.0493	Low
R-squared		0.98
Adj R-squared		0.97
Pred R-squared		0.95
Adeq precision		32.58

As it can be easily derived, a simplified quadratic function and a second order factorial one can justify the response factor H_f according to the Equation (4.10) and (4.11). Both the analysis led to the same results, in terms of significant effects and performance indexes; in fact, the Predicted R-Squared are, in agreement with the Adjusted R-Squared from a quantitative point of view. At the same time, the index Adequate Precision measures the signal to noise ratio. A ratio greater than 4 is suitable, and the numerical results indicates an adequate signal. Anyway, the addition of the partial sheet thickness to the considered factors improves the quality of the analysis, for this reason it could be preferred the model proposed in equation (4.11) to better explore the space of the solutions.

However, rather than the analytical result, synthesised by means of a simplified factorial equation, it was considered more interesting to focalise the attention on the robustness of the analysis and on the perspective that a relevant role on the final height H_f is firstly played by the wall inclination angle imposed during the former part and the local sheet thickness, predicted by using the sine law.

Starting by this assumption, the previous procedure (4.9) was redefined taking into account the first deformed part and testing a new algorithm able to consider the material characteristics change. Such as already specified, from a formability point of view, two opposite phenomena determine the output of a SPIF operation: work hardening and stretching. While the former can improve the results, increasing the blank strength, the effect of sheet thinning strongly penalises the product integrity. For these reasons, in order to optimise and generalise the applicability of equation (4.9), it is necessary to introduce a reduction coefficient to reduce the limiting specimen depth obtained for single and independent slope. More in detail, it is close to the reduction in thickness at the end of the first part of the geometry, according to the sine law . Taking into account only α_1 angle values closer to the

critical one, Figure 4.15 shows the predicted depth, corrected or not, together to the experimental values.

For sake of clearness, it is necessary to specify the meaning for each terms:

$$H_{2_exp} = H_f - H_1 \quad (4.12)$$

$$H_{2_Pred} = \{\text{equation (4.9) applied directly to the second part of the geometry}\} \quad (4.13)$$

$$H_{2_Pred_Corr} = H_{2_Pred} \cdot K \quad (4.14)$$

being

$$K \cong \begin{cases} 1 & \alpha_1 \leq \alpha_2 \leq \alpha_{max} \text{ or} \\ & (\alpha_1 > \alpha_{max} \text{ and } \alpha_2 < \alpha_{max}) \\ \sin(\frac{\pi}{2} - \alpha_1) & elsewhere \end{cases} \quad (4.15)$$

Naturally, the mean value for H_{2_exp} was firstly calculated from all the repetitions. As it can be easily recognised, a good overlapping between the experimental height H_{2_exp} and the analytical prediction $H_{2_Pred_Corr}$, corrected multiplying by the round value local thickness t_1 , was obtained.

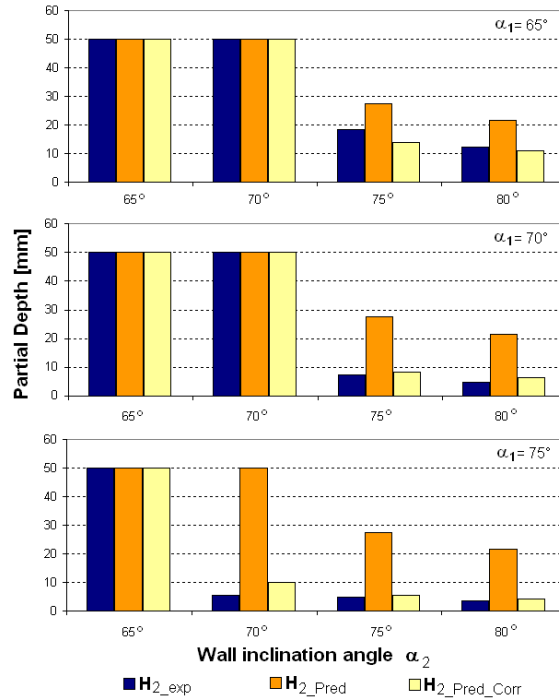


Figure 4.15: Comparison between experimental and analytical results.

This assumption, according to the empirical study of the phenomena, allows to perform a new algorithm, preliminarily derived for simple slope and deep component and now generalised on double slopes.

4.4.4 Numerical analysis

Model design

Despite it is a common opinion among the researchers that experimental approach usually supplies more robust data as compared to numerical simulation, nowadays remarkable improvements were introduced in the FE analysis thus dramatically enhancing its suitability. In the research here addressed, the code Dynaform® was used as simulation tool. It implements the dynamic equilibrium equations and results very efficient, also for the use of a smart remeshing criterion, based on the strain controlled shell element subdividing. The simulation is conditionally stable because the imposed high speed of the punch may induce dumping phenomena. For this reason a check on the total kinetic energy was done, verifying that the imposed quota is less than the 10% of the total plastic energy, so that the dynamic effect in the simulation is negligible. The material behaviour has been supplied by a proper power law while the tool has been modelled as rigid surface.

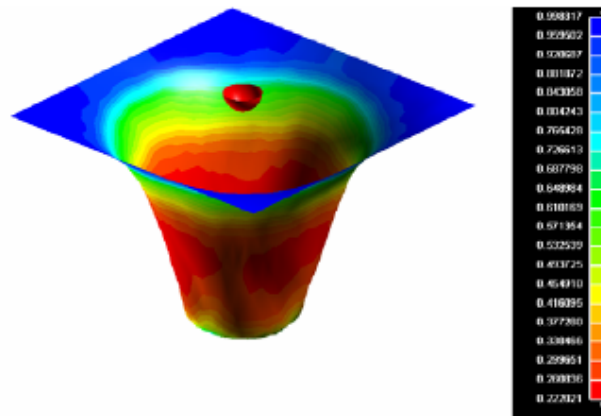


Figure 4.7: Thickness distribution with $\alpha_1=65^\circ$ and $\alpha_2=70^\circ$

Thinning analysis

At the end of the numerical simulations, each test was compared with the experimental one. The comparisons of both numerical and experimental measures are shown respectively for $\alpha_1= [65^\circ-70^\circ-75^\circ]$ in the next figures 4.8, 4.9 and 4.10. As it can be observed, a good matching was determined for the whole campaign; from a quantitative point of view, in fact, the maximum error is of the tenth of millimeters.

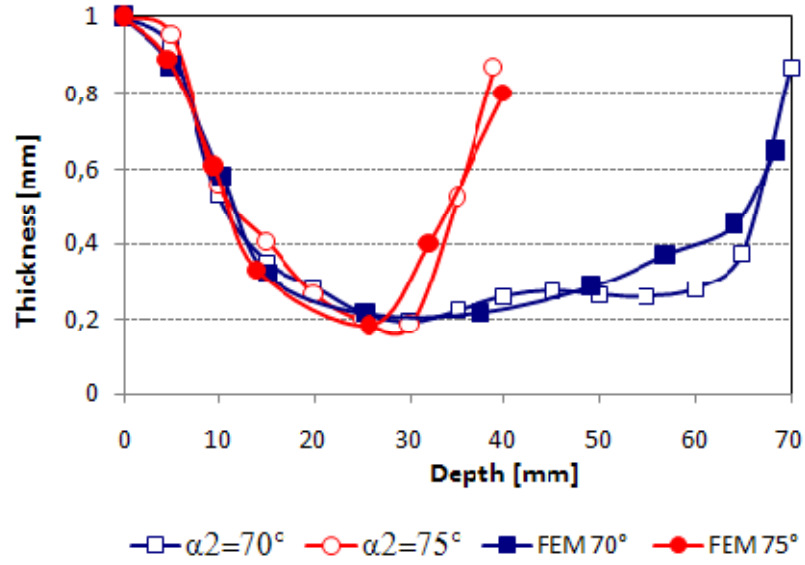


Figure 4.8: Experimental-Numerical comparisons for $\alpha_1=65^\circ$.

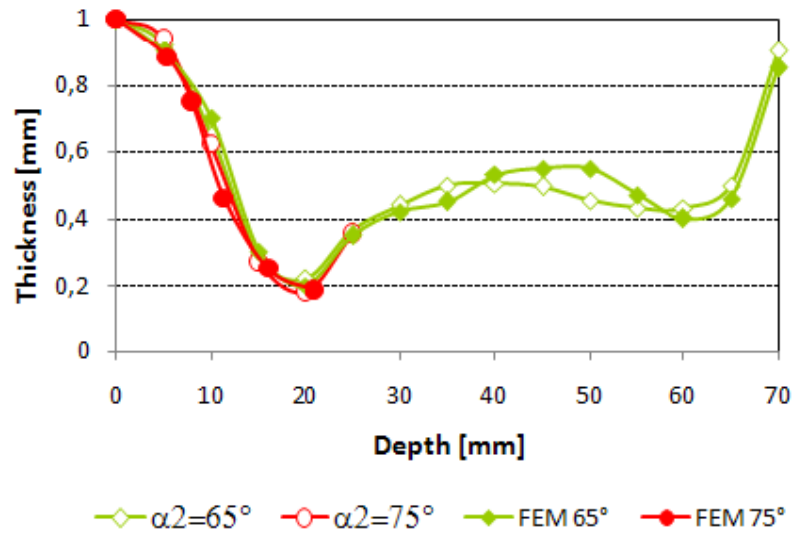


Figure 4.9: Experimental-Numerical comparisons for $\alpha_1=70^\circ$.

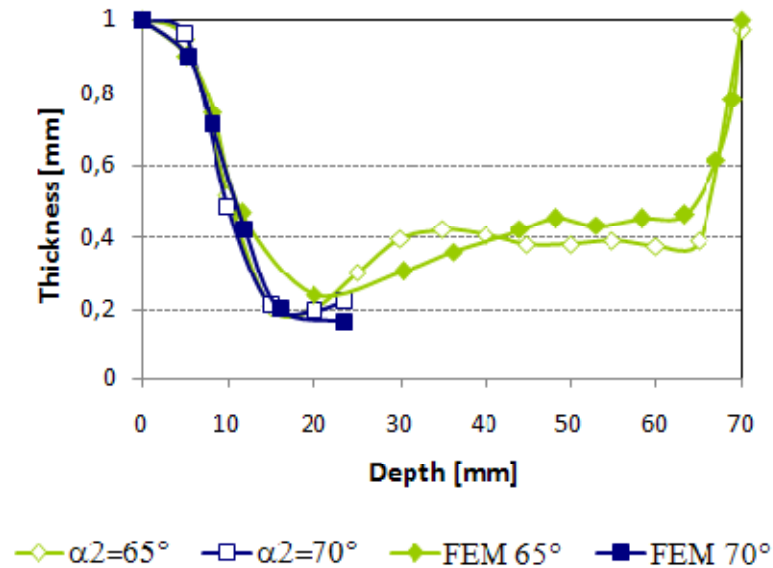


Figure 4.10: Experimental-Numerical comparison for $\alpha_1=75^\circ$.

These results confirm the suitability of the FE simulation to predict material thinning even in IF processes. In this case, for instance, this constitutes an interesting result since, as observed in the previous figures, breaking occurs when thickness reaches more or less the value of 0.20 mm.

Concluding on numerical simulation of double slope

An effective design tool in AISF of multi-slopes shapes was set-up permitting to assess some interesting conclusions:

- despite the process mechanics in AISF is strongly localised, the product feasibility is not simply related to the process conditions and material properties but the sheet behaviour is directly influenced by the 3D profile;
- a suitable numerical model represents a good trade-off between CPU times and results reliability.

Starting from these assumptions, even if the model was validated on double-slope specimens, the approach can be easily extended to monitoring and control multi-slopes shapes.

4.4.5 Concluding on double slope formability analysis

Nevertheless SPIF is strongly characterised by a localised process mechanics, the common idea that only what happens in the forming zone determines material formability limit is not

completely true for complex and varying geometry. In fact, having a look at Figure 4.15, it is clear that formability is influenced by the history of material deformation.

Thus, a pragmatic way to operate is the extension of the available knowledge for single slope processes introducing a penalty coefficient which reduces the estimated depth proportionally to the previous calculated thinning.

On the other hand, it is clear that further researchers have to be focused on this matter in order to get a wider knowledge about material damage in Incremental Forming of sheet metal.

This topic, together to dimensional accuracy, will constitute the challenge of the next years in this field.

4.5 Multi slope formability analysis

4.5.1 Multislope IF process

It is a common opinion that the incremental sheet forming process mechanics is not yet well understood. In fact, it is known that formability is very high as compared to traditional stamping processes but it is not well explained why [FAM06, BTH07].

What is more, many researches agree on the localization of deformation which limits the analysis just at the forming zone. On the other hand, some experimental tests show that material seems to have memory of the forming history up to the current zone.

Thus, research in this field can be subdivided into two categories: the former tries to explain what happens in the material starting from a microscale point of view; the latter classifies the results adopting a macroscale approach, building reliable tools which link the process performance to the input set. This investigation belongs to this second way.

In that approach, it is important to generate cases which reproduce the reality in order to obtain reliable data for the modelling step.

In Incremental Forming it is known that the punch describes a trajectory which is always tangential to the CAD surface of the workpiece. These surfaces are conceptually absolutely general and some limitations introduced by the researcher are sometimes too strong.

In the present work this constraint was relaxed as possible designing a very “flexible” shape, characterised by three slopes with three different heights (Figure 4.16).

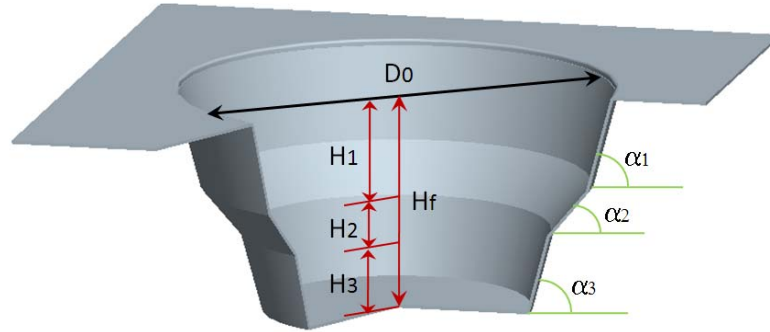


Figure 4.16: The investigated multislope shape.

Of course, a surface presents curve profiles but, locally, more slopes can be a good approximation. In fact, in IF the section is always reproduced by a sequence of linear slopes due to the distance vector between two different spires.

On the other hand, for the chosen geometries a number of slopes equal to three is enough to characterise and determine the material behaviour in the investigated process.

At the same time, to make the analysis more robust, additional effects were considered. First of all, in order to take into account all the deformation paths, two different geometries were investigated, namely a frustum of cone and a frustum of pyramid. The former, in fact, is characterised by a homogeneous profile along the planar section which results roughly in an uni-axial strain while the second is characterised by points of discontinuity in the corner. The latter induce a deformation tensor close to a biaxial one. In this way it is possible to include the different deformation paths that occur in the incremental sheet forming process.

Finally, the main process parameters were included as input factors. According to literature, the tool diameter, the step size and the sheet thickness were considered to make the analysis complete and consistent from a mechanical point of view.

A number of ten factors were included in the analysis and the number of experiments was reduced through a careful application of a proper statistical approach for the design of the experiments.

4.5.2 Experimental campaign

As explained in the previous section, a set of tests was designed aimed at manufacturing cones and pyramids in AA1050-O sheet.

In this study, ten 2-level factors were considered as reported in table 4.7.

Table 4.7. Investigated factors and their levels.

<i>Factors</i>			<i>Low (-1)</i>	<i>High (1)</i>
<i>A</i>	1° slope angle	α_1	65°	75°
<i>B</i>	2° slope angle	α_2	65°	75°
<i>C</i>	3° slope angle	α_3	65°	75°
<i>D</i>	1° height	H_1	20mm	30mm
<i>E</i>	2° height	H_2	15mm	25mm
<i>F</i>	3° height	H_3	15mm	25mm
<i>G</i>	Sheet thickness	s	1mm	2mm
<i>H</i>	Geometry	G	<i>Cone</i>	<i>Pyramid</i>
<i>J</i>	Tool Diameter	D_p	12mm	18mm
<i>K</i>	Tool depth step	p	0.3mm	1mm

The twelve experiments fixed by the experimental plan, a Plackett-Burman (PB) design shown in coded levels in Table 4.8, were executed by using a proper clamping equipment mounted on a CNC milling machine, working on 240x240mm² aluminum sheets (Figure 4.17).

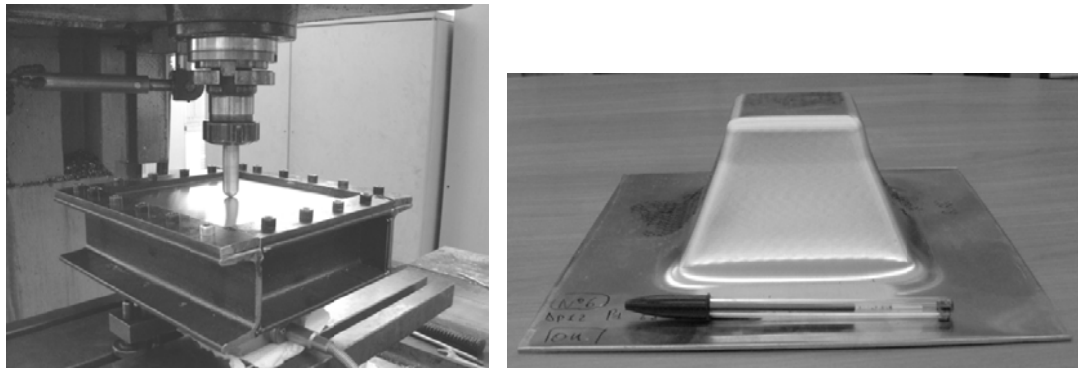


Figure 4.17: Experimental equipment and component.

As response variable, the percent ratio between the actual specimen height and the designed one was utilized. Table 4.8 reports such a response for each test. For sake of clearness, Figure 4.18 displays the comparison between expected final height (H_f) and measured one (H_{exp}). As it can be observed, the results are well distributed between safe and unsafe ones, thus ensuring the robustness and reliability of the analysis.

Table 4.8. The 12-run Plackett-Burman design for factors *A-K*, and the responses obtained.

Run	<i>A</i>	<i>B</i>	<i>C</i>	<i>D</i>	<i>E</i>	<i>F</i>	<i>G</i>	<i>H</i>	<i>J</i>	<i>K</i>	Responses
1	1	-1	1	-1	-1	-1	1	1	1	-1	88
2	1	1	-1	1	-1	-1	-1	1	1	1	43.33
3	-1	1	1	-1	1	-1	-1	-1	1	1	61.67
4	1	-1	1	1	-1	1	-1	-1	-1	1	29.71
5	1	1	-1	1	1	-1	1	-1	-1	-1	40.29
6	1	1	1	-1	1	1	-1	1	-1	-1	26.43
7	-1	1	1	1	-1	1	1	-1	1	-1	100
8	-1	-1	1	1	1	-1	1	1	-1	1	100
9	-1	-1	-1	1	1	1	-1	1	1	-1	100
10	1	-1	-1	-1	1	1	1	-1	1	1	100
11	-1	1	-1	-1	-1	1	1	1	-1	1	60.83
12	-1	-1	-1	-1	-1	-1	-1	-1	-1	-1	100

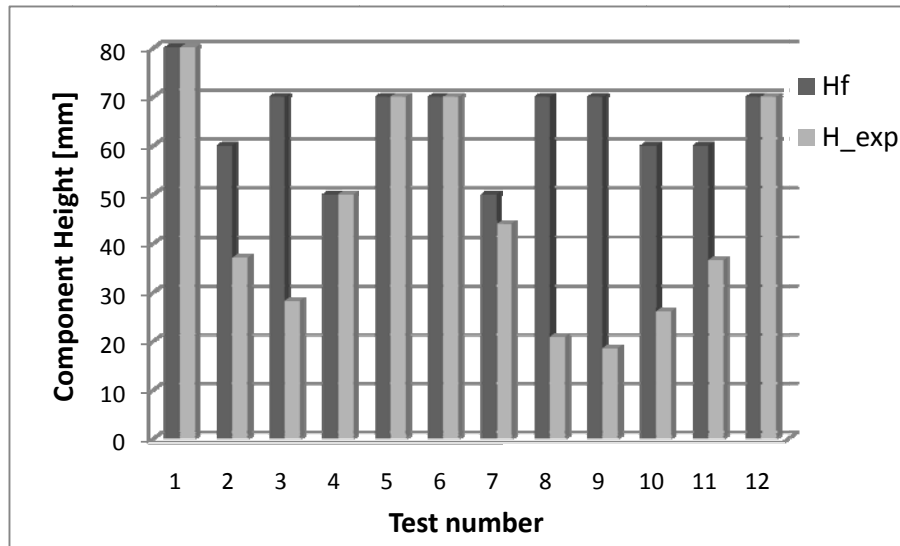


Figure 4.18: Comparison between expected final height (H_f) and measured one (H_{exp}). Test are reported in their actual order (randomized).

To ensure the same conditions during the whole experimental campaign, the blank was supported by a backing plate; more in detail, both circular and square backing plates, with side L_0 and diameter D_0 of 140 mm, were used to manufacture cones and pyramids

respectively. The initial outer diameter or base was fixed taking into account the tool geometry and keeping constant the distance between the backing plate and the first coil of the trajectory.

Naturally, considering the two levels imposed by the experimental plan, the lowest and the highest value for each factor were properly chosen: as regarding the tool diameter, for instance, 12 mm and 18 mm tool dimension were used; at the same time, the incremental step size was varied between 0.3 and 1mm.

According to the material formability limit, which individuates in about 70° the critical wall inclination angle for an AA1050-O aluminum alloy, the low and the high values of this factor were respectively fixed equal to 65° and 75° . Previous researches, carried out on the single slope (see section 4.3) highlighted that slope angles lower than the critical one can be safely manufactured to obtain very deep geometries; on the contrary, increasing the wall inclination angle the formability decreases, allowing only a limited component depth.

As regarding the partial height of each slice, they varied between 15 and 25 mm: the above specified range represents the suitable tradeoff between the achievement of stationary conditions and the test quickness. On the contrary, the first slice was oversized of 10 mm in order to reduce the transient effect due to the sheet bending during the first coils.

4.5.3 Statistical analysis

The 12-run PB design, used in this study to accommodate the 10 factors identified as potentially important (Table 4.8), is a popular screening design which allows to study up to 11 factors in just 12 runs. It belongs to the class of PB designs developed by Plackett and Burman [PB46], in which the number of runs is a multiple of 4. Due to their complex aliasing patterns, analysis of such designs has traditionally been limited to main effects only, assuming that interactions among factors are negligible. By adopting this approach, however, important interactions may go unidentified in real analyses; in such cases, misleading results will be obtained from the design.

This led several authors to perform specialized methods that allow to consider the interactions in addition to the main effects. One of such methods, proposed by Box and Meyer [BM93, BHH05], was used to analyze the data in Table 4.8. Box-Meyer method aims at discovering the active factors, that is those which significantly affect the response through their main effects and/or interactions. It considers all the possible subsets of active factors, each subset stating a particular combination of factors as active. Posterior probabilities are

thus calculated for each of these subsets, and finally (marginal) posterior probabilities are obtained for each factor [BM93]. These marginal probabilities are used to summarize the activity of the factors.

In implementing the method, the maximum order of interactions to be entertained has to be chosen; in the special case in which interactions are neglected, main effects are only taken into account as conventional methods. For the PB design in Table 4.8, analysis with up to three-factor interactions was run. The marginal posterior probabilities for factors A - K are reported in Figure 4.19; the computations were carried out using the BsMD package for R language [Bar06]. Factors A , B and D (α_1 , α_2 and H_1) clearly stand out as active, while the remaining factors turn out to be unimportant. This implies that factors α_1 , α_2 and H_1 are those involved in significant main effects and/or interactions, but the analysis cannot reveal which main effects and/or interactions are significant.

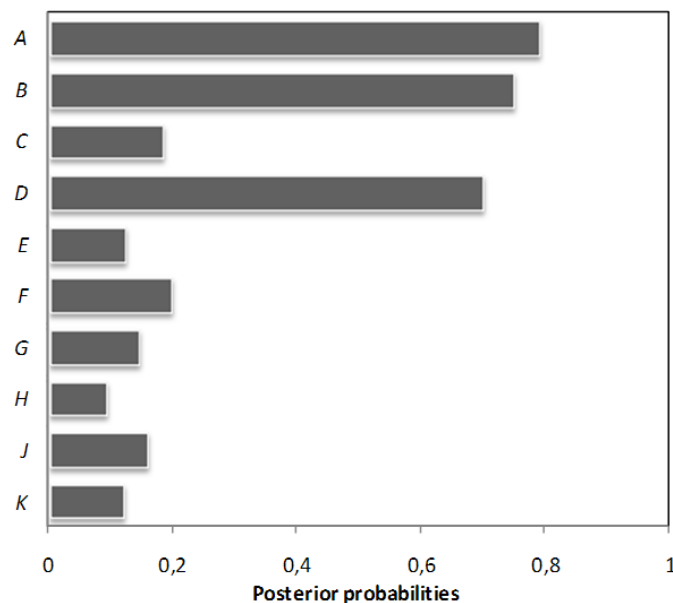


Figure 4.19: Marginal posterior probabilities for factors A - K , Box-Meyer analysis.

To do this, further model-fitting procedures or additional experiments are generally required. In this case, however, we can take advantage of a remarkable *projectivity* property of the 12-run PB design [BHH05]. In fact, this design is of *projectivity* 3, which implies that a full 2^3 design in the identified active factors A , B and D is produced; moreover, 4 out of the 8 runs are replicated twice. Such projected design allows to perform a standard factorial analysis for factors A , B and D ; in addition, duplicated runs may be used to estimate the standard error of each effect to give a more reliable analysis. The projected design, arranged

in standard order, is shown in Table 4.9 together with the corresponding data. A normal plot of effects is displayed in Figure 4.20, giving indication that the main effect of factor *D* and the *AB* interaction are negligible, while all the other effects are significantly different from 0, including the three-factor interaction.

Analysis of the projected design supplemented Box-Meyer screening analysis of the PB design. In particular it gave opportunity to perform a detailed study of the effects for the 3 factors previously emerged as active. It is worthwhile noting that factor *D* was judged active because it is involved in significant two-factor and three-factor interactions with the other two active factors, but its main effect is negligible. If the 12-run PB design were analyzed via conventional methods which discard interactions, factor *D* (H_1) would be missed.

Table 4.9. The projected 2^3 design (in standard order) and the data for factors *A, B, D*.

Run	A	B	D	Responses	
1	-1	-1	-1	100	
2	1	-1	-1	100	88
3	-1	1	-1	61,67	60,83
4	1	1	-1	26,43	
5	-1	-1	1	100	100
6	1	-1	1	29,71	
7	-1	1	1	100	
8	1	1	1	40,29	43,33

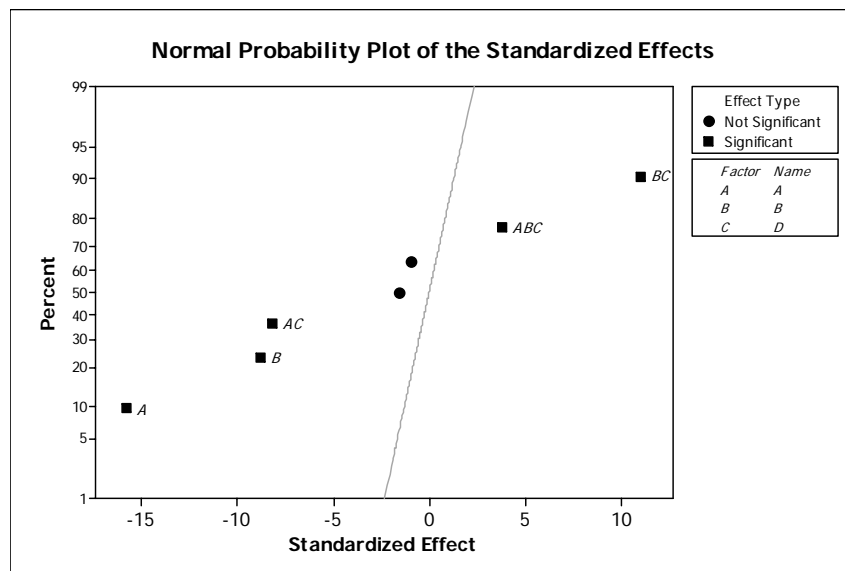


Figure 4.20: Normal plot of effects, projected 2^3 design in factors *A, B, D*.

4.5.4 Conclusions on multislope analysis

The potential of the 12-run PB design was used for investigating the 10 factors included in the experiment. At the screening stage, Box-Meyer analysis method pointed to factors α_1 , α_2 and H_1 as important factors to be considered in subsequent analyses. Such conclusion allows for the possibility that the identified active factors are involved in influential interactions. Indeed, the analysis of the projected full factorial design in these active factors revealed that interactions are important in explaining the data, including the three-factor interaction. Any traditional analysis would fail to uncover these significant interactions, giving misleading results because of the complicated alias structure inherent in PB designs such as that utilized in this investigation.

This could represent a suitable way to be pursued in order to well asses the IF processes for which the cost of the tests is sometimes very high. In fact, the screening of a large number of process variables can be executed with little resources, orienting the researchers toward the investigation of the most influential parameters.

4.6 Thinning analysis in AISF processes

4.6.1 AISF process evidences

In general, Incremental Sheet Forming may be described as a simple process in which a rotating hemispherical punch moves along a properly designed trajectory and deforms a clamped sheet [PK03, YY03, JMH+05]. Being the sheet fully clamped on the periphery, the deformation mechanics is basically stretching, i.e. it causes a corresponding thickness reduction according to material incompressibility.

Actually, the Sine Law may supply only a rough and average approximation [KN99], since it largely fails at least in two regions, as highlighted by some researchers [SMS+99]. In particular, thickness values larger than the ones calculated by the Sine Law occur in the zones of the blank close to the clamping area which are not interested by the punch action and are free to bend. On the contrary, lower thickness values arise in the plastically deformed zone, where the material results strongly stretched (Figure 4.21).

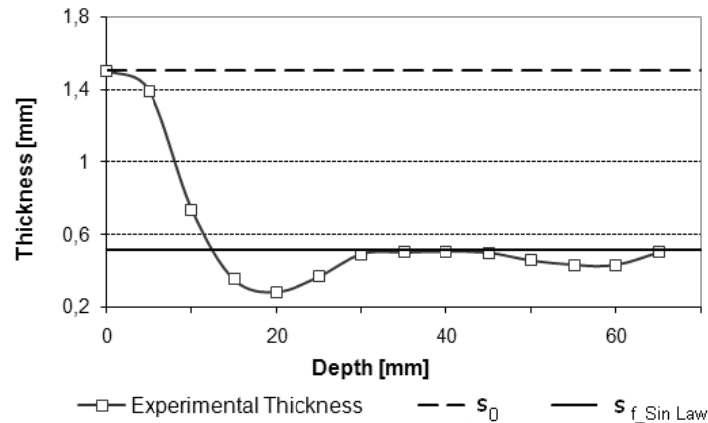


Figure 4.21: Typical thickness distribution in AISF process

Contemporary, the sine law takes into account only the influence of two process parameters, while it is well known that other factors strongly influence the process performances.

According to the above considerations, it is easy to understand that incremental forming process design strongly requires a more efficient modeling tool to predict thinning occurrence during the process. To pursue this aim, a simple trial and error approach could result time consuming and not very effective; on the contrary, a robust design of the experiments is required.

In the following investigation the RSM has been implemented, starting by the application of a Central Composite Design (CCD) face centered hyper-space.

In particular, being n the number of factors each one characterised by k levels, the traditional fully orthogonal plane (that corresponds to k^n experiments), can be reduced in $k^{(n-1)}$ tests only. Naturally, the ANOVA analysis, the Normal Probability Plot and others performance indexes complete the RSM, allowing to evaluate the experimental data robustness and the prediction model reliability.

4.6.2 Experimental campaign

Starting from the available base of knowledge on the considered process [JMH+05, KP03, KN99, AFF+03], a set of experiments was properly designed and executed in order to deeply analyze the role played by the process parameters correlation with respect to the thickness distribution.

According to some investigations on the utilized material [AFF+03], namely an Aluminum Alloy 1050–O, the tests were carried out varying those process parameters which directly affect formability, such as the tool diameter (D_p), the tool depth step (p), the wall inclination angle (α) and, finally, the sheet thickness (s). Other variables, like the tool speed rotation or the tool feed rate, were kept constant to reduce the problem complexity and because they have not a major influence on material formability [AFF+03]. The tool path on a plane is a closed loop which usually consists of straight lines, smooth curves and corners. In order to measure the thickness distribution, a homogeneous profile was preferred and in particular a frustum of cone was chosen as specimen shape for the experimental campaign. The major base diameter (D_0) and the final height (H_f) were fixed equal to 90 mm and 60 mm respectively. Naturally, each test was executed up to the failure occurrence or, vice versa, up to the desired depth.

The experiments were executed on a Mazak Nexus milling machine centre, equipped with a clamping device and a baking plate to ensure the sheet locking. An emulsion of mineral oil was utilized to lubricate the interface between the punch and the sheet.

As introduced in the previous chapter, the experiments were analyzed following the Response Surface Methodology. Each experiment was firstly designed as belonging to a CCD face centered hyper-space in order to reduce the number of tests (Figure 4.22). In particular, taking into account four factors and three levels for each one, 27 tests were performed.

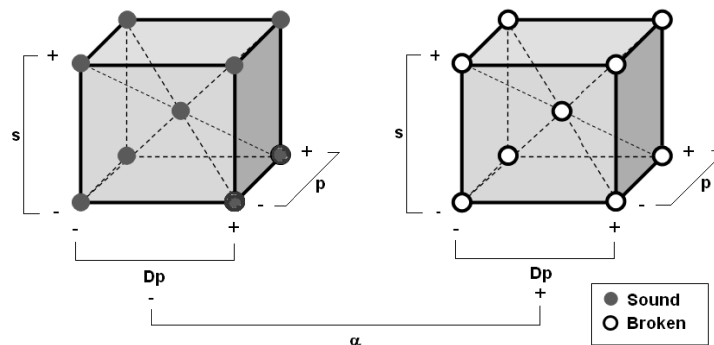


Figure 4.22 The investigated experimental plane

Furthermore, as concern the response variable, it was derived by the measure of the minimum thickness. In Table 4.10 the lowest and the highest values for the investigated range are displayed. According to the formability limit of the utilized material, the wall

inclination angle was varied in the range of [65° - 75°], keeping the critical value for the investigated material, i.e. 70°, as the central point. Naturally, the thickness distribution was evaluated varying the process parameters both in stationary condition and in failure one.

Before invoking the statistical analysis, some conclusions can be derived by a qualitative observation of the measured thickness distribution for changing process conditions. First of all, the main influence seemed to be played by the initial value of the thickness (Figure 4.23) and the wall inclination angle (Figure 4.24) in agreement with the Sine Law [KN99]. In fact, varying one of those factors, both the output of the process (in terms of sound or broken component) and the minimum thickness reached change too.

Table 4.10. Extreme Value of the Experimental Plane.

Parameters	Lowest Value	Highest Value
Sheet Thickness (s)	1mm	2mm
Wall Inclination Angle (α)	65°	75°
Tool Diameter (D_p)	12mm	18mm
Tool Depth Step (p)	0.3mm	1mm

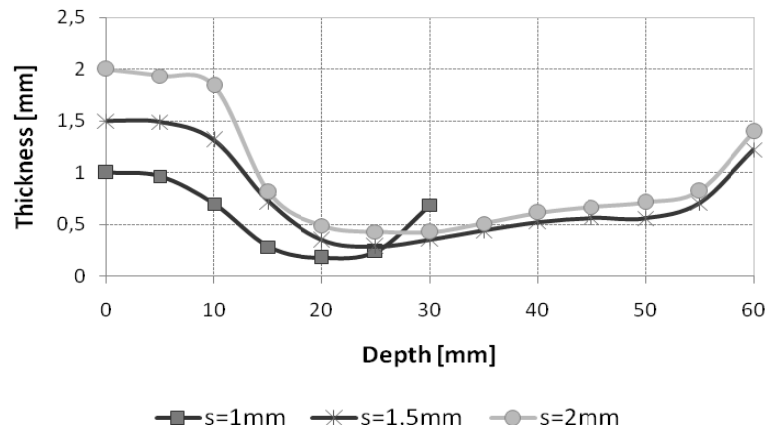


Figure 4.23: Thickness distribution at the varying of the initial sheet thickness ($\alpha=70^\circ$, $D_p=15\text{mm}$, $p=0.65\text{mm}$)

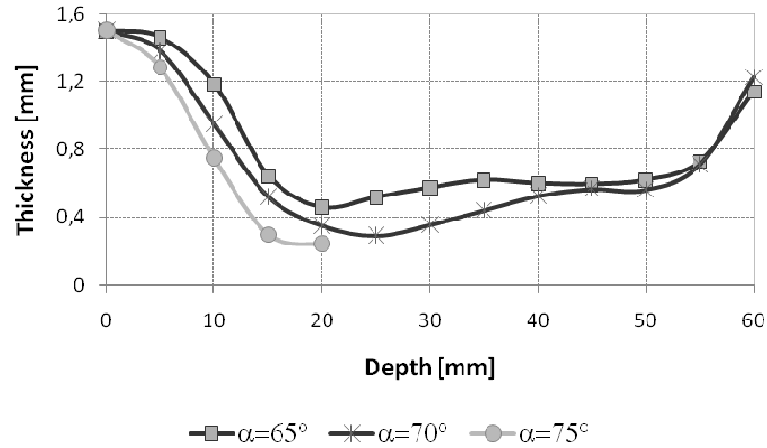


Figure 4.24: Thickness distribution at the varying of the wall inclination angle ($s=1.5\text{mm}$, $D_p=15\text{mm}$, $p=0.65\text{mm}$)

In particular, reducing the initial thickness or increasing the wall slope angle the minimum thickness measured decreases, moving close to the instability process condition.

On the other hand, none conclusion can be derived by a qualitative observation of the thickness trends at the varying of the other two process parameters (Figures 4.25 and 4.26), neither about any possible correlation among them. On the contrary, a proper application of RSM could help to skip this lack of knowledge.

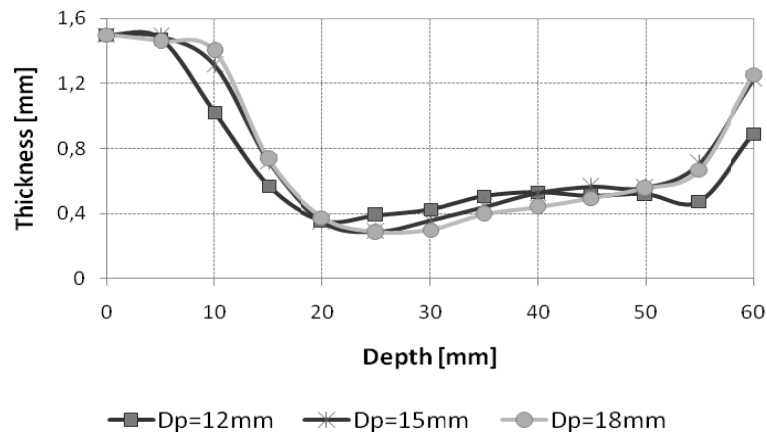


Figure 4.25: Thickness distribution at the varying of the tool diameter ($s=1.5\text{mm}$, $\alpha=70^\circ$, $p=0.65\text{mm}$)

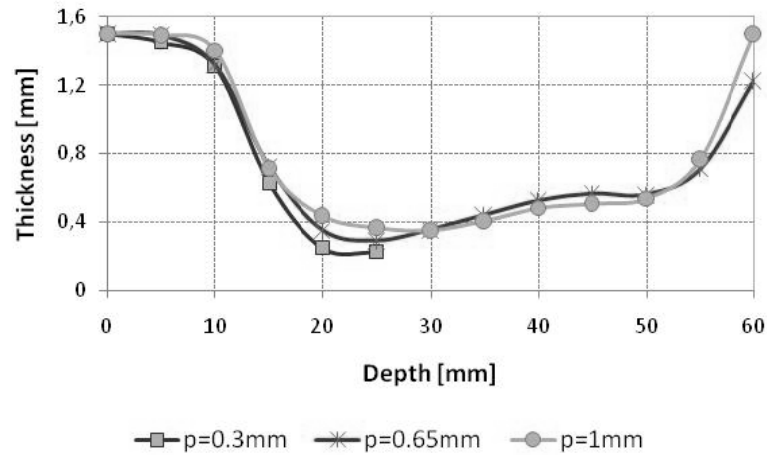


Figure 4.26: Thickness distribution at the varying of the tool depth step ($s=1.5\text{mm}$, $\alpha=70^\circ$, $D_p=15\text{mm}$)

4.6.3 Statistical analysis of the results

From a statistical analysis point of view, the attention was focalized on a single value supplied by the minimum thickness rather than on the whole distribution. In this way, the 27 tests, represented by a proper combination of the pattern (s, α, D_p, p) were analysed by means of the ANOVA in order to determine the better function f which fully explains the relationship between input and output as follows:

$$s_{min} = f(s, \alpha, D_p, p) \quad (4.16)$$

Starting by the ANOVA analysis and the Lack of Fit tests, which allows to determine the function f that ensures the smallest lack-of-fit in the prediction of the output variable, the quadratic model resulted the best way to explain the experimental results (see Table 4.11).

Table 4.11. Model definition.

Source	p-value	R^2	R^2_{corr}	R^2_{pred}	PRESS	Result
Linear	< 0.0001	0.81	0.78	0.69	0.21	
Factorial	0.0002	0.92	0.88	0.74	0.18	
Quadratic	0.0072	0.99	0.97	0.93	0.05	<i>Suggested</i>
Cubic	0.0360	0.99	0.99	0.67	0.23	<i>Aliased</i>

According to that, the experimental data were subsequently analyzed in order to highlight the effects of the single independent factors and their interactions on the dependent one (see Table 4.12).

Table 4.12. ANOVA results.

Factors	p-value	Influence on s_{min}
s	< 0.0001	High
α	< 0.0001	High
D_p	< 0.0001	High
p	0.0003	High
s^2	0.5360	No
α^2	0.0005	High
D_p^2	0.0229	Low
p^2	0.5360	No
αs	0.0001	High
$D_p * s$	0.0121	Medium
$p * s$	0.7719	No
$\alpha * D_p$	0.0812	Low
$\alpha * p$	0.9229	No
$D_p * p$	0.9229	No

As it can be easily observed, the first order factors are the most significant to influence the process heaviness, according with the state of the art in matter of formability [KP03, KN99, AFF+03]. At the same time, the second order wall angle and the interaction between this one and the initial value of the thickness result highly significant, as suggested by the Sine Law in a simplest way [KN99]. On the other hand, the interaction between the tool diameter and the initial sheet thickness or the wall angle such as its second order factor are partially significant to influence the output value.

Neglecting the not significant factors, it is possible to simplify the quadratic model to describe the investigated phenomenon. The analytical result of the analysis is reported in the next equation (4.17):

$$s_{min} = 10.63 - 0.15 D_p + 0.081 p + 2.24 s - 0.29 \alpha - 0.012 D_p \cdot s + 7.92 \cdot 10^{-4} D_p \cdot \alpha - 0.026 s \cdot \alpha + 3.51 \cdot 10^{-3} D_p^2 + 2.06 \cdot 10^{-3} \alpha^2 \quad (4.17)$$

The model suitability was statistically evaluated taking into account some performance indexes, such as the $R^2=98\%$, the $R^2_{\text{corr}}= 97\%$, the $R^2_{\text{Pred}}= 96\%$, rather than the Normal Probability Plot (Figure 4.27) and the Prediction Capability Diagram (Figure 4.28).

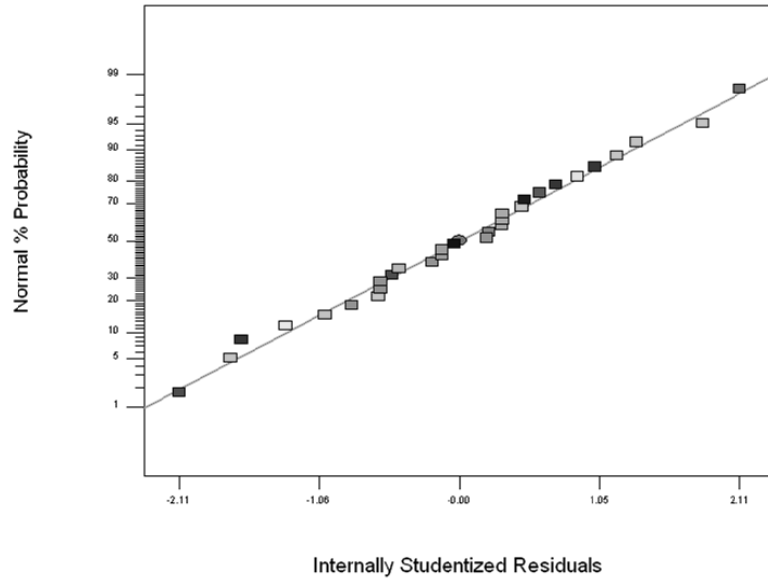


Figure 4.27: Normal Probability Plot

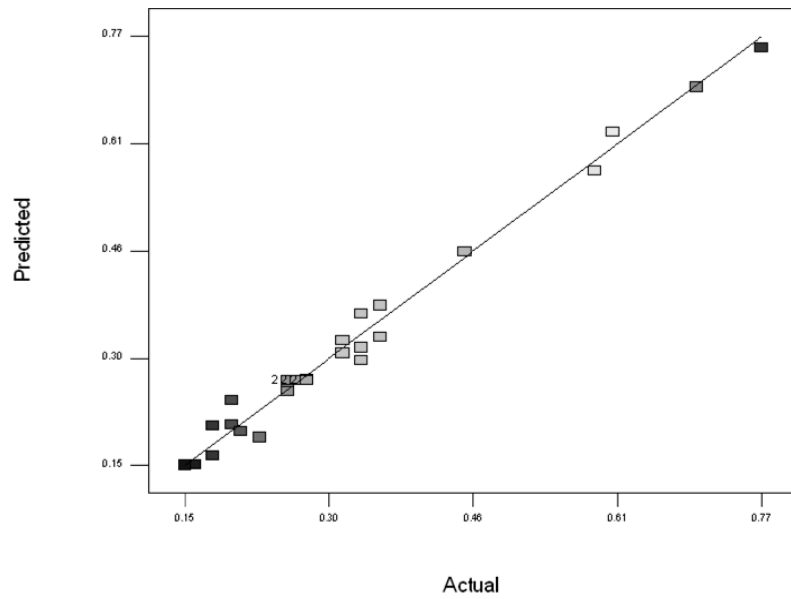


Figure 4.28: Prediction Capability Diagram

4.6.4 Concluding on thinning in AISF

A simple model to relate the minimum thickness and the process parameters in Incremental Sheet Forming process was proposed. This can suggest a new way to evaluate material formability during process design since it seems that material cannot overcome a threshold thinning.

In particular, the Sin Law usually supplies an average thickness value while its actual distribution is often more complex. Using the proposed model, it is possible to predict with a good accuracy the minimum thickness in the zone where the stretching is more severe.

Naturally, further investigations are required to definitively assess and generalize the proposed model.

Study on AISF accuracy

5.1 Introduction and scope of this chapter

In this chapter an overview on the state of art in the springback compensation is reported in order to introduce a wide study on geometrical part deviation in AISF. In detail, an investigation involving several material and several shape is carried out and presented with regard to the secondary operations of part trimming. This investigation is reported to explain the springback role and its influence at varying of material and shape.

Starting from this base of knowledge an investigation on numerical capability to predict the spring is reported. In fact to avoid the “trial and error” approach should be favourable to predict the part deviation by numerical model. Finally a novel approach to improve the geometrical part accuracy is presented.

5.2 State of the art on the accuracy and springback compensation

Several references deal with the problem of geometric accuracy in AISF: Junk [Jun03] discusses springback in AISF in view of both process-related and workpiece related parameters. In a series of experiments it is shown that the use of a full positive die, an alternating tool direction, a large blank holder force, a small wall angle of the desired geometry, as well as a material with a high hardening exponent n (for definition see Eq.(3.1)) have a positive influence on the geometric accuracy of the final shape. Also, it is shown that a better accuracy is obtained when a pyramid is formed using two-stage TPIF instead of single-step TPIF. However, the potential of multi-stage forming with respect to improving the geometric accuracy is not exploited. An algorithm for correcting the tool path is presented, which tries to find a geometry based on which a tool path can be calculated that yields a “correct” part without deviations. The first step is to manufacture a part using a tool path that is calculated from the CAD model of the desired shape. After digitizing this part, deviation vectors between the actual and the desired geometry are determined. The correction module derives a new geometry for tool path generation by mirroring the geometry obtained after

forming about the target geometry Figure 5.1. The mirrored deviation vectors can be scaled in length by

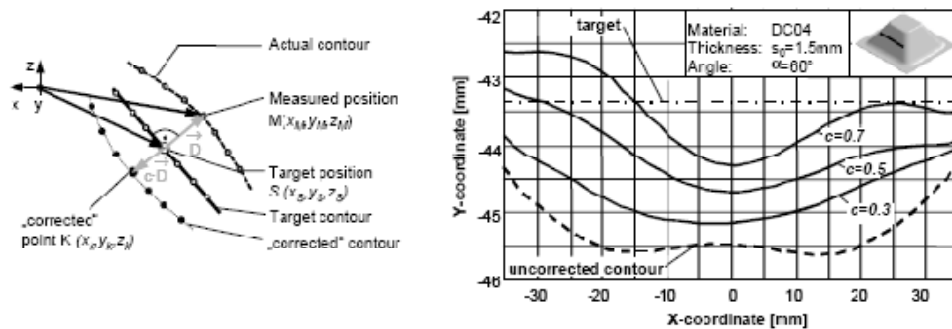


Figure 5.1: Illustration of the correlation algorithm proposed in [Jun03] for the improvement of the geometric accuracy

a correction factor c . The end points of the vectors are used to define a new part geometry, which is used to determine an updated tool path. Hence, it is assumed that springback can be compensated by imposing bulges in the opposite direction to those observed on the first part. For a pyramidal part, the algorithm was shown to yield reduced deviations, which is due to the fact that the initial bulge was replaced by a few smaller ones intersecting the desired target shape (Figure 5.1, right). Ambrogio *et al.* [AFG+05] use a neural network in combination with 2D finite element calculations to determine improved trajectories. A linear relationship between springback in the horizontal (X) and vertical (Y) directions is observed,

$$\Delta X = K\Delta Y, \quad (5.1)$$

where K assumes a value between 0.22 and 0.28 for the cases investigated. As stated in [Jun03], 2D FE calculations are not sufficient to model AISF. Calculation times for 3D FE models of AISF render an extension of the approach to full scale models impossible. According to Ambrogio *et al.* [ACD+04], the step-down and the forming tool diameter have the largest impact on the geometric accuracy among all process parameters. A smaller forming tool and a small step-down are reported to be beneficial for the accuracy. A modified trajectory for a truncated pyramid is presented, where an increased initial slope is introduced in the tool path. The geometric shape obtained is reported to be much closer to the desired one, but no exact values are given. Jadhav [JGH03, Jad04] discusses an optimisation of the basic process parameters that include the vertical step-down, the feed rate, the tool diameter, as well as the tool path. Experiments were carried out to identify the optimum process variables, considering the influence of the feed rate, the tool diameter, the vertical step-down and the tool path type (uni- or bi-directional and helical) on the geometric deviation, the

forming time, the thickness variation and the surface finish. It is proposed to use a concave tool path that represents a bulge in the direction opposite to the bulge that occurs with the standard tool path, similar to the approach in [Jun03]. Verbert *et al.* [VDL07] use feature detection to identify characteristic features of a part, such as planes, edges, free-form surfaces, etc. An optimized tool path is determined for each specific feature which is shown to yield a better overall accuracy in a single-step forming operation. Bambach [Bam08] proposed a multistage strategy in order to improve the part geometry and studied the possibility to combine that strategy with thermal treatments obtaining a relevant reduction of springback phenomena.

5.2.1 Discussion of the state of the art. All approaches, except the multistage strategy proposed by Bambach [Bam08], that were summarized in the previous section are based on an “over-bending” of the tool path in the direction opposite to the bulge that is induced by single-step forming. This bulge is either measured or it is assumed a priori that bulges will occur. The limit of this approach can be illustrated with the forming of a straight side wall of a pyramid. Assuming that a pyramid is initially manufactured with a tool path which is calculated directly from the CAD file, bulges will be found on the side walls. These bulges point inwards in SPIF and outwards in TPIF, i.e. usually in the direction opposite to the direction in which the sheet metal is pushed during forming. The initial tool path is aligned parallel to the side walls. When a corrected tool path is used that points in the direction opposite to the bulging, the forming tool will travel on a trajectory that is longer than the initial one. It is clear that this approach will never yield a flat side wall, since the sheet metal is primarily stretched during AISF. In plain words, the created side wall will always be too long to fit in-between the corners of the part so that bulges will occur. Depending on the tool path and process parameters employed, the initial bulge will be replaced by several smaller bulges, thereby reducing the overall deviations but making the side wall “wavier”. The approaches found in the literature motivate departure from single-pass forming strategies and an investigation of multi-pass strategies as a possible way to improve the accuracy. Starting from this considerations Bambach [Bam03] proposed the multi-stage strategy and the annealing after forming, but the thermal treatment can be an expensive additive operation. For the aforementioned motivation in this chapter, after a deeper experimental and numerical study on geometrical accuracy of the incrementally formed parts a new approach is proposed.

5.3 A study on the accuracy in Incremental Forming process

It is well known that material coupling is carried out after trimming, when it could change its shape after the new equilibrium. In this section the above concept is kept in touch and a wide experimental campaign has been set-up in order to acquire experimental information on the effect of unclamping and trimming after incremental forming processes.

However, many of these studies are based on the analysis of the components after the forming step, when material is already clamped on the frame, or after unclamping. But, from an industrial point of view, it is clear that the most consistent measure is relative to the component after the trimming step, when the part is theoretically ready to use.

For the reasons above described, in this section a study on the role of springback in Incremental Forming, after the trimming step, is proposed.

For sake of completeness, three different materials have been investigated and three different geometries have been designed, in order to reproduce some elements present in general, like high curvatures, narrow corners and double curvatures. The aim of the present analysis was to simulate what happens, in general, when component is firstly formed and then trimmed, varying geometry and material, and comparing the experimental results with the expected geometry modelled in the CAD files.

In this way some general conclusions can be drawn and a consistent knowledge becomes available for the process analysts to take some critical decisions when complex shapes have to be manufactured.

All these aspects are accurately discussed in the next paragraphs.

5.3.1 Geometrical considerations on springback

Springback is a complex phenomenon in forming, depending on both the properties of the material, such as its yields stress, Young's modulus and strain hardening coefficient, and the geometrical conditions of the material, such as the sheet thickness and the product shape [FFG⁺98]. The idea that drove the present study is focused on the evaluation of the above factors and, for this purpose, a careful attention was paid on the shape definition. Considering the adopted manufacturing process, it is a common point of view that the total amount of the sheet springback is directly dependent on the final product geometry: the presence of points of discontinuity or corners increases the material rigidity, while a free-form, characterised by the continuous intersection of convex and concave curvatures, is more penalised by the elastic behaviour.

Thus, in order to produce all the possible effects on a deformed component the different geometries were classified into three categories which produce all the. This is possible, of course, taking into account shapes which are characterised by known boundary conditions: in this case they are all concave shapes, with a limited depth respect to the dimension of the blank.

In formal words, being S the space of the possible deformation modes after the process, it can be built as the sum of the sub-spaces S_j corresponding to the deformation modes (due to the springback) of the single geometric categories.

The three categories above mentioned are:

- a frustum of cone, which represents a homogeneous geometry with a symmetric section (Figure 5.2.a);
- a frustum of pyramid, characterised both by points of rigidity and points more free to move, the latter in the middle of the sides (Figure 5.2.b);
- a free-form flower wise, which is determined by the intersection of circumference parts, causing heavier change of the wall inclination (Figure 5.2.c).

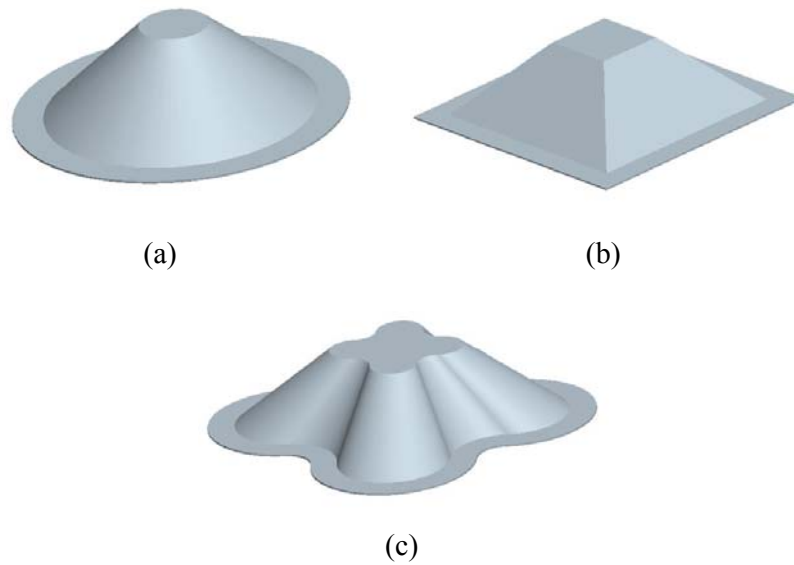


Figure 5.2: The investigated geometries

In formal terms, it is possible to write:

$$S_c \cup S_p \cup S_f \subseteq S \quad (5.2)$$

where S_c , S_p and S_f are the sub-spaces of the possible deformation modes, due to the springback, for cones, pyramids and free-forms respectively.

Naturally, according with the aim to reduce the geometrical complexity and to asses the equation 1, some geometrical conditions were kept constant all over the shapes. First of all, the major base dimension was fixed equal to 80 mm both for the circumference diameter and for the pyramid and free-form sides. Contemporary, a final height of 40 mm and a wall inclination angle varying into the range of 40 – 45 degrees were chosen to fully define the geometries.

5.3.2 Experimental investigation

The present research was carried out with the aim to analyse the sheet springback both at the end of the manufacturing step and after the component trimming. This task was developed in order to investigate aspects which led to derive some suitable guidelines for the application of Single Point Incremental Forming, from an industrial point of view. Anyway, due to the problem complexity, it was considered strategic to reduce the factors of the experimental plane, fixing the process parameters during the manufacturing phase. On the contrary, the varying effect was assigned to the material behaviour; more in detail, three different materials were considered, namely two aluminium alloys (AA 1050 – O and AA 5754 – H22) and one deep drawing steel (DC04), and each of them was utilised to manufacture the specified shapes. The chemical properties of the above said materials are highlighted in Table 5.1.

Table 5.1. Materials chemical compositions (% of mass)

	Al	Cu	Fe	Mg	Mn	Si	Ti	V	Zn
AA 1050 – O	99.5	0.05	0.4	0.05	0.05	0.25	0.03	0.05	0.05
	Al	Cr	Cu	Fe	Mg	Mn	Si	Ti	Zn
AA 5754 – H22	94.2	0.3	0.1	0.4	2.9	0.5	0.4	0.15	0.2
	C	Cr	Al	Mn	Ni	Ti	Sn	S	Mo
DC04	0.05	0.03	0.047	0.22	0.01	0.003	0.001	0.007	0.01

As regarding the Incremental Forming process conditions, a tool diameter of 12 mm and a constant tool depth step, equal to 1 mm, were used for the whole campaign; at the same time a tool speed rotation equal to 300 r.p.m. and a tool feed rate of about 600 mm/min. On the

contrary, during the trimming phase, a small end mill was properly used setting the rotation speed and feed, and using a pitch equal to 0.1 mm, in order to remove a few material for each loop.

The experimental campaign was executed on a CNC work centre, both for the incremental forming operation and for the trimming phase. An emulsion of mineral oil was provided during the experiments.

Naturally, the tests were repeated three times in order to validate the results, avoiding the possibility of relevant errors in the measuring procedure.

An example of the incremental forming process and the trimming one, for the manufacturing of a free form component, is shown in the next Figure 5.3.

To better define the springback evolution two “check points” were fixed during the experimental campaign: first of all, a preliminary measure of the component geometry was executed at the end of the manufacturing step, keeping the clamping action but removing the tool from the sheet; secondly, the same measure was repeated after the trimming phase in order to evaluate the quality of the final product according to the project constraints.

To execute this measure, a reverse engineering approach was implemented and a Laser based scanning system was utilised to pursue the above goals [VMC97]. A Minolta Vivid 300 laser scanning systems was adopted for the proposed research (Figure 2.8): this system is able to rebuild the product geometry by using a Laser source which illuminates a body by a reflected beam.

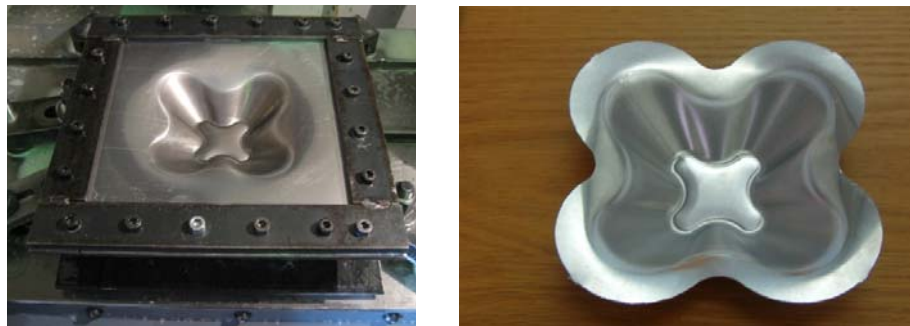


Figure 5.3: Results of the intermediate and final step in the manufacturing of the free-form component

According to the procedure defined in chapter 2 (in section 2.4.4) two virtual models were considered for each test; they exactly reproduce the end of the manufacturing phase (Figure 5.4.(a)) and the trimmed component (Figure 5.4.(b)).

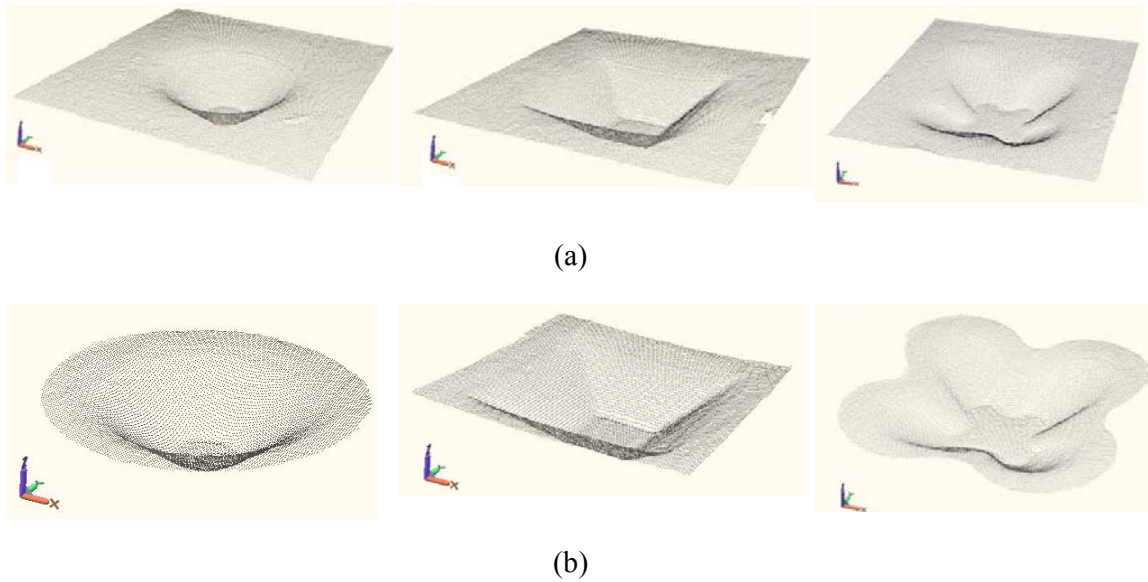


Figure 5.4: Virtual models after the manufacturing phase (a) and after the sheet trimming (b)

Naturally, a proper reference system was set-up in order to ensure the same positioning of the workpiece during the measurement phase. In this way, it was possible to compare the acquired geometries with respect to the absolute coordinate system and to carry out any requested comparison with the CAD model of the manufacturing specimens.

5.3.3 Discussion of the results

The “*data manipulation*” phase was developed utilizing “*RapidFormTM 2004*”, a proper software provided by INUS Technology as showed in chapter 2.

A first interesting qualitative result can be obtained taking into account the reported maps. As expected, a relevant discrepancy between the desired profiles and the real ones is easily discernible, in the column (a), for each of the geometries. What is more, for all of them, it is possible to state that the larger difference is localized in the flange where the sheet is not well supported. In fact, no proper back-plates were used. This problem is particularly evident in the free-forms.

On the contrary, a good precision was measured in the sloped wall, also in the free form. The worst result concerns the pyramid, probably because the presence of long straight lines in the trajectory maximizes the role played by the local sheet rigidity. The latter, in fact, changes depending both on the distance from the clamping equipment and the geometry corners.

Finally, the specimen bottom always shows a lifting-up of about 1-2 mm as compared to the imposed depth.

These issues immediately suggest to modify the part-program in order to reduce this inaccuracy as proposed by Ambrogio et al [AFD⁺04].

Here it is very interesting to observe how is significant the trimming phase in terms of geometry precision. Having a look at the column (b) of the Figure 5.5, which reports the differences between the already clamped formed parts and the trimmed ones, it is possible to note that the entity of the differences is very low and practically always less than 1 mm. This is not true only for the pyramidal shape: in this case, the large flat generated surfaces again results in bigger errors.

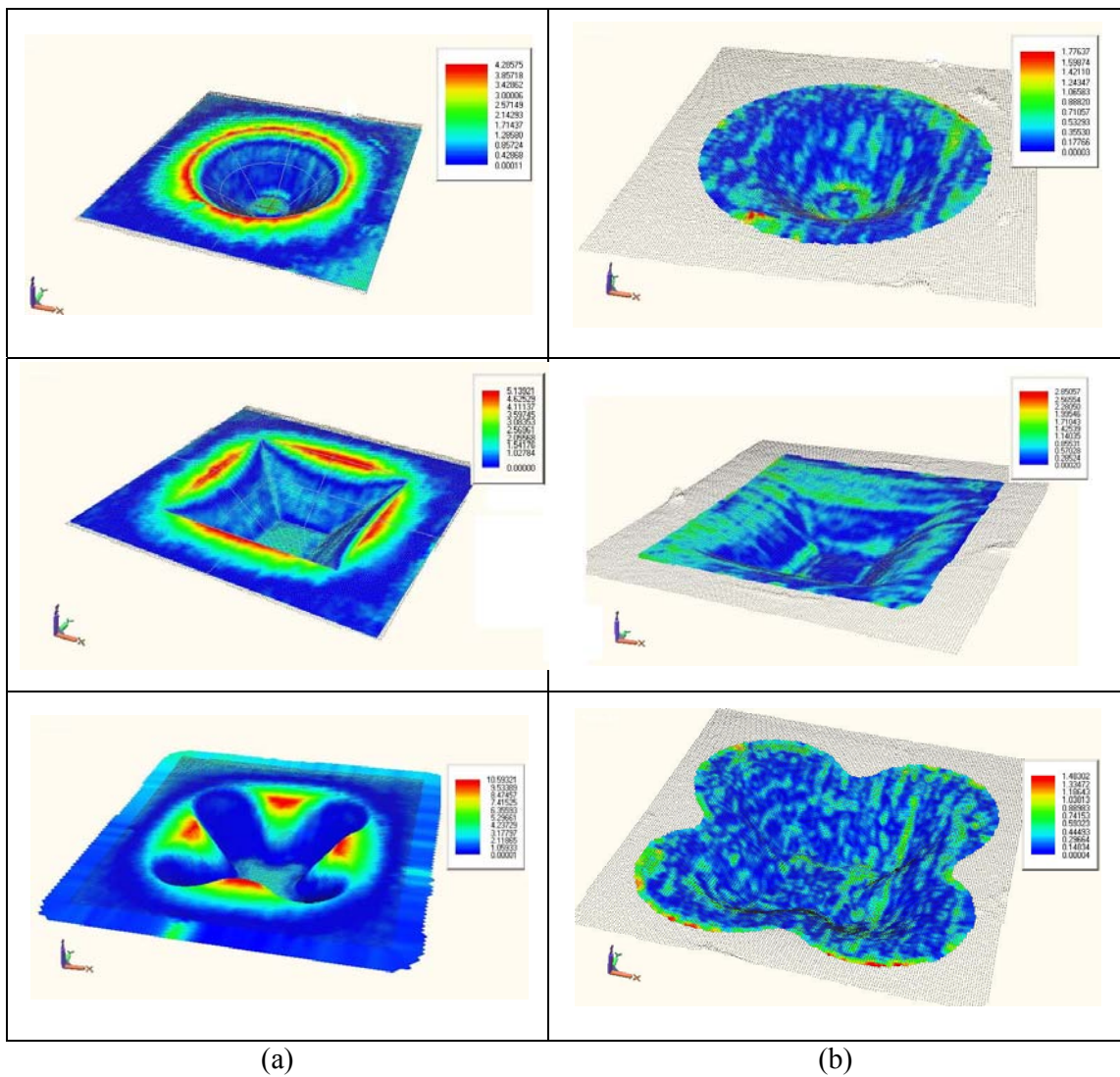


Figure 5.5: Comparisons between the CAD model and the manufactured one at the end of the SPIF process (a) and between the last and trimmed product (b) for AA 5754 – H22

These considerations, based only on the qualitative analysis of the maps, can be partially assessed utilising the data of the tables 5.2 and 5.3.

Table 5.2. Geometrical discrepancies evaluated between the CAD model and the manufactured component

	Frustum of Cone			Frustum of Pyramid			Free – form		
	ϵ_{ave}	ϵ_{max}	σ	ϵ_{ave}	ϵ_{max}	σ	ϵ_{ave}	ϵ_{max}	σ
	[mm]	[mm]	[mm]	[mm]	[mm]	[mm]	[mm]	[mm]	[mm]
AA 1050 – O	1.10	4.0	1.04	1.52	5.5	1.79	1.90	11.1	2.09
AA 5754 – H22	0.93	3.8	0.81	1.17	5.1	1.17	1.69	10.5	2.03
DC04	0.90	3.5	0.76	1.23	5.0	1.17	1.71	10.0	2.02

Table 5.3. Geometrical discrepancies evaluated between the manufactured and trimmed component

	Frustum of Cone			Frustum of Pyramid			Free – form		
	ϵ_{ave}	ϵ_{max}	σ	ϵ_{ave}	ϵ_{max}	σ	ϵ_{ave}	ϵ_{max}	σ
	[mm]	[mm]	[mm]	[mm]	[mm]	[mm]	[mm]	[mm]	[mm]
AA 1050 – O	0.31	0.70	0.27	0.54	2.5	0.51	0.27	0.7	0.22
AA 5754 – H22	0.29	0.60	0.27	0.50	1.2	0.35	0.31	0.8	0.26
DC04	0.29	0.55	0.26	0.51	1.2	0.35	0.34	0.7	0.28

In the tables, in fact, the average error and its standard deviation is reported for all the shapes. There were taken into account both the comparisons between the CAD model and the deformed part and between the latter and the trimmed one.

Unfortunately, the average error is not able to distinguish the different zones (flange, sloped wall and bottom), however it supplies a sort of magnitude of the actual error.

It is easy to discern that there is about a factor ten between the error revealed comparing the CAD model and the formed parts and the one measured between the shape before and after trimming.

5.3.4 Conclusions on the experimental measure of part accuracy

An experimental campaign aimed to the measuring of the geometrical error in incremental forming, before and after the trimming phase, is carried out. As conclusions, also taking into

account that today a precision below 1 mm in medium dimension components is regarded as a good performance for the investigated process, it is possible to state that:

- no very significant differences in the behaviour were noted utilising all the selected materials;
- the presence of large flat surfaces, like the ones which characterize the pyramid, increases the part inaccuracy, both in forming and trimming steps;
- in the free forms, the most critical zone becomes the flange because no proper back-plates are designed and mounted on the equipment;
- the error amount that can be ascribed to the trimming phase is very low and one order below the error generated in the forming process.

For the above reasons, at this level of knowledge on the incremental forming process, probably the research effort could be focused on the improvement of precision in forming phase, trying to approach the desired geometry and neglecting, in the first attempts, the role played by the trimming.

Concluding, in this task, the strategy based on the arbitrary modification of the simple CAD-CAM generated tool trajectory could be the most suitable way to define a general methodology to implement when single point incremental forming process is used.

5.4 Numerical capability to predict the springback

Up to now, the numerical simulation did not supply significant aid to the designers, due to the problem complexity and the very long simulation time when an elasto-plastic analysis has to be carried out. For this reason an experimental trial and error approach is often preferred. An innovative approach is represented by the application of numerical analysis based on a coupled explicit-implicit formulation. In this section, some results of a wide research on the application of explicit-implicit code for the dimensional accuracy analysis are proposed. Both the problems related to the dimensional accuracy and springback phenomenon after the manufacturing step and the trimming operation are analysed from an experimental and a numerical point of view. In this way, some relevant issues, as well as the FEM capability, have been derived by the comparisons with the experiments.

Nowadays the use of numerical simulation can represent a strategic keypoint for the process analysis [AFG⁺04]. Anyway, the absence of symmetry in the problem and the high

blank dimension respect to the tool, impose the use of explicit dynamic analysis in order to reduce the simulation time. These numerical tools are not able to supply accurate results all over the process: in other words, while good predictions are possible taking into account some issues like material thinning, plastic behaviour, required load, the elastic equilibrium after the punch removing and, especially, after shape trimming, is not calculated with the expected precision [NL99]. As a result, the final predicted shape can be significantly different respect to the experimental one and, in this case, it is clear that the use of the code as design tool becomes meaningless.

In the study here addressed, a wide analysis was carried out with the aim to well understand the potentiality of a numerical model for predicting all the above said geometrical problem. For this reasons, different shapes and materials were considered, in order to obtain a representative sample for the investigation. Contemporary, the geometrical error detections were executed both after the punch removing, with the blank already clamped, and after trimming, in order to well describe the material behaviour.

Naturally, the same campaign was numerically designed and executed and, at the end, some guidelines were derived by the comparison with the experiments.

5.4.1 Numerical capability

Many approaches to simulate springback have been recently proposed, including explicit-explicit, static explicit-static explicit, and even one step method [Wag02]. It should be observed that due to inherent numerical sensitivity implicit schemes for both loading and unloading have been popular, as well as attempts to link dynamic explicit simulations of forming operation to static implicit simulation of springback. In particular, Narasimhan et al. [Wag02] showed that an explicit implicit sequential procedure can be utilized to predict springback distortions in an automotive component. At the same time, explicit models are usually preferred to implicit ones in the simulation of the forming stages since they generally provide faster and more reliable performances. What is more, springback stages do not involve contact problems and the workpiece remains purely elastic during springback; in this way many numerical difficulties disappear and the solution convergence time is reasonable.

Actually, to well define the code capability a preliminary comparison between the simple explicit solution and the one obtained with an explicit-implicit sequential procedure was carried out considering the geometry resulting from the particular stress distribution at the end of the manufacturing step. To do that, a frustum of cone was chosen as specimen profile and

single test was firstly experimentally and then numerically executed, in order to compare the final geometry obtained with both implicit and explicit formulations.

For this purpose, LS-Dyna commercial code was utilized: the code is based on an explicit formulation starting from the dynamic equilibrium of the considered structure; what is more, it takes into account the springback phenomena following an hybrid approach based on the explicit loading - implicit unloading analysis of the process. Further details of the implemented model will be provided in the next paragraphs.

In this way the F.E. analysis is able to furnish the final shape of the part the punch removal (Figure 5.6)

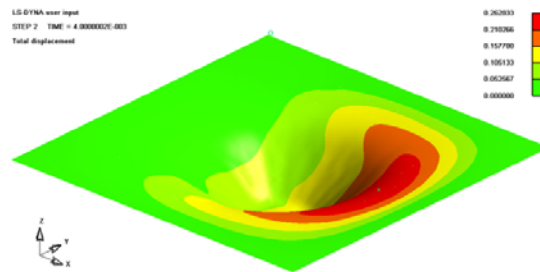


Figure 5.6: Numerically measured total displacement at the punch removal.

A qualitative analysis derived by the comparison between measured final geometry of the part after punch removal and the numerical ones showed the same behavior for both explicit and implicit formulations (Figure 5.7).

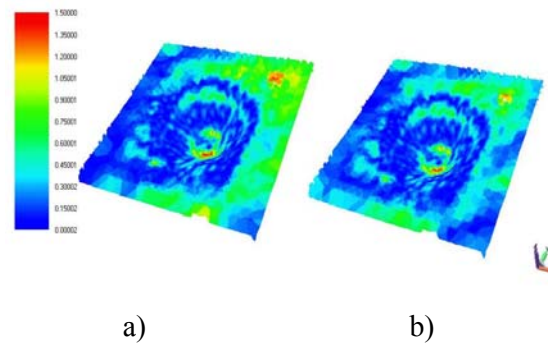


Figure 5.7: Comparisons between the measured final geometry of the part and both the explicit (a) and the implicit (b) formulation results.

It should be observed that an improvement in terms of mean error has been calculated with the implicit step,

More in detail, the mean error and the standard deviation measured by the above specified comparisons are shown in the Table 5.4.

TABLE 5.4. Explicit and implicit error distribution.

	Mean	StdDev
Explicit vs. Experimental	0.03	0.38
Implicit vs. Experimental	0.01	0.35

According to these results and to the aim of this investigation, the implicit elastic step, to calculate the final shape of the component, was implemented in the following to evaluate the geometrical error entity at the end of an incremental forming operation in more general conditions.

5.4.2 Numerical analysis

As experimentally observed, after the forming operation springback occurs since the forming tool is removed and the internal stress state of the component is not equilibrated by the external actions anymore; for this reason an elastic deformation occurs up to reach a new geometry for which the residual internal stress state is self equilibrated. The inhomogeneous distributions of strains along the formed sheet thickness together with the elasto-plastic behaviour of the workpiece material determine the occurrence of the springback phenomenon. What is more, as trimming is developed new springback phenomena are observed in the produced part since, again, the internal residual stress state is not equilibrated and a new equilibrium configuration is reached through an elastic distortion of the component.

In order to justify this phenomenon the described FE analysis was developed for the whole experimental campaign in order to evaluate the geometrical error at the end of the manufacturing step and after the trimming one.

All the simulations were developed in three phases: a forming one and two springback analyses. In the forming simulation the explicit formulation was utilized, in turn for the springback simulation, occurring both after the removing of the punch (Step 1) and after the blank trimming (Step 2), the implicit formulation of the code was implemented.

According with the model adopted in the previous paragraphs, the blank was meshed through about 450 quadrilateral shell elements and a three level geometric remeshing strategy was applied all over the numerical simulations; in particular, the Belyschko-Lin-Tsay (B-T) shell element [AH02], with five integration points along the thickness, was used. As far as the punch velocity is regarded an artificially increased value equal to 2m/s was utilized, checking that the kinetic energy was below the 10% of the deformation work, in order to minimize any inertia effect characterizing incremental forming simulation. Frictional actions were

considered through a Coulomb model with a coefficient equal to 0.12. As far as the implicit analyses of springback are regarded, all the numerical parameters introduced in the forming stage were assumed except for the type of element. Actually for such analyses the full integrated shell element was always used on the basis of preliminary investigations. Such choice does not determine any relevant increase in the computational time but, in turn, gives the most effective results in terms of prediction of the final geometry of the formed part after springback phenomena occurring both after forming and trimming stages. According to the material characteristics, the DC04 steel showed an anisotropic behaviour and the known Lankford's anisotropy were properly introduced into the model (i.e. $r_{0^\circ}=1.5$; $r_{45^\circ}=1.3$; $r_{90^\circ}=2.1$). In turn the Aluminium alloy AA-1050 showed a very limited anisotropy. To take into account the latter experimental results two different yield criteria were considered: the Barlat-Lian [BL89] and the classic Von Mises. The former takes into account the material anisotropy and was utilized for steel sheet incremental forming simulations; the Von Mises yield criterion was utilized to model the Aluminium material. It is necessary to underline that in all the simulations, for both the considered materials, an isotropic hardening law was taken into account.

The elastic behaviour measured at the end of the simulations carried out on DC04 for all the geometries are displayed in the next Figure 5.8.

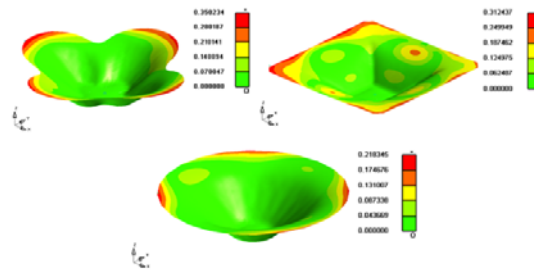


Figure 5.8: Total displacement after the trimming for DC04.

5.4.3 Discussion of the results

In order to develop a proper comparison between the experimental results in terms of clouds of measured points, and the numerical predictions, a few error function are introduced (Table 5.5-5.6).

To do that, a proper CAD software was adopted: more in detail, the analysis was performed into the “RAPIDFORMtm 2006” environment, produced by INUS technology. This software allows the comparison between two surfaces showing the relative error automatically.

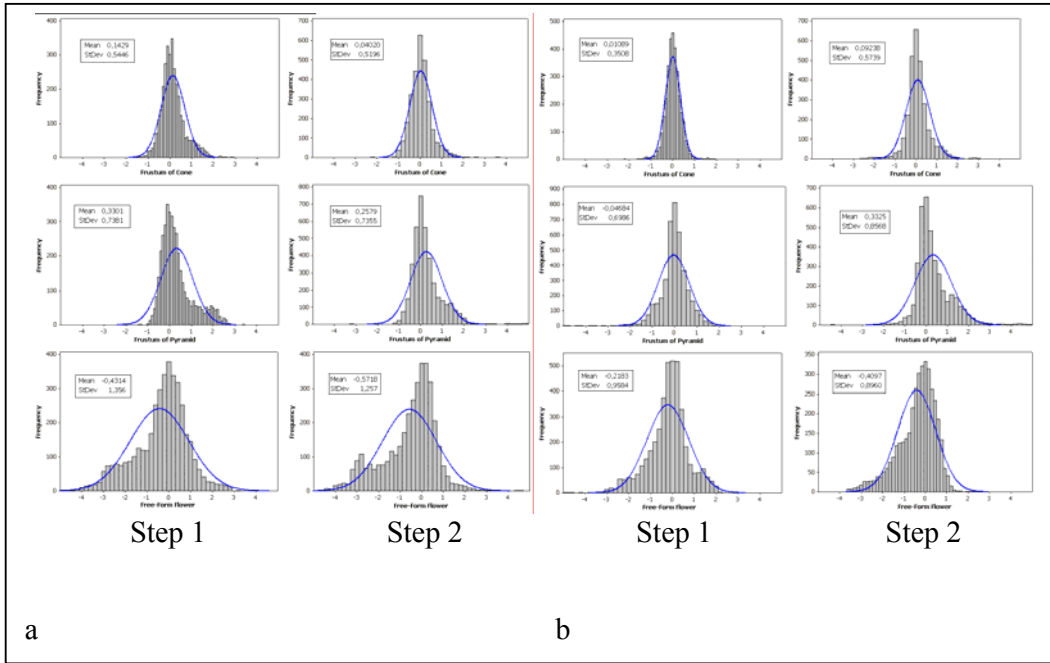


Figure 5.9: Error distribution for the tests carried out on AA 1050-O (a) and on DC04 (b)

It should be observed that the clouds of points were managed and positioned in the space by means of an optimisation procedure that minimize the error between the considered surfaces. After the registration phase, the discrepancies between the geometries can be graphically displayed by means of a 3D map and analytically evaluated by the equivalent error distribution. Both these results are presented in the following Figure 5.9 a),b).

TABLE 5.5. Numerical model suitability measured by the comparison with the real product at the end of the manufacturing step (Step 1).

		Mean	StdDev	Variance	Maximum Abs
Frustum of Cone	AA1050-O	0.011	0.351	0.123	2.20
	DC04	0.143	0.545	0.296	2.87
Frustum of Pyramid	AA1050-O	-0.047	0.699	0.488	6.02
	DC04	0.330	0.738	0.545	3.41
Free-Form Flower	AA1050-O	-0.218	0.958	0.919	6.82
	DC04	-0.431	1.356	1.839	7.97

TABLE 5.6. Numerical model suitability measured by the comparison with the real product at the end of the trimming (Step 2).

		Mean	StdDev	Variance	Maximum Abs
Frustum of Cone	AA1050-O	0.092	0.574	0.329	3.95
	DC04	0.040	0.519	0.270	3.92
Frustum of Pyramid	AA1050-O	0.332	0.857	0.734	4.95
	DC04	0.258	0.736	0.541	5.04
Free-Form	AA1050-O	0.409	0.896	0.803	3.66
Flower	DC04	-0.572	1.257	1.580	4.69

As shown the discrepancies between the numerical and the experimental model increase with the complexity of the shape; in particular, a lower error was measured in the frustum of cone, while the higher error was calculated in the free-form flower shape. This trend was observed both at the end of the manufacturing step and after the trimming, so that for both the considered materials.

5.4.4 Conclusions on numerical capability

The numerical procedure is based on the explicit model to simulate the forming stage and an implicit model to calculate the elastic deformation occurring after the tool removal and after the trimming of the flange.

This is a typical approach when numerical prediction of forming springback is carried out. In this case, incremental forming process was studied and, in particular, the dependence of the material behaviour and shape complexity on the final geometry was investigated.

The obtained results are effective; further investigations on the effectiveness of the numerical procedure have to be developed taking into account the influence of the numerical parameters such as the work hardening model, the type of element and so on.

5.5 A novel approach: the back-drawing strategy

In this paragraphs a simple approach is proposed, based on the self capability of the process to correct the inaccuracy when different step of Incremental Forming are carried out on both the part surfaces. In particular, it is demonstrated that a relevant increasing in the accuracy is obtainable at the second repeated step, while new ones do not affect the accuracy sensitively.

The above approach open a new scenario since it allows to maintain the basic equipment (without any support) and does not require any further knowledge concerning the material behaviour after the punch action.

As analyzed in the discussion of the state of art on accuracy (section 5.2, 5.3.1) many approaches were proposed in the past in order to reduce the natural geometrical errors resulting by the dieless deformation [MAF07]. They are based on different approaches, among them the following are the most interesting:

- the use of different kind of material supports. Nevertheless the tooling complexity remains always reduced as compared to the conventional stamping, this methodology is not well appreciated by the scientists since it is a sort of hybrid technology which forces the concept of the AISF process toward a more traditional one [ACC⁺08];

- the use of off-line procedures, mainly based on analytical approaches or on some heuristics, which are able to predict material behaviour and then modify the tool trajectory accordingly. This procedures are of course relatively expensive, especially in manufacturing of complex shape, since a number of numerical and experimental tests are required in order to acquire a suitable base of knowledge [ADF⁺07, ACF⁺07];

- the use of on-line procedures, based on the measure of the current position of the sheet and the use of a simple controller able to compensate the material diverting respect to the ideal surface [BHA04]. This is theoretically very precise since there is a feedback step by step on the sheet position but it is expensive due to the need of the inspector directly mounted on the CNC machine. Furthermore, springback effect after trimming is not considered.

In this section a new approach is presented. The basic idea is to use the self capability of the tool-sheet system to automatically compensate the material diverting when the sheet is deformed, alternatively, on both the sides.

On a normal 4 axes numerical controlled machine it is possible to easily rotate the sheets operating on the other side whenever is desired. It is very easy to understand that operating in this way the process mechanics can be absolutely unknown, since only the theoretical tangent trajectory is imposed on every side, respectively. Of course, this approach increases the cycle time whose slowness is already one of the main drawback of AISF process. However, in the other approaches some preliminary tests are required to supply the knowledge to perform every control strategy.

5.5.1 Back drawing: the Experimental Campaign

First of all, in the present investigation, the following processes are defined:

- Incremental Forming (IF), in which the punch operates only on the top face;
- Back-Drawing Incremental Forming (BIF), in which the punch operates firstly on the top face and then on the bottom one (Figure 5.10);
- Double Incremental Forming (DIF), in which Back-Drawing Incremental Forming is executed two times, consecutively.

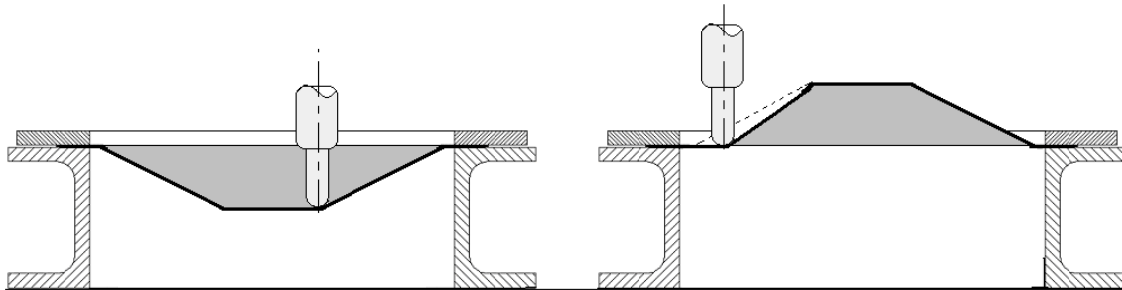


Figure 5.10: The two steps of the Back-Drawing Incremental Forming

Observing the Figure 5.11, it is possible to verify how the strong increase of accuracy is due to the Back-Drawing Incremental Forming step. Double Incremental Forming process (DIF) introduces a certain benefit, however in the opinion of the author its use is not reliable as trade-off between process duration and obtainable advantages.

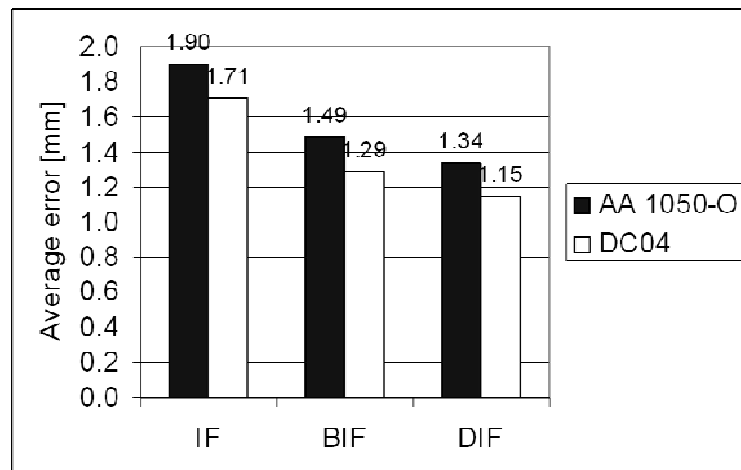


Figure 5.11: Error trend vs. incremental forming repetitions ($p=1\text{mm}$, $s=1\text{mm}$)

For this reason, all the considerations below will be referred to the accuracy increase reachable moving from IF to BIF.

While the sheet thickness (s) and the tool depth step (p) were properly varied during the whole campaign, the other process parameters were kept constant; in particular, the punch diameter (D_p) was 12 mm, the punch rotation speed (S) was 120 r.p.m., the feed (F) was 700 m/min and mineral oil was used as lubricant.

Table 5.7. Error (in mm) for IF and BIF processes for DC04 and AA1050-O, for changing process conditions.

Process Parameters	DC04		AA1050 - O	
	IF	BIF	IF	BIF
	ϵ_{ave} [mm]	ϵ_{ave} [mm]	ϵ_{ave} [mm]	ϵ_{ave} [mm]
p=0.3mm - s=1mm	1.46	1.22	1.75	1.48
p=0.3mm - s=2mm	2.31	1.87	1.05	0.88
p=1mm - s=1mm	1.71	1.29	1.90	1.49
p=1mm - t=2mm	2.48	2.10	1.60	1.31

Table 5.7 gives a synthetic overview of the results while the next Figures 5.12-5.19 give an idea of the inaccuracy in the whole field on the free-form, at the end of the Back-Drawing Incremental Forming process (DIF), for different sheet thickness and depth step.

It is confirmed that the accuracy increases of the 20%-25% executing BIF process instead of IF one, without any other correction.

At the same time, it is possible to observe how the depth step does not play a relevant role (while it is very important as formability is regarded). On the contrary, sheet thickness strongly affects accuracy, playing a different role for AA1050-O and DC04: the former shows a better accuracy for the thicker sheet (up to 0.88mm as average error) while the latter shows a better accuracy when thinner sheets are deformed (up to 1.22 mm as average error).

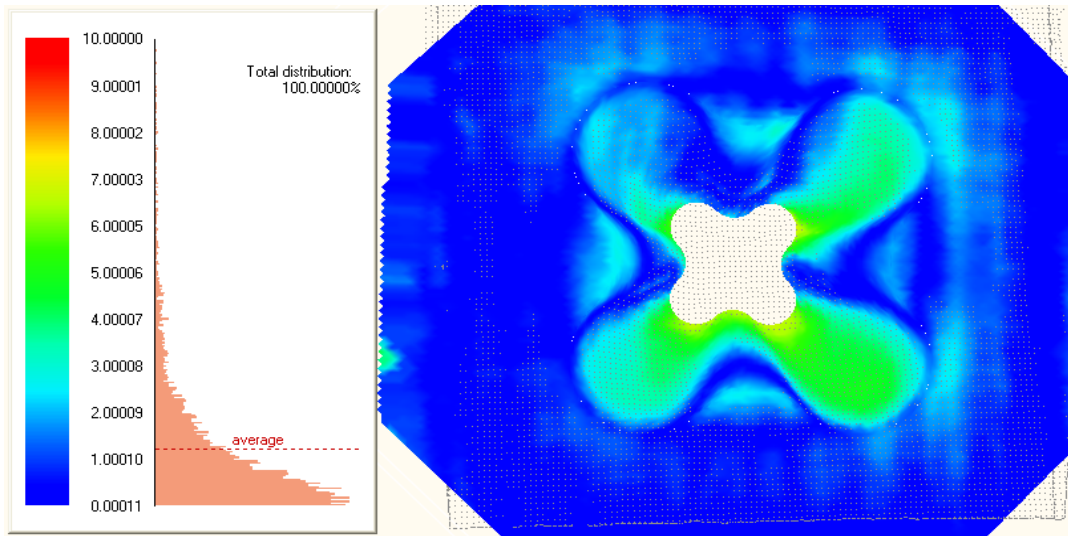


Figure 5.12: Whole field diverting on DC04 Steel (Depth step $p=0.3\text{mm}$; thickness $s=1\text{mm}$)

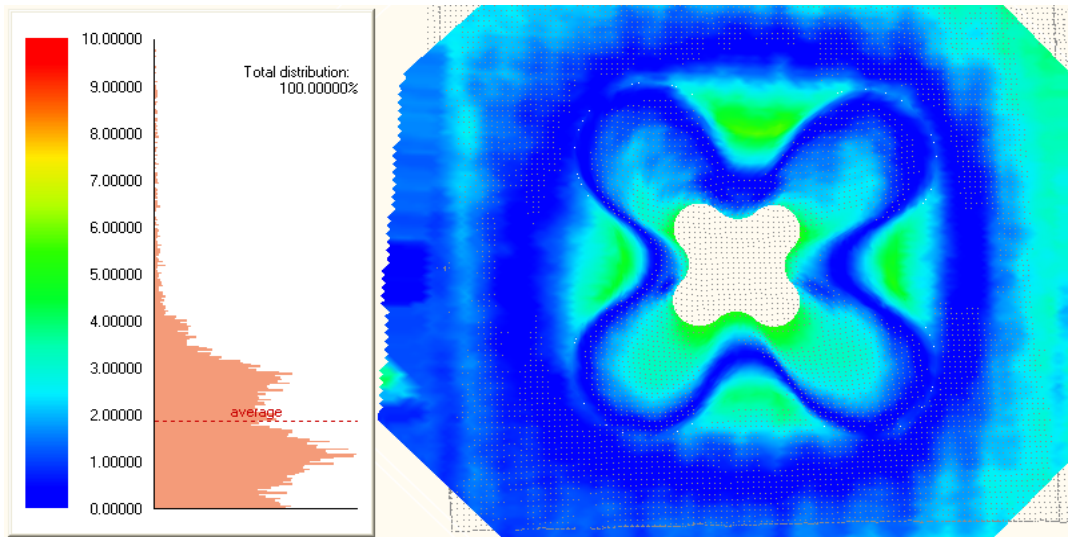


Figure 5.13 Whole field diverting on DC04 Steel (Depth step $p=0.3\text{mm}$; thickness $s=2\text{mm}$)

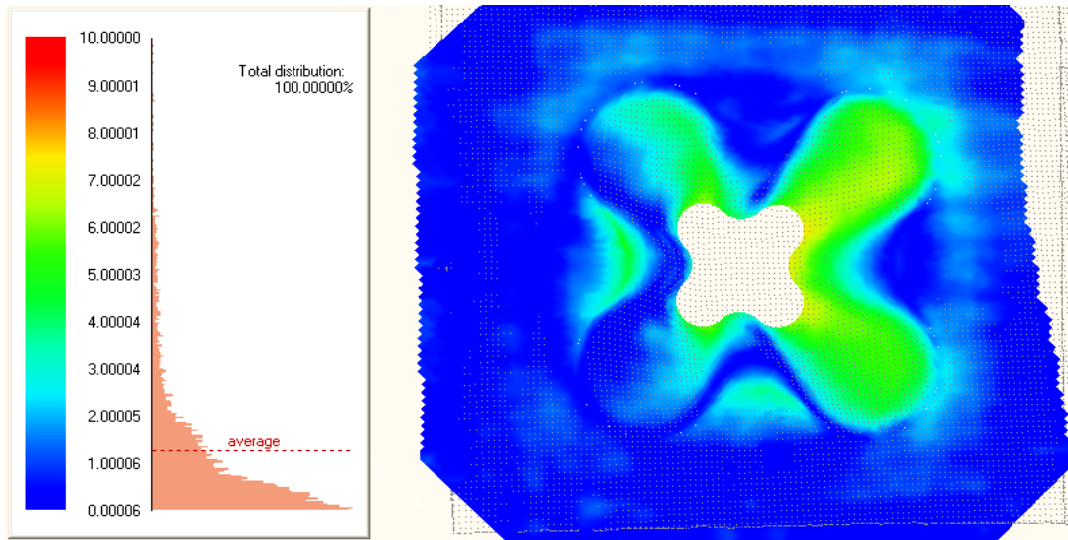


Figure 5.14: Whole field diverting on DC04 Steel (Depth step $p=1\text{mm}$; thickness $s=1\text{mm}$)

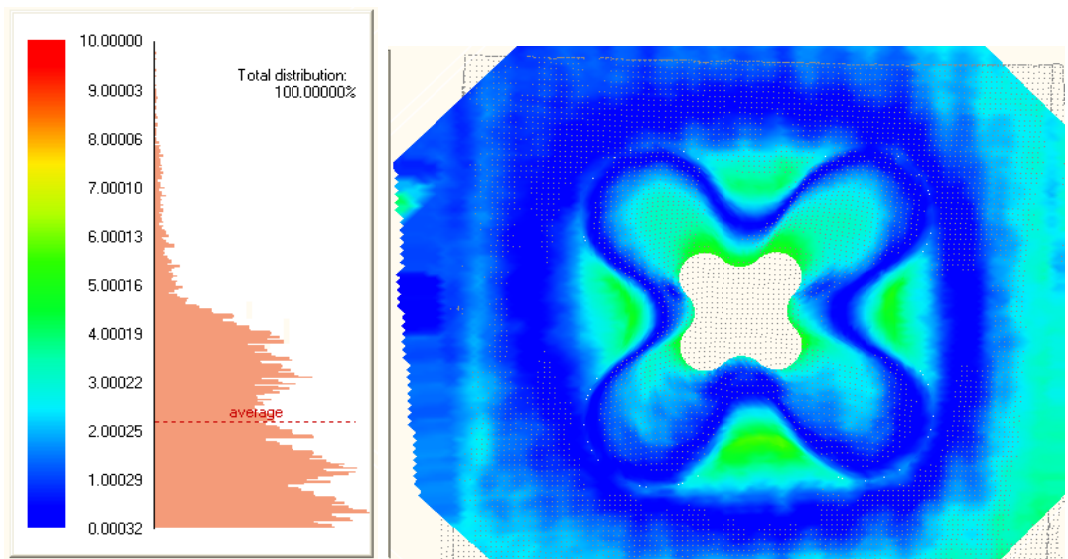


Figure 5.15: Whole field diverting on DC04 Steel (Depth step $p=1\text{mm}$; thickness $s=2\text{mm}$).

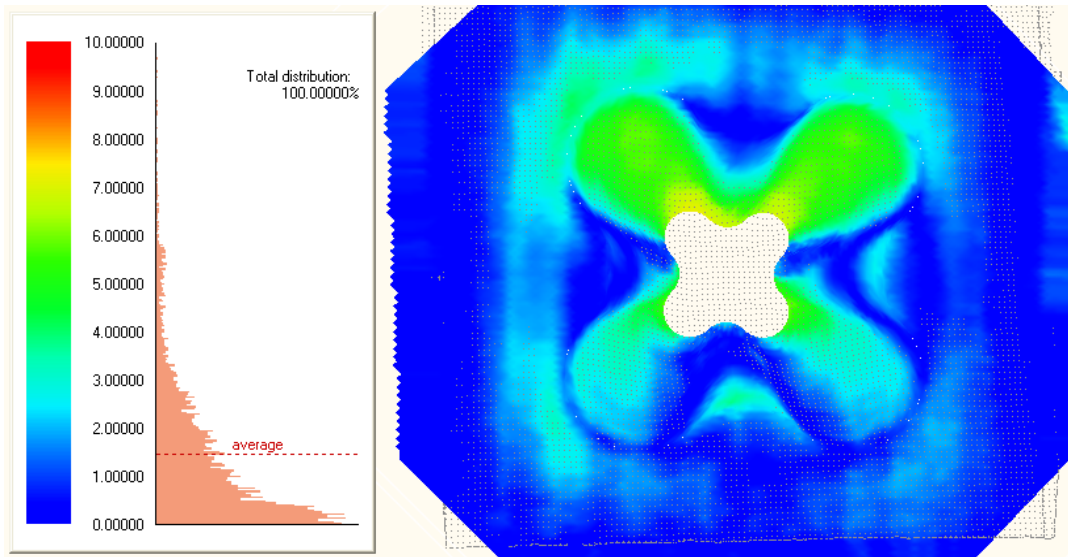


Figure 5.16: Whole field diverting on AA1050-O Aluminium Alloy (Depth step $p=0.3\text{mm}$; thickness $s=1\text{mm}$)

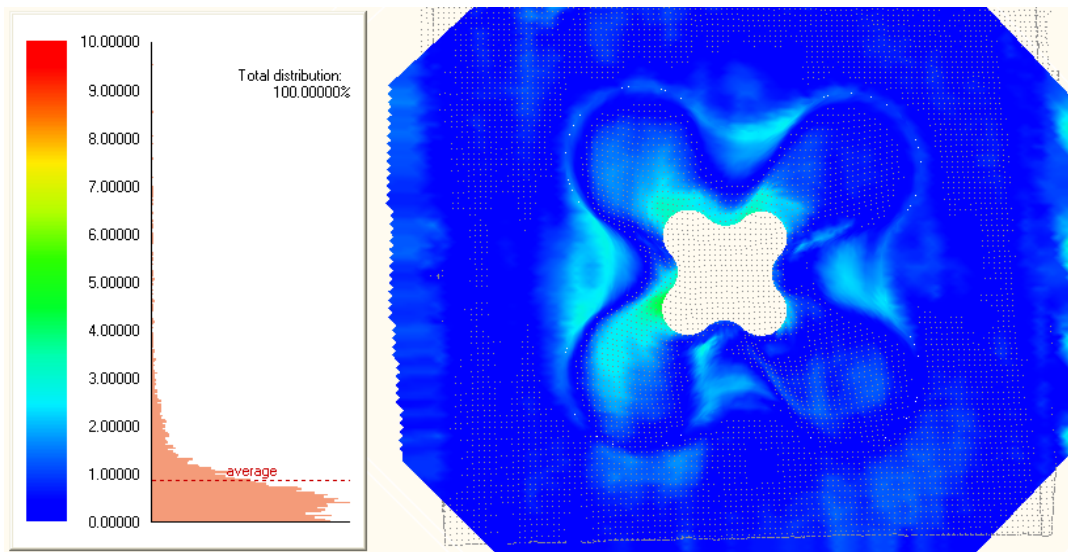


Figure 5.17: Whole field diverting on AA1050-O Aluminium Alloy (Depth step $p=0.3\text{mm}$; thickness $s=2\text{mm}$)

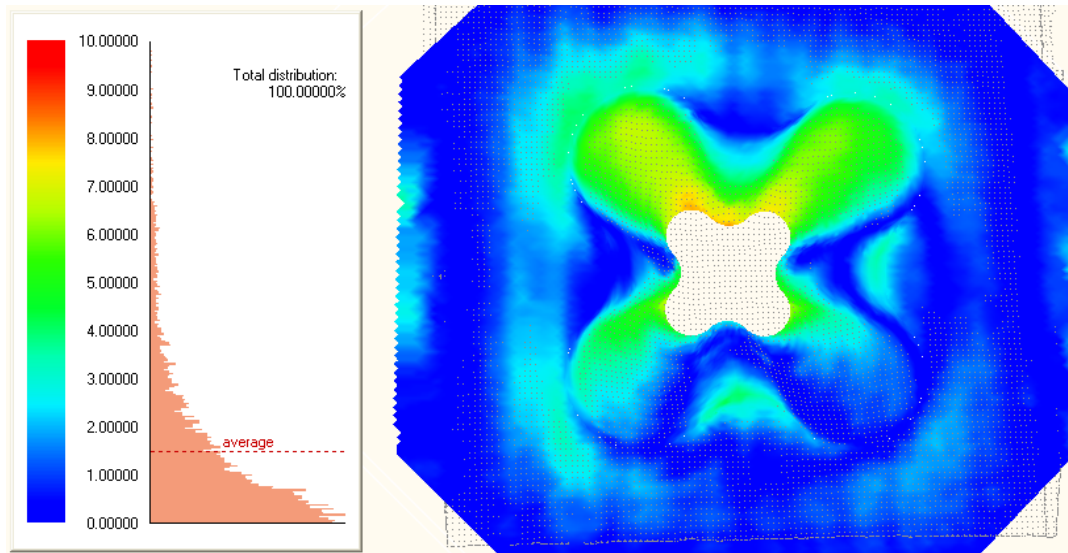


Figure 5.18: Whole field diverting on AA1050-O Aluminium Alloy (Depth step $p=1\text{mm}$; thickness $s=1\text{mm}$)

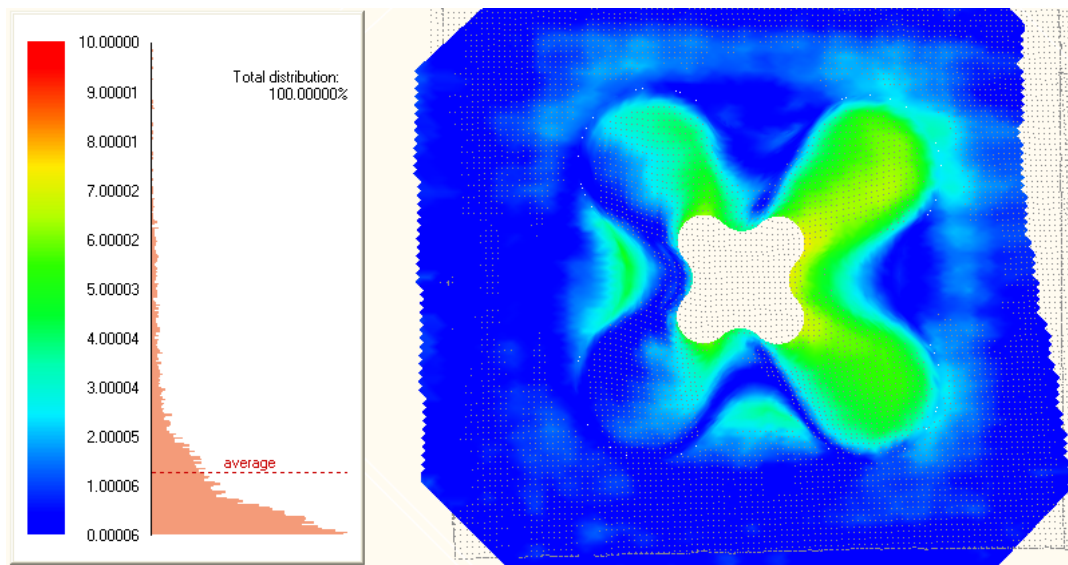


Figure 5.19: Whole field diverting on AA1050-O Aluminium Alloy (Depth step $p=1\text{mm}$; thickness $s=2\text{mm}$)

5.5.2 Conclusion on the back-drawing strategy

As a conclusion of this study, it is possible to state that Back-Drawing Incremental Forming process can constitute an interesting way to increase the process accuracy since it derives only by geometrical considerations, without any knowledge of the complex phenomena involved in the material diverting.

Of course the process time doubles but this can be a reasonable “cost” when accuracy of IF parts is not considered suitable. The process can be iterated (DIF) obtaining again an accuracy increase; anyway, it was experimentally demonstrated that accuracy enhancing reduces with the number of iterations.

Finally, it was shown that a higher thickness allows a higher accuracy when working AA1050-O while the inverse evidence concerns DC04 Steel for which a lower thickness is suggested.

Strategies to control the thickness distribution in SPIF

6.1 Introduction and scope of this chapter

As showed in the previous chapters the material formability is strictly dependent from the material thinning. Moreover the not uniform thickness distribution border a wide application of AISF processes in industrial field. In this chapter a possibility to control and enhance the thickness uniformity is presented by changing the tool trajectory.

6.2 Formability and thickness distribution

It is well known that Single Point Incremental Forming process (SPIF), which corresponds to the simplest configuration of Incremental Sheet Forming Process, runs using a simple frame which locks the sheet during the forming action of a hemispherical punch moving along a designed trajectory [JMH+05]. For this reason SPIF requires a simple tooling and a 3 axes CNC machine allows the relative positioning of both workpiece and punch.

What is more, all the deformation of the sheet is due to thinning since no material flow is allowed. In fact, it was demonstrated that a controlled material flow driven by the punch does not improve the performance significantly [AFG+05].

More in detail, the stress field in the punch-sheet contact point surrounding causes a local thinning and, consequently, new surface generation which allows to form complex 3D shapes starting from a flat sheet.

On the other hand, the approaches commonly used for SPIF trajectories design derive from machining knowledge and, for this reason, paths tangent to the desired shape are usually generated. This could not be the optimal solution as it is demonstrated by some researchers [KN99]. In simple words, it is possible to deform more material respect to the one theoretically enough to obtain the target shape. What is more, larger is the surface on which deformation is imposed, better is the thinning distribution since more material contributes to

the overall manufacturing process. In addition, it is possible to impose to material a proper deformation along a sloped wall, avoiding some singularities due to the process mechanics, as shown in the following.

According to the above considerations, it is quite obvious that an effective design and control of incremental forming operations requires an accurate and reliable modelling of thinning, which cannot be based only on the simple Sine Law [KN99].

Even applying a simple trajectory along a sloped wall (conical shape), it is well known that the Sine Law may supply only a rough approximation, since it largely fails at least in two regions; more in detail: a thickness value larger than the one calculated by the Sine Law occurs in the zones of the blank not interested by the punch actions; on the other hand, lower thickness values arise in the plastically deformed zone.

In the next Figure 6.1 both the force at the punch-blank interface and the thickness distributions obtained from experiments carried out on AA 1050-O, 1.5mm thick, are displayed. The wall angle reproduced during the test was fixed to 70° , which corresponds to the maximum wall angle that can be safely manufactured with this alloy. The typical distribution, measured for severe but not dangerous values of the wall inclination angle, shows a polynomial trend for the normal force and a corresponding decreasing thickness [AFG+05]. Furthermore, being the bending role limited with respect to the stretching one, a higher thinning occurs after the first loops, which corresponds to a reduction of the punch force, consequently. If the process conditions are severe, but not enough to determine material failure, after this first stage, the process tends to become stationary; consequently the punch force reaches again a steady state value and, simultaneously, the thickness approaches the Sine Law value. In this way, being Incremental Forming characterized by localized deformation, thinning remains a local effect and the thin section does not influence material integrity when severe but not dangerous conditions are manufactured.

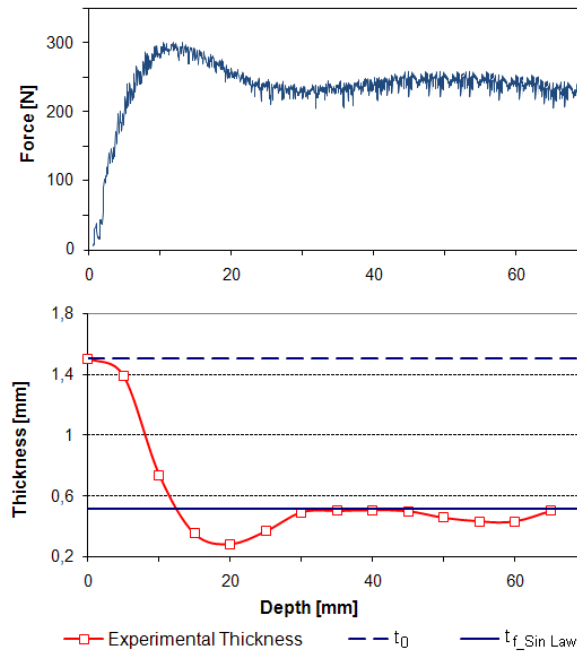


Figure 6.1. Punch force and thickness distribution obtainable in SPIF process.

Starting by these considerations thickness distribution could be improved modifying the local effect of the deformation obtaining a more homogeneous profile; in other words, it is possible to change the strain distributions and/or to work in a different way the same portion of the blank material in order to improve the thickness distribution. Concluding, also the tool trajectory can be considered as a process parameter in order to optimise the final thickness distribution.

6.3 Tool path optimization

As previously introduced, this chapter is aimed at investigating the tool path impact on the thickness distribution. In fact, it was observed that a not uniform thinning could penalize material formability (Figure 6.1); anyway, due to the particular process mechanics, it is interesting to understand how changing the tool trajectory it is possible to spread the thickness along the working profile.

With this aim, among all the possible solutions, four approaches in terms of tool trajectory were tested and compared (Figure 6.2):

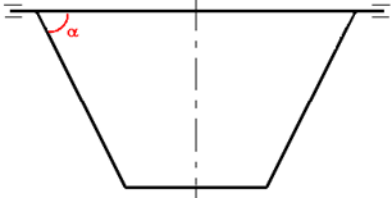
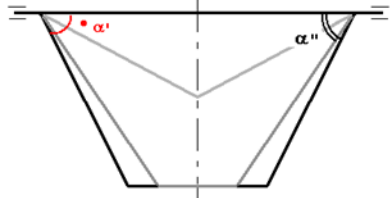
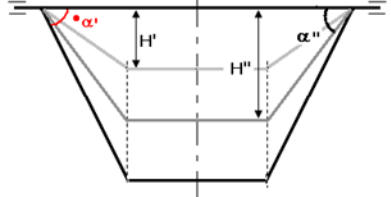
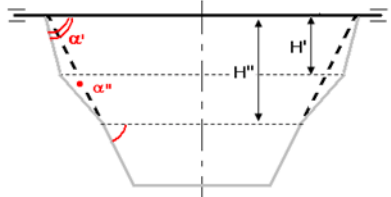
	<p>Single Slope</p> <p>$\alpha = \text{target value}$</p>
	<p>Incremental Slope</p> <p>$\alpha' = 1/2 \alpha$ $\alpha'' = \alpha - 10^\circ$</p>
	<p>Wall Slope</p> <p>$\alpha' = 1/3 \alpha$ $\alpha'' = 2/3 \alpha$</p> <p>$H' = 1/3 H_r$ $H'' = 2/3 H_r$</p>
	<p>Decremental Slope</p> <p>$\alpha' = \alpha + 10^\circ$ $\alpha'' = \alpha - 10^\circ$</p> <p>$H' = \text{beginning of localised thinning}$ $H'' = \text{end of localised over-thinning}$</p>

Figure 6.2. Details of the investigated tool paths.

- Single Slope (SS) – which corresponds to the conventional negative tool path (from outer to inner and from higher to deeper);
- Incremental Slope (IS) – based on the idea to work more material than the strictly required, deforming the part of blank usually not involved in manufacturing step. Invoking the volume constancy, in fact, the aim of this approach is to evaluate the contribute of this additional material to the localized thinning;
- Wall Slope (WS) – it is well known that in SPIF hardening phenomenon balances the stretching one, restoring the stationary conditions after the transitory [AFG+05]. Starting by this idea, a proper trajectory was implemented to test the effect of material hardening; more deeply, the same portion of material was repeatedly worked in subsequent steps with progressive depth: considering the finale shape, the total deformation was split into three steps having the wall angle equal to $1/3\alpha$, $2/3\alpha$ and, finally, α .

- Decremental Slope (DS) – the last approach is based on the assumption that in the first loops material is not efficiently utilized (thinned) since the bending effects tends to delay the stretching phase. Thus, a higher wall angle is artificially used in the first steps in order to make less heavy the stretching phase that follows the first loops. Known the wall inclination angle α , a differential of $\pm 10^\circ$ was applied subdividing into equal parts the punch descent.

No more than three multiple trajectories were executed for each couple shape-strategy as a trade-off between benefits and process slowness. Furthermore, although in the literature it is possible to recognize other approaches [KN99], to introduce a compressive and positive stress distribution into the sheet, they were not considered here, being the work focalized on the simplest configuration (i.e. SPIF) which does not requires any external equipments.

6.4 Experimental evidences

The tool paths comparison was firstly experimentally executed, taking into account an AA1050-O blank material, 1 mm thick. To simplify the investigation, the final geometry was a frustum of cone, having a 90mm major base and a final depth of 50mm; a punch having 12mm diameter and a step size of 1mm were utilised. Finally, according to the formability behavior of the utilized material, just a couple of wall angles, i.e. 60° and 70° , were considered as target values in order to test the proposed tool paths both in stationary and limit conditions.

At the end of each experiment, the thickness distribution was measured by using an optical microscope supplied by Leica, (Figure 6.3).

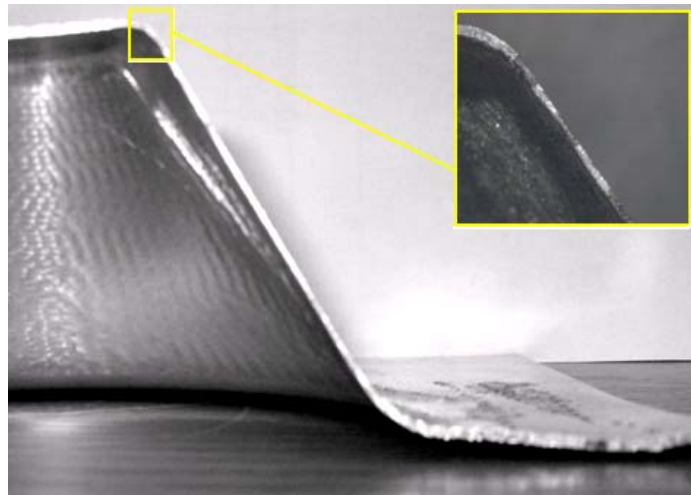


Figure 6.3. Experimental profile.

As expected, changing the tool trajectory, thinning evolves in a different way.

In the next Figures 6.4 and 6.5, the thickness distributions obtained from the experimental campaign, for each target angle (60° and 70°) and tool trajectory (SS,IS,WS and DS), are displayed.

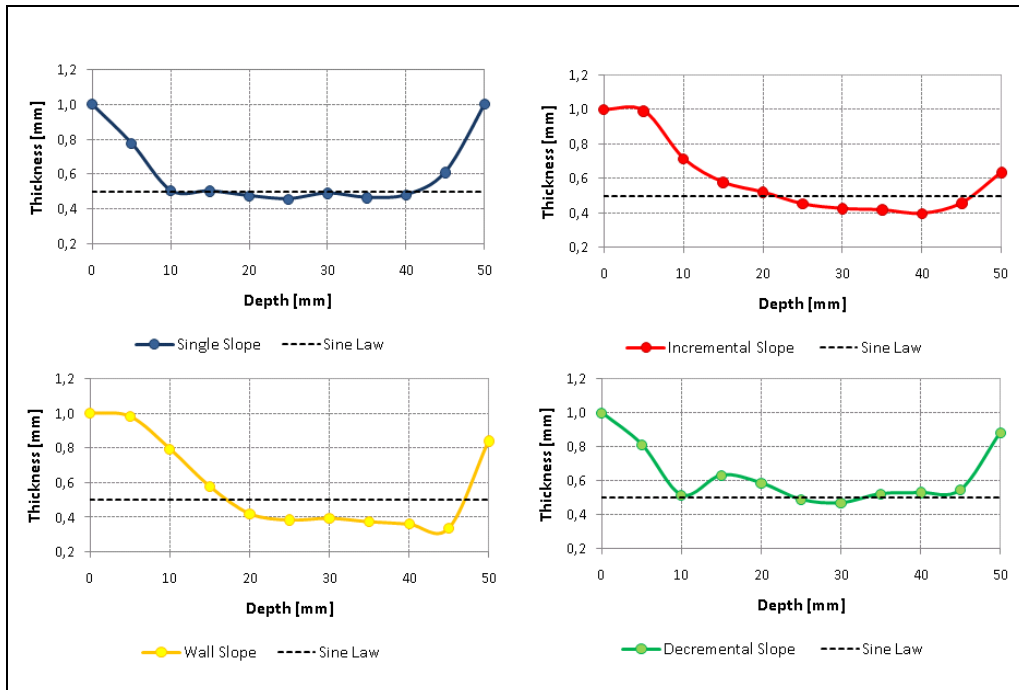


Figure 6.4. Thickness distributions for the investigated tool trajectories and wall inclination angle $\alpha = 60^\circ$.

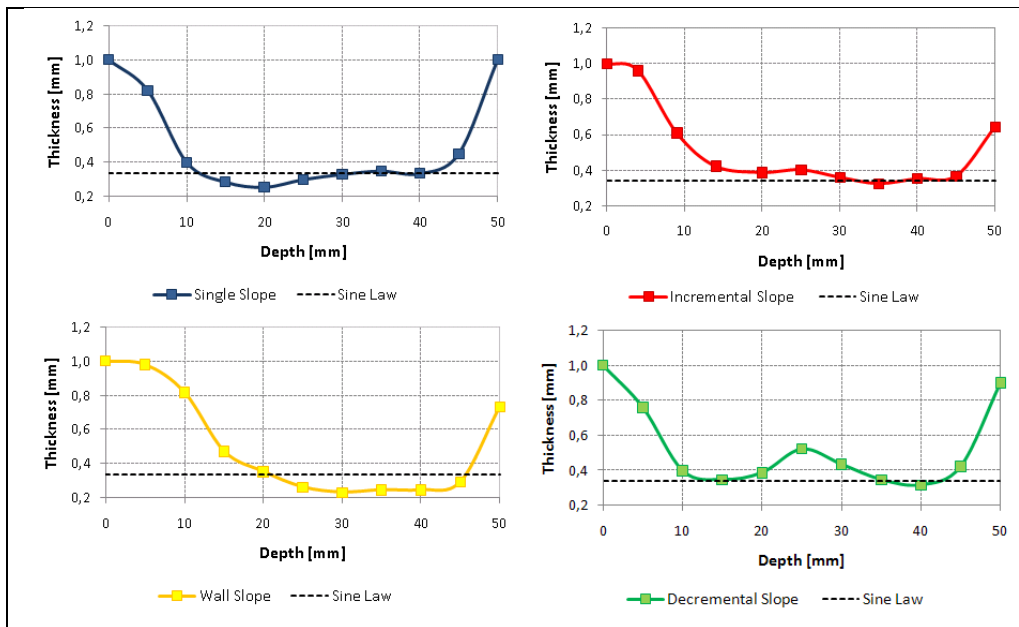


Figure 6.5. Thickness distributions for the investigated tool trajectories and wall inclination angle $\alpha = 70^\circ$.

Observing the above trends, some conclusions can be derived:

- Single Slope tests give back the well known thickness distribution with a larger localised thinning in the experiment carried out with a 70° wall angle. Naturally, the last wall angle represents the critical one for the utilised aluminium alloy, 1 mm thick. For this reason the displayed thickness distributions are also representative of the process limit, without any kind of optimisation;
- applying an Incremental Slope, a lower thinning is measurable on the finale profile. As expected, it can be blamed to the contribute of the additional worked material; in fact, thanks to the partial thinning of the base, the material usually involved results less stretched. In this way, the thickness reaches slowly the Sine Law value;
- the Wall Slope allows to reduce the initial thinning, but introduces a larger variability in the total distribution; in particular, after the former advantage, a thickness lower than the one predicted by the Sine Law was observed close to the minor base. Here, material results more stretched due to the higher hardening that characterises the upper part of the profile, reducing the contribution of the surrounding zones to deformation;
- the Decremental Slope modifies the profile completely introducing a higher variability (and flexibility) in thickness distribution; more in detail, being the first imposed angle higher than the desired one, a sudden thickness reduction can be observed in the first millimetres of depth while, for the same reason, due to the lower wall angle applied in the second part of the tool trajectory, a thicker profile can be detected. In this way, a thickness higher than the one predicted by the Sine Law is always obtained.

Focalizing the attention on the lowest thickness measured for all the investigated specimens and comparing that with the one predicted by the Sine Law, it can be observed a reduction of the sheet thinning with a proper design of the tool trajectory. The lowest thickness measured in the experimental campaign are shown in Table 6.1. The benefits of a not conventional tool path are more evident increasing the process heaviness, as in 70° test; in fact, implementing the DS strategy, the minimum thickness is 40% higher than the SS one.

	Single Slope	Incremental Slope	Wall Slope	Decremental Slope	Sine Law
$\alpha = 60^\circ$	0.46	0.40	0.34	0.47	0.50
$\alpha = 70^\circ$	0.25	0.34	0.23	0.35	0.34

Table 6.1. Smallest thickness measured at the varying of the tool path.

Neglecting Wall Slope results since no advantages were observed, similar performances have been obtained with IS and DS strategies.

However, two drawbacks affect both Incremental and Decremental approaches outputs. In fact, geometrical considerations penalize the Incremental Slope applicability, generating a defect on the minor base where, increasing wall angle, the shape is not completely recovered (Figure 6.6). At the same time, Decremental Slope could results in a not accurate geometry, due to the discontinuities on the wall, reducing the part quality (Figure 6.7).

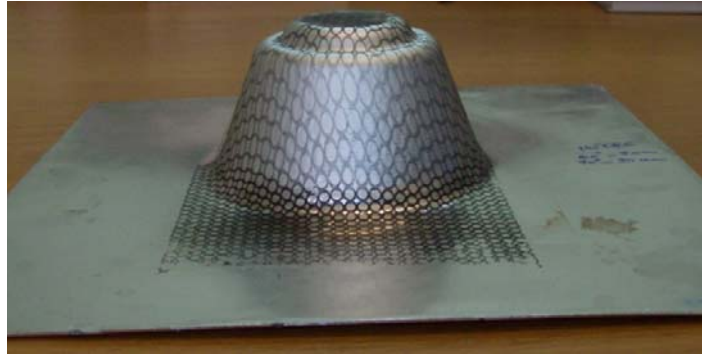


Figure 6.6: Possible defect in Incremental Slope trajectory.

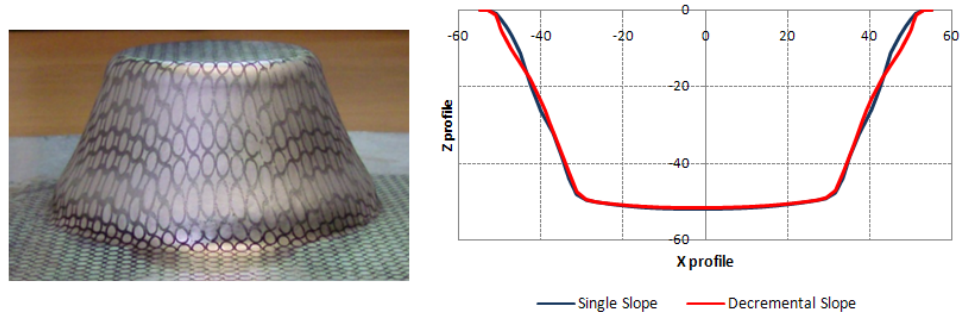


Figure 6.7: Possible loss of accuracy using Decremental Slope.

Of course a trial and error task could reduce both these defects, leading to an optimal solution. For instance it is possible to design a non-linear punch descent in DS. But it is clear that this task is time consuming and a more efficient methodology has to be developed.

Higher advantages, in terms of shortness of the analysis, can be derived introducing a numerical model which allows to better understand the process mechanics.

6.5 Numerical simulation

Nowadays the numerical simulation reached a satisfactory robustness, becoming a reliable tool also for sheet metal forming processes analysis. Naturally, the explicit formulation is the better solution, considering the long process time of AISF processes.

In the study here addressed LS-Dyna ® code was used as simulation tool. It implements the dynamic equations and results very efficient for this kind of process mechanics [ZRT+07]. The punch was modelled as rigid tool and properly meshed, while the blank was meshed with squared 4-nodes shell elements, 2mm in dimension. The Tsay-Hill formulation, with five integration points along the thickness, was applied to the blank elements. Furthermore, the adaptive mesh control was neglected, in order to avoid some instability phenomena. The Barlat-Lian model was used to characterize material yielding behaviour. In order to characterise the material strength tensile tests were previously executed on strips, with different levels of yielding, to consider the larger elongation at rupture occurring in AISF. Both the time scaling and the mass scaling approaches were utilised, verifying the energy condition of the model during the simulation. In particular, considering the utilised explicit formulation, a check on the total kinetic energy was done, verifying that the imposed quota was lower than the 5% of the internal energy. Finally, as regard the time scaling, the simulation time was about one hour with a time step of 2.5×10^{-6} sec, utilising a Xeon dual processor.

Both the profiles, having the wall inclination angles equal to 60° and 70° , were simulated. The above specified model was tested by comparing the output with the previous manufacturing conditions (Figures 6.4 and 6.5). The next Figures 6.8 and 6.9 show the shaded maps of the predicted thickness and the relative comparison between numerical and experimental cases. As it is possible to observe, a good match is reached, thus confirming the model robustness.

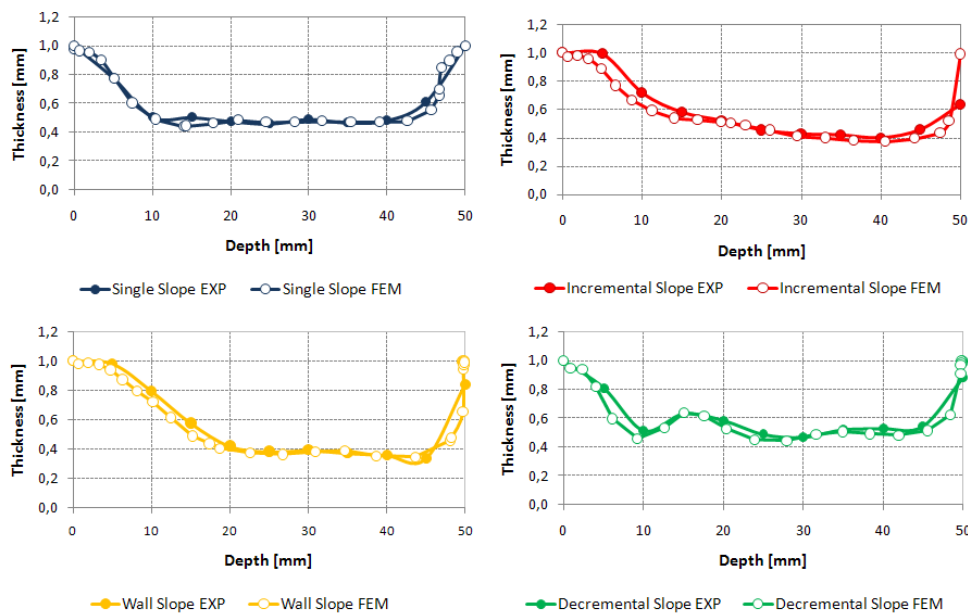


Figure 6.8. Comparison between experimental and numerical thickness distributions, $\alpha = 60^\circ$.

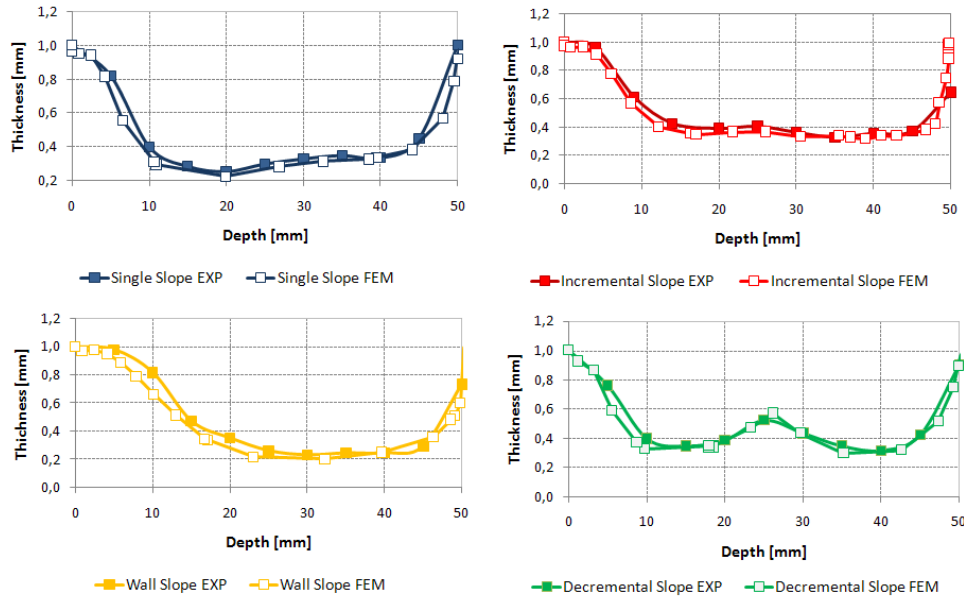


Figure 6.9. Comparison between experimental and numerical thickness distributions, $\alpha = 70^\circ$.

The results authorize to use the numerical tool for optimising the tool trajectory. A numerical simulation, in fact, requires a variable time between 60 and 180 minutes, depending on the number of runs on the same specimens, using a high performance dual processor personal computer.

6.6 Conclusion on the proposed strategy to optimize the thickness distribution

In the previous sections, the tool trajectory was considered as a process variable in Single Point Incremental Forming while usually it is directly derived from the knowledge in machining field.

Four different strategies to generate the tool path have been implemented and analyzed, showing how it is possible to obtain the same final shape modifying the thickness distribution in the specimen. These trajectories are derived starting by the idea to involve material not strictly required from a theoretical point of view or to deform material according to proper but not conventional guidelines. In this way, formability can be conveniently enhanced.

At the same time, optimization task cannot be based only on trial and error approach, thus it was shown how numerical simulation reached the required robustness and suitability.

Warm and Hybrid Incremental Forming

7.1 Introduction and scope of this chapter

Earth overheating and weather changing pushed, in the recent years, the attention of people on pollution and its impact on the future of our life. Thus, a new sensibility on CO₂ emissions is worldwide recognizable and scientists effort is focused on this task [KGK03]. Nowadays words such as sustainability and environment friendly processes belong to the common language, although sometimes the implementative aspects are not so clear.

Within this framework, it is quite obvious that the development of new materials characterized by a favorable strength vs. mass ratio surely represents a strategic issue: such materials would permit to manufacture lightweight vehicles, allowing lower CO₂ emissions.

New materials, in turn, introduce some criticisms, mainly related to the higher costs and sometimes to the lower workability [NAG⁺06]. Among new materials, Magnesium alloys show interesting features, since their cost is not prohibitive and there is already some technical knowledge available on their workability which permits feasible applications. In fact, some components in automotive and transportation industry are already produced in Magnesium alloys.

More in detail, Magnesium alloys require a forming temperature higher than room temperature and it is usually worked in “warm conditions”, namely at a temperature ranging between 200°C and 300°C [ITO⁺04,ZYW06]. These temperatures, in fact, permit to activate new sliding planes and dramatically increase material formability.

Furthermore, in the last few years another trend is clearly discernible in the metal forming industries, namely the development of flexible forming processes, well suitable for small scale or niche productions [JMH⁺05]. One of the most recent and interesting processes is Incremental Forming, which has shown, among the other advantages, the enhancement of material formability due to the peculiar process mechanics [FFM02]. Several incremental forming applications have been proposed in technical literature, mainly on steels and aluminum alloys.

This chapter reports some results of a wide study focused on the application of incremental forming to magnesium alloys. The main objective of the research was the analysis of process suitability, through the evaluation of material formability and the assessment of the role of the most important process parameters. With this aim, a proper equipment to carry out Incremental Forming experiments at the varying of temperature was developed and a wide experimental campaign was properly designed by DOE.

Moreover, as detailed in [Bam08], for a wider industrial use of AISF it is mandatory to find solutions to the main limitations of the process, which are: (i) the long process time, (ii) the sheet thinning, (iii) the limited geometrical accuracy and (iv) the lack of dedicated process planning and modelling tools.

In this chapter, a new hybrid process is analysed, the combination of AISF and stretch forming (SF). This new process combination will be motivated in the ‘state of the art’ section by analysing the work that has been done so far to overcome the limitations of AISF. Each of the process limits will be analysed separately, and hypotheses about the benefit of combining AISF with stretch forming will be formulated. The process combination will be analysed in section 7.3, which starts with the development of a forming machine that combines AISF and stretch forming. A ‘spherical cap’ with a circumferential groove is used to analyse and compare the hybrid process and the basic AISF process regarding sheet thinning and forming time. Finally, an overview over current developments of dedicated CAX algorithms and finite element models for SF+AISF are given, which are essential steps towards an application of the new hybrid process.

7.2 Warm Incremental Forming

7.2.1 Experimental evidences and preliminary investigations

First of all a preliminary investigation was carried out in order to verify formability of Magnesium alloy AZ31 at room temperature. Figure 7.1 shows that formability is very low, while it enhances increasing test temperature.

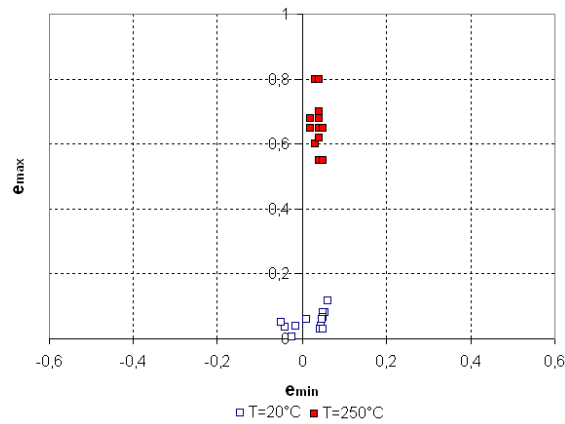


Figure 7.1: Strains at failure at different temperatures.

More in detail, at room temperature failure occurred for a depth of just few millimeters, also forming a truncated cone with a very small wall angle (Table 7.1).

These preliminary results assign a relevant role to the forming temperature: therefore a wide experimental campaign in warm forming conditions was designed.

Wall Angle	Final Height
20°	20.5mm
25°	6.5mm
30°	3 mm

Table 7.1: Failure conditions at room temperature.

7.2.2 The experimental equipment

Figure 7.2 shows the developed experimental equipment. It allows to form truncated cones characterized by different thicknesses up to a temperature of 400°C.

The initial sheet diameter is 130 mm and it is clamped through a proper blankholder; a backing plate is used in order to reduce the bending effect at the die corner. The working area has a diameter of 100 mm. A particular attention was paid to the design of the heating and insulation system, in order to achieve an effective thermal control on the sheet and to avoid thermal gradients. This aim was pursued through numerical simulations and tests.

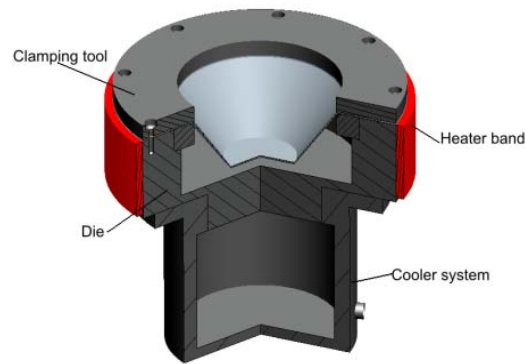


Figure 7.2: The experimental equipment.

The final solution consists of a heater band placed along the external surface of the die, governed by a PID controller with three thermocouples placed at different radii on the specimen. All over the tests, the differences among the measured data were always lower than 5°C.

The tests were carried out on AZ31–O sheets and the target geometry was a truncated cone with a major diameter (D_0) of 100 mm and a depth (H) of 40 mm; the value of the minor diameter depended on the value of the wall inclination angle α . All the experiments were carried out on a 3-axis CNC milling machine; a proper cooling system was necessary to avoid heat transfer to the machine. MoS_2 was utilized to lubricate the interface between punch and sheet. Figure 7.3 reports a sound specimen obtained during the experiments.

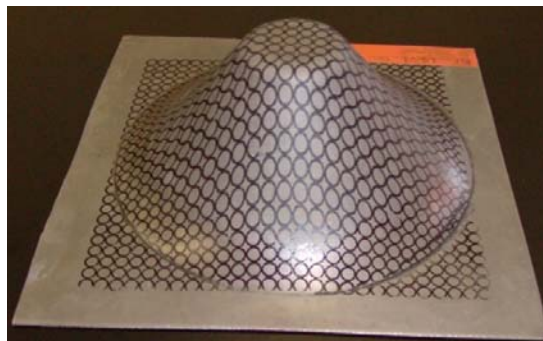


Figure 7.3: A sound specimen ($\alpha=50^\circ$).

7.2.3 Fracture evidences

The experimental tests provided some interesting evidences about material breaking.

During Incremental Forming at elevated temperature, an oxide layer forms on the surface of the sheet. This layer deeply influences material strength, increasing the required load, but, in the meantime makes the material brittle on the surface.

This circumstance causes a particular fracture evidence, as reported in Figure 7.4. Different layers of material slide the one on the other, generating a break and, thus, process failure.

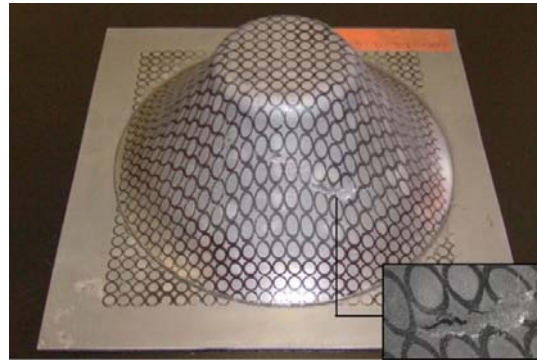


Figure 7.4: Material failure due to oxidation.

7.2.4 Plan of the experiments and main results

In order to determine the formability limits of AZ31 in Incremental Forming, as well as to determine the correlations between formability and process parameters, an experimental campaign was carried out based on a proper Design of Experiments (DOE).

Starting from the available base of knowledge three main process parameters were taken into account namely: the punch diameter (D_p), the tool depth step (p) and the sheet temperature (T). Three levels for each of them were considered. In particular, as concerns sheet temperature, the considered range was 200-300°C, which corresponds to the maximum formability conditions [CH03, Lee07].

On the other hand, for sake of simplicity, sheet thickness was fixed equal to 1 mm all over the tests. Furthermore, since the aim of the research was to assess failure conditions, the wall inclination angle was increased by 2.5° up to reach the critical value (α_{max}) for each set of parameters. In order to reduce the number of experiments, maintaining, in the meantime, the statistical consistency of the results, a CCD plan was executed instead of a fully orthogonal one. Table 7.2 shows the plan ranges.

Parameters	Factors Levels	
	Lowest	Highest
Sheet Temperature	200° C	300° C
Punch Diameter	12 mm	18 mm
Tool Depth Step	0.3 mm	1,0 mm

Table 7.2: Ranges of the experimental plan.

The sheets were previously electro-chemically marked with circles (3 mm diameter), in order to measure the major strain at failure (FLD₀ value): all over the tests, the minor strain was always close to zero.

Tables 7.3 and 7.4 summarize some of the experimental results for the extreme temperature values: the limiting wall inclination angle increases at increasing sheet temperature. The maximum α value was 60° at 300°C.

These results confirm the significant enhancement on material workability associated to warm forming conditions.

		Tool Depth Step			
		0.3 mm		1 mm	
		Tool Diameter			
		12 mm	18 mm	12 mm	18 mm
Slope Angle	45°	Sound	Sound	Sound	Sound
	50°	Sound	Sound	Sound	NO
	55°	NO	NO	NO	
	60°				
	65°				

Table 7.3: Experimental results at 200°C.

		Tool Depth Step			
		0.3 mm		1 mm	
		Tool Diameter			
		12 mm	18 mm	12 mm	18 mm
Slope Angle	45°	Sound	Sound	Sound	Sound
	50°	Sound	Sound	Sound	Sound
	55°	Sound	Sound	Sound	NO
	60°	Sound	NO	NO	
	65°	NO			

Table 7.4: Experimental results at 300°C.

All over the experimental campaign a Kistler piezoelectric dynamometer was used, fixed to the clamping equipment, to measure the forming force.

The comparison of the measured forces permits to assess that the forming load increases increasing the tool depth step, the wall inclination angle and the tool diameter, while it decreases increasing the test temperature. The forming load strongly depends on the tool depth step value; figure 7.5 shows that at increasing the latter parameter in the mentioned range, the measured forming force increases of about 40%.

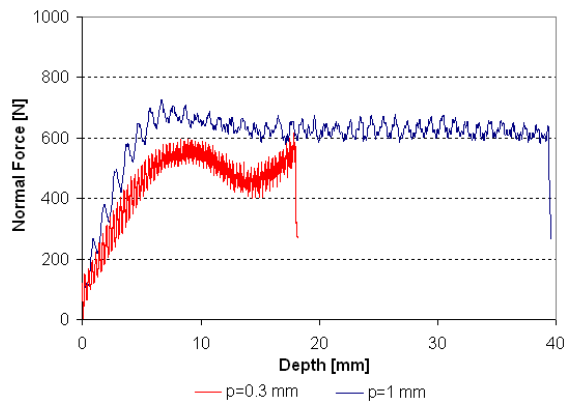


Figure 7.5: Forming load vs. tool depth step trend.

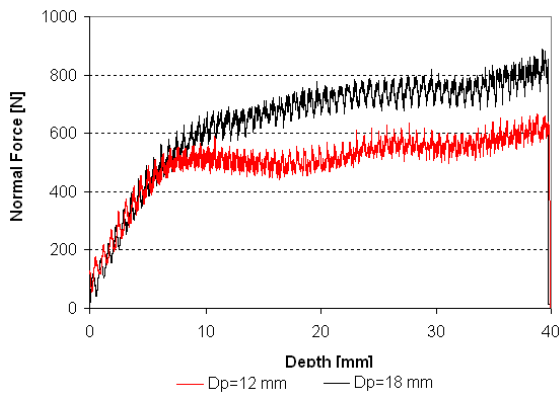


Figure 7.6: Forming load vs. tool diameter.

On the contrary, less significant effects were observed varying the tool diameter even if about 25% of spread is recognized (Figure 7.6). The strongest dependence is, as easily predictable, on the testing temperature. Figure 7.7 shows that a reduction up to 50% was measured between experiments carried out at 200°C and 300°C respectively. Furthermore, for a $\alpha=55^\circ$ material breakage occurred at 200°C while a sound component was formed at 250°C and more.

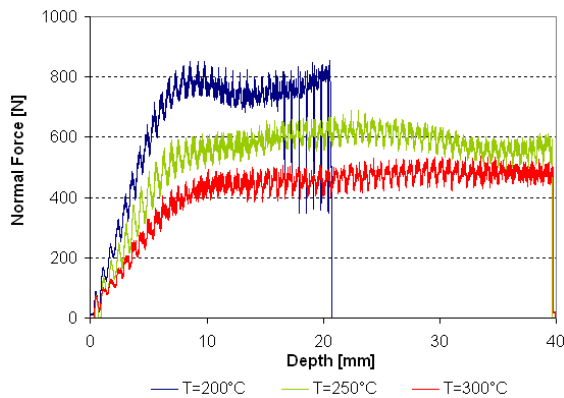


Figure 7.7: Forming load vs. temperature trend.

Figures 7.8-7.10 reports some interesting results on material formability varying the process parameters. Formability was measured through the mean value and the standard deviation of FLD_0 .

The highest FLD_0 value was measured during the test executed at 250°C, with the smallest tool depth step ($FLD_0=1,6$). This result is fully consistent, in terms of forming temperature, with the state of the art on magnesium formability in conventional forming processes. All over the temperature range, the best formability results were always obtained utilizing the smallest tool depth step. On the contrary, no general considerations on tool diameter can be assessed because no monotonic results were found.

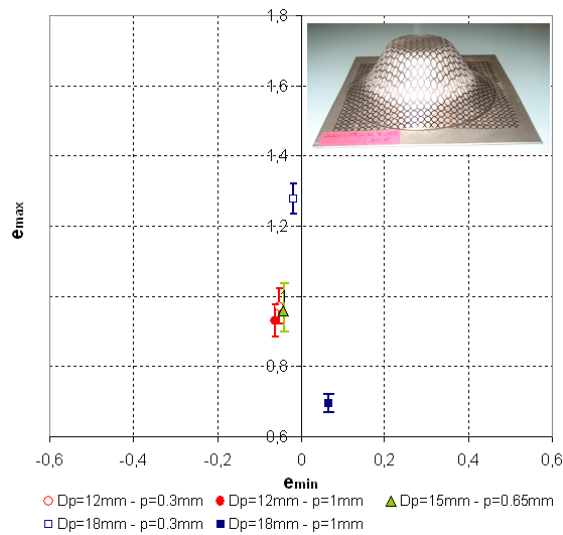


Figure 7.8: FLD_0 at 200° C (mean value and standard deviation).

Finally the measured formability data were utilized for a rigorous statistical analysis.

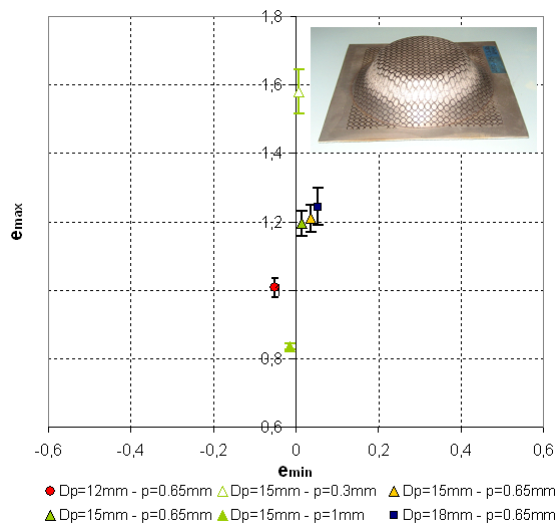


Figure 7.9: FLD_0 at 250° C (mean value and standard deviation).

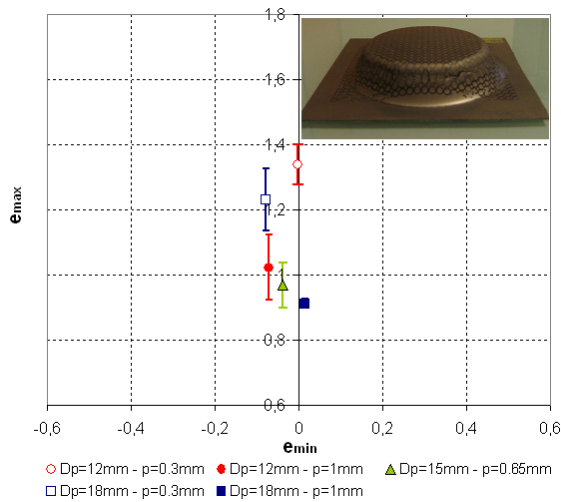


Figure 7.10: FLD_0 at $300^{\circ}C$ (mean value and standard deviation).

In particular, applying the response surface statistical model, an ANOVA analysis was run in order to investigate the effect of each input variable (namely the process parameters) and their interactions on the output (the formability). ANOVA analysis definitely confirmed the main role played by the forming temperature (Table 7.5).

Variable	Influence on FLD_0
T	High
D_p	Low
P	High
$D_p \cdot p$	Medium
$D_p \cdot T$	No
$T \cdot p$	No
T^2	High
D_p^2	No
p^2	No

Table 7.5: Influence of input variables on FLD_0 .

In the meantime, FLD_0 is also influenced by the tool depth step and its interaction with the tool diameter. On the contrary the dependence on the punch diameter D_p is quite small. Both these statements are consistent with the results reported in previous figures and tables.

The robustness of the results is confirmed by the high correlation indexes equal to $R^2=91\%$ and $R^2_{Adjusted}=90\%$; they denote the goodness of the fitting surface, the efficiency of which is also confirmed by the analysis of the residuals statistical distribution.

7.2.5 Conclusion on the Warm Incremental Forming Process

In this work a wide investigation on the effects of some process parameters on Incremental Forming of AZ31 Magnesium alloy was carried out.

Some important conclusions can be stated:

- a dramatic formability enhancement is possible working magnesium in warm conditions;
- Incremental Forming seems to be an effective process in the investigated conditions;
- the influence of temperature and tool depth step on formability are quite relevant, while the role of tool diameter is negligible in the investigated range;
- maximum formability occurs at 250°C; this result is fully consistent with the one obtained for other forming processes, like deep drawing.

7.3 Hybrid Incremental Forming Process

The main drawbacks of AISF processes presented in the previous sections are here addressed and discussed in order to motivate the idea to build from scratch a new hybrid process, namely Hybrid Incremental Forming process and obtained combining AISF with stretch forming (SF) process.

The relevant AISF limit are due to:

Sheet thinning

Thinning in AISF depends on the wall angle α according to the so-called sine law [KN99]:

For parts with wall angles greater than 60-70 degrees, multistage forming strategies have to be used to avoid excessive thinning [HAB⁺04]. In multistage forming, a pre-form, several intermediate shapes and the final part geometry are formed by AISF. As reported by Hirt et al. [HAB05] a process time of approximately 7 hours is required to produce a square box of 200 x 200 x 60 mm³ in 15 forming stages. The intermediate stages had to be found by trial and error. As a consequence, this approach cannot be easily transferred to more complex parts. An improved forming strategy detailed in [HAB05] generates a pre-form by stretching the sheet metal roughly over the male die using AISF with a large step-down. A stiffening brace was manufactured using this strategy [HAB05], but pre-stretching by AISF leads to large forming forces and increases the likelihood of wrinkling, which makes it hard to transfer this approach to other part geometries.

Geometric accuracy

Recently, Micari et al. [MAF07] have studied the feasibility of some forming strategies that aim at improving the accuracy of parts formed by AISF, identifying tool path ‘overbending’ as a promising approach to improve the accuracy of a part. In contrast, the work detailed in [HAB+04] shows that ‘overbending’ induces waves on the formed part, and that a part manufactured by AISF will contain considerable residual stresses as a consequence of the cyclic loading and unloading during forming.

Forming time

AISF is an incremental forming process. The time to manufacture a part is determined by the length of the tool path and the average travelling speed of the forming tool. Bambach [Bam08] shows that the process time required to manufacture a conical frustum of height h , bottom radius $r=h$ and top radius $2r$ scales quadratically with h : Assuming an average speed of 500 mm/s and a step-down of 0.2 mm for the tool path, the forming time is already greater than one day for a conical frustum of 1 m height.

Finite elements modelling

An overview of process models for AISF is given in [JMH+05, Bam08, HAB04]. In particular, [HAB04] analyses the CPU time required to simulate the forming of the conical frustum mentioned in the preceding paragraph on a single processor machine using a dynamic explicit code. The FEA takes almost 10 days using tool path with a step-down of 0.5 mm, and more than 20 days with a step-down of 0.2 mm. This makes FEA prohibitive for larger parts. Although it is not inconceivable that ways will be found in the future to overcome the process limits of AISF and to enable model-based process planning, an alternative process will be analysed in this paper: the combination of AISF and stretch forming.

All these issues motivate the idea of a novel process as above reported.

The concept of the new hybrid process is illustrated in Figure 7.11, which indicates that stretch forming is used to create a pre-form in a first forming step. Stretch forming will not yield the final part geometry (otherwise the process combination would not be necessary). Hence, features such as pockets, corrugations or grooves that are not formed during SF are formed using AISF.

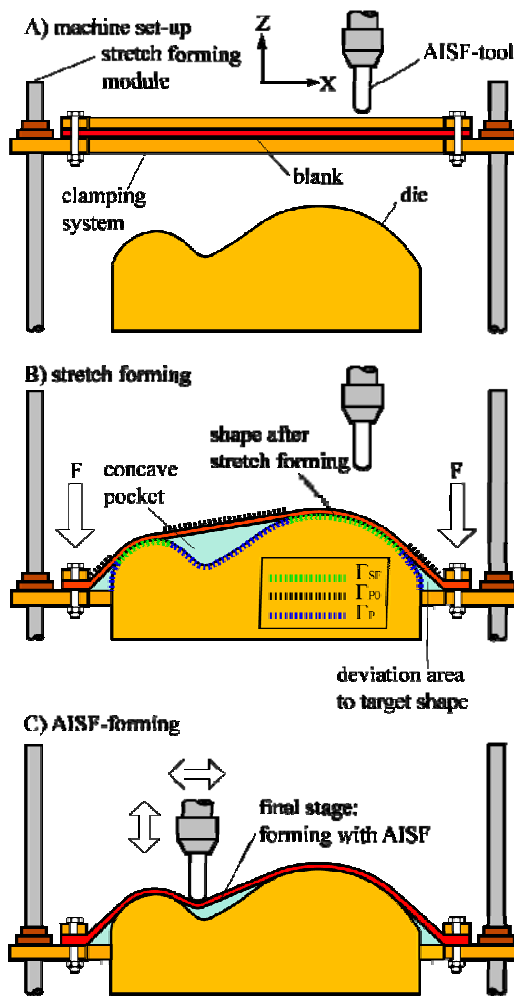


Figure 7.11: Principle of the process combination.

For the discussion to follow, it is useful to introduce designations for the surface area of the sheet in contact with the die after stretch forming, Γ_{SF} , and its complement, the surface area of the sheet that is not in contact with the die after stretch forming, denoted by Γ_{P0} . Γ_{P0} is available to form those part features by AISF that cannot be formed by stretch forming. These features cover a surface area Γ_P , which is the area of the die that is not in contact with the sheet metal after stretch forming. The following advantages are expected from the combination of AISF and SF:

1. The process time of AISF increases with the surface area covered by the tool path. The process time for stretch forming scales with the total height of the part. Hence, the combination of AISF and SF is expected to have a shorter process time for shallow parts with a large surface area.
2. For a given part, AISF and SF yield a different distribution of sheet thinning. If a pre-form can be produced by SF that leaves more sheet thickness for part features such as pockets (Γ_{P0}) than would be available if the same pre-form were produced by AISF, the

process combination should yield less thinning in the pocket areas compared to AISF. Thus, the process combination should offer new possibilities to overcome the thinning limits of AISF.

3. Stretch forming is known to yield parts with a good accuracy due to the tensile state of stress [Lan90]. AISF could benefit from stretch forming in two ways: (i) by creating a pre-form using SF that would be more accurate than a pre-form manufactured by AISF. (ii) by superimposing tensile stresses during AISF, i.e. by applying stretch forming simultaneously to AISF in order to reduce the residual stresses induced by the cyclic bending and unbending.

4. In the same way as the forming time is reduced, the time needed for the simulation of the process should be smaller for SF+AISF compared to AISF. Hence, process planning and optimisation would become more viable for the process combination than for AISF.

The statements 1-4 do not hold for arbitrary parts. It will be necessary to identify part geometries for which the process does offer these advantages. Due to the restricted space, only the hypotheses 1, 2 and 4 are tested in this paper. A hemispherical base geometry with circumferential groove is used to analyse the possible benefits of the process combination compared to pure AISF. As detailed above, the machine set-up will be discussed first before the experimental tests are given.

7.3.1 Process Investigation: the experimental set-up

Figure 7.12 shows an AMINO DNLC-RB forming machine in which the original hydraulic control system of the frame was replaced by 4 screws jacks driven by a servo motor. The screw movements are controlled by a closed-loop control system. With this set-up, a downward force of 50 kN can be exerted in order to perform stretch forming experiments on soft materials, e.g. aluminium alloys.

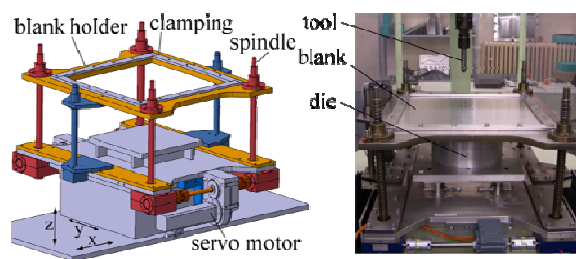


Figure 7.12: The experimental set up.

7.3.2 Experimental test

As mentioned above, a hemispherical part with circumferential grooves serves as benchmark part for the analysis of the sheet thinning induced by the combined process. Two experiments will be presented:

1. The forming of a section of a hemisphere without pockets was considered in order to analyse the differences in material flow induced by AISF and SF. The aim was to analyse sheet thinning using a simple part for which both AISF and stretch forming can be treated analytically.
2. The forming of a section of a hemisphere with a groove around the circumference is analysed to show the benefit of the process combination of AISF and SF compared to pure AISF both in terms of sheet thinning and forming time.

7.3.3 Forming of a hemisphere

A cap of a hemisphere was formed by AISF and by stretch forming using a die of 240 mm radius and 1 mm AA1050-O sheets. The forming depth was 25 mm, which was sufficient to show the different thinning behaviour of AISF and SF. The measured thickness distributions are given in Figure 7.13. The sheet thickness in AISF decreases in radial direction with increasing wall angle, in accordance with the sine law.

Sheet thinning in stretch forming over a hemispherical punch has been analysed e.g. in [Cha00]. Under frictionless conditions, the maximum amount of thinning occurs at the pole. With non-zero friction, the maximum thinning can be found at a certain distance from the pole. After the maximum, the sheet thinning drops in radial direction, which is in contrast to the course of sheet thinning obtained by AISF. Two conclusions can be drawn from this result:

1. Stretch forming can be used to induce thinning in areas that would not be deformed by AISF, in this case in the pole. Hence, the combination of AISF and SF offers the possibility to achieve a more homogeneous thickness distribution compared to either SF or AISF.
2. There is a certain point along the radius where AISF and SF induce the same amount of thinning. Beyond that point, less thinning is generated by SF than by AISF. If a pocket is lying beyond that point, more material would be available to form the pocket when a pre-form made by SF is used.

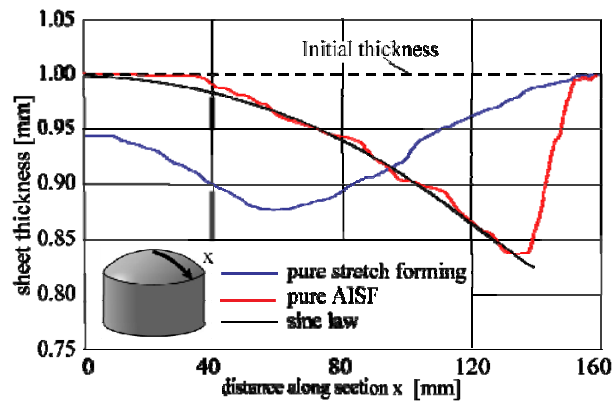


Figure 7.13: Comparison of thickness reduction induced by AISF and stretch forming.

From the theory of stretch forming over a hemispherical punch it follows that the position of maximum thinning in SF and the radial thickness distribution changes with the forming depth. The point at which AISF and SF yield equal thickness reduction is shifted radially outwards for greater forming depths.

In order to verify the second statement, a section of a hemisphere with a circumferential pocket was formed (Figure 7.14) using a male aluminium die and DC06 mild steel sheets with a sheet thickness of 0.7 mm. In the case of the hybrid SF+AISF process, a pre-form is created by stretching the sheet over the die to a forming depth of 80 mm. After that, the circumferential groove is formed by AISF. To have comparable conditions to stretch forming, the AISF process is performed in two stages: first, a pre-form is created that corresponds to the pre-form created by SF. In a second forming step, the pocket area is created. For the AISF operations, both in hybrid and in pure AISF, a punch diameter of 30 mm and a tool step down of 0.1 mm were used.

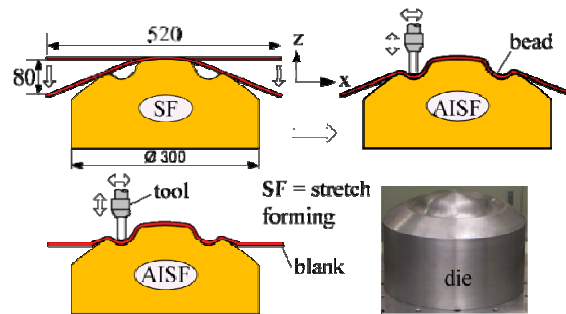


Figure 7.14: Comparison of AISF and SF+AISF for a spherical cap with a groove.

Figure 7.15 shows the comparison of the thickness distribution obtained with the hybrid process and pure AISF along a radial section. Both for AISF and SF+AISF, the maximum thickness reduction was measured in the groove. The maximum measured thinning is smaller

for SF+AISF and the distribution of the thickness along the section is more uniform than in the case of pure AISF.

It is worth mentioning that the stretch forming unit does not offer enough force to manufacture a complete hemisphere by stretch forming of steel sheets. Hence, only a spherical cap was considered, and the groove had to be placed in an area where the advantage of the process combination is not overly pronounced.

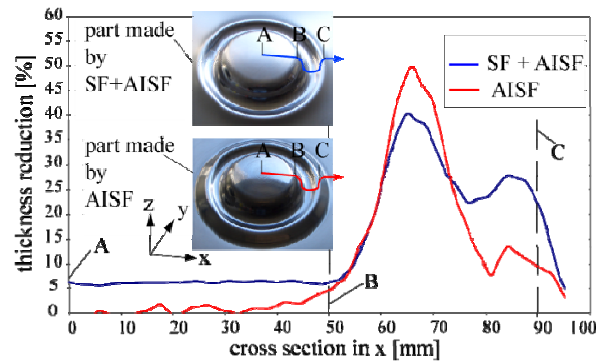


Figure 7.15: Comparison of thickness for pure AISF and AISF+SF.

7.3.4 Process modelling

A finite element model was set up in LS-DYNA for the forming of the grooved sphere both for pure AISF and the combined process. In the FE model for SF+AISF, the sheet was meshed with 13,500 shell elements for the first forming stage, i.e. the stretch forming. Automatic remeshing was applied in the AISF forming step which yielded approximately 30,000 elements at the end of the simulation. The CPU time for the simulation of the stretch forming step was 2 hours, while the simulation of the forming of the groove took approximately 6 days on a 2 processor machine. Figure 7 shows the distribution of major surface strains measured on the formed part using a ‘gom ARGUS’ system in comparison with the numerical results.

The numerical and experimental results show a similar deformation pattern. The comparison of the results along a radial section line in Figure 7.16 shows that the FEA predicts well the strains found in the experiment.

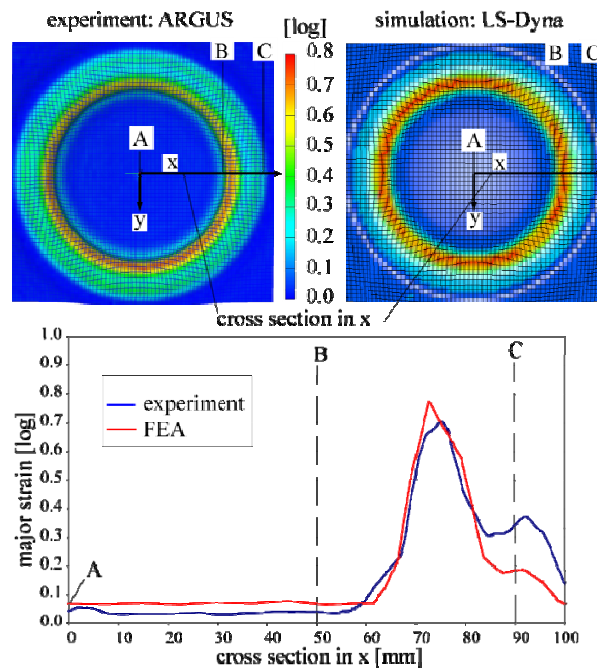


Figure 7.16: Comparison of FEA and experiments for SF+AISF.

In the simulation of pure AISF, a fine mesh with 30,000 elements has to be used from the beginning. Due to the length of the tool path, 39 days were needed to simulate the whole AISF process. Figure 7.17 shows a comparison of measured and simulated major strains along a radial section, similar to Figure 7.16. Trials showed that the simulation cannot be speed up by applying more mass scaling or using less elements without losing accuracy.

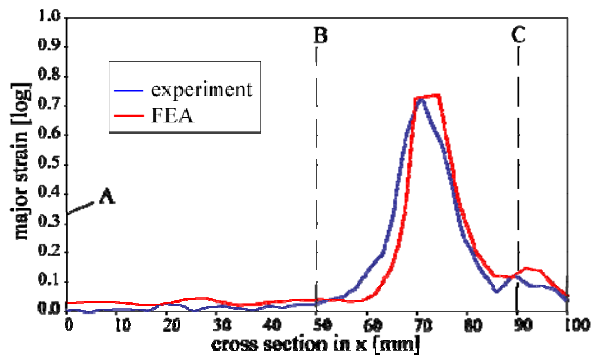


Figure 7.17: Comparison of FEA and experiments for AISF.

The results show that SF+AISF has the advantage that the simulation of the stretch forming can be completed in a relatively short time, even for a larger part, which makes it possible to simulate and optimise at least the first forming stage.

7.3.5 CAX developments

In order to save time through the process combination of AISF and SF compared to pure AISF, the time needed for the stretch forming and the time needed to form the remaining features using AISF must be minimised. However, the areas Γ , Γ_{p0} and Γ_p shown in Figure 2 are not known a priori, but are the result of the stretch forming operation and the springback after forming. For a minimum forming time per part, it is necessary to identify the regions which have to be formed by AISF. Since the prediction of the part shape after SF concerning the thickness distribution and geometry is not possible analytically for complicated shapes, the utilisation of FEA is indispensable.

To detect the sections that need AISF processing, the process chain depicted in Figure 7.18 was developed, which enables to optimise the process time and provides the NC-codes for both SF and AISF. First, the target part is transferred to Unigraphics NX. With NX, the NC-path for SF is generated and transferred to LS-DYNA. The stretch forming simulation in LS-DYNA yields the part geometry and sheet thickness distribution. This information is transferred back to NX. An algorithm that detects deviations between the simulated geometry and the target geometry was implemented in UG NX. This algorithm identifies the areas that need to be deformed by AISF and creates the NC-path programmes for the forming of these areas. This approach was used to optimise the tool paths for the benchmark part. The forming time using AISF was 35 min, which could be reduced to 20 min in the combined process.

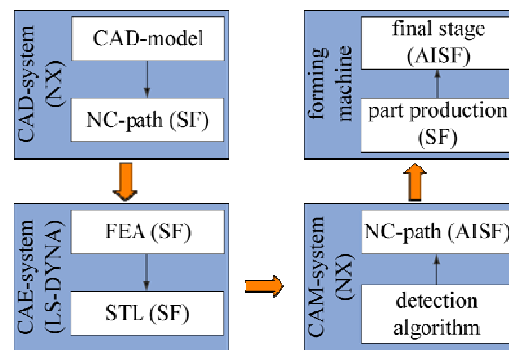


Figure 7.18: CAX process chain.

7.3.6 Summary and outlook on the proposed hybrid process

A new hybrid process, the combination of AISF and stretch forming was put forward and investigated in this paper. It can be concluded that with the process combination of AISF and SF

- a noticeable reduction of production time compared to AISF is possible, especially when the areas that need to be processed by AISF are identified in advance,

- in comparison to AISF a more uniform thickness distribution with a reduced amount of maximum thinning can be achieved
- process planning based on FEA seems to be more viable than for AISF

Future research will focus on the effect of the process combination of SF and AISF on the geometrical accuracy and the forming limits. The latter is important when part features such as pockets have to be formed from a pre-stretched sheet. From an application point of view it seems important to consider industrial parts in the future.

Conclusions

New methods of forming sheet metal are, nowadays, available as answer to the modern market trend; the manufacturing field strongly continues to ask either custom manufactured parts or small batch production quantities, with a very short time to market between the design phase and the manufacture of the product.

In this contest, Asymmetric Incremental Sheet Forming is an “ideal candidate” for making complicated shapes from sheet metal in a easy way. It makes the forming of sheet metal a flexible operation and is a technology easily available for all facilities having access to a three axis CNC milling machine. As highlighted in the former chapter of the thesis, there are two variations to the process: the first is characterized by two contacts points, where one of the parts is a partial or a full die; the other one, instead, is related to a single contact point, which impress local deformation to the sheet. In particular, on the last kind was focalized the attention of the present PhD thesis.

Although a relatively new process, its potentiality is already defined by the scientific community, in fact several research groups are involved in its development. With this perspective, the present works has tried to contribute to the process well understanding, by means of a detailed study on the process fundamental aspects, on the implementation of a suitable numerical model and, finally, on the feasibility analysis related to the process industrial application.

More in detail, after a careful analysis of the state of art, some specific research contexts have been fixed, following two different approaches and goals. From one side, the necessity to improve and acquire more base of knowledge on the process main aspects seems to be impellent, in order to increase the process stability. For this purpose, a particular attention was paid to the formability property, which strongly emphasizes the peculiar process mechanics; contemporary, great attention was dedicated to define some “spy variables” of process stability, such us the thickness distribution along the profile or the force trend revealed with an on-line measurement instrument.

On the other side, the evaluation of the process suitability from an industrial point of view seems to be a strategic point. With this perspective, a lot of time and resource of the PhD

course was spent on the analysis of the main drawbacks which affect SPIF technique. First of all, the geometrical accuracy was widely investigated from experimental and numerical points of view. Several optimization strategies have been performed, in order to improve the component accuracy.

Finally new processes have been introduced namely Warm Incremental Forming and Hybrid Incremental Forming in order to extend the formability or, in the case of Hybrid Incremental Forming, to overcome some process limitations such as process time , geometrical accuracy and part feasibility.

References

- [ABB+08] Ambrogio G., Bruni C., Bruschi S., Filice L., Ghiotti A., Simoncini M.: *Int J Mater Form*, DOI 10.1007/s12289-008-0027-y (2008).
- [ABF+07] Ambrogio G., Bruni C., Filice L., Gabrielli F., 2007, On the Formability of Magnesium Alloy sheets in warm conditions, *Key Engineering Materials* 344, pp. 55-62.
- [ACC+08] Attanasio A., Ceretti E., Giardini C., Mazzone L., Asymmetric two points incremental forming: improving surface quality and geometric accuracy by tool path optimization, *International Journal of Material Processing Technology*, Vol. 197 (2008), 59-67.
- [ACF+07] Ambrogio G., Cozza V., Filice L., Micari F., An analytical model for improving precision in Single Point Incremental Forming, *International Journal of Material Processing Technology*, Vol. 191 (2007), 92-95.
- [ADF+05] Ambrogio G., De Napoli L., Filice L., Gagliardi F., Muzzupappa M., Application of Incremental Forming process for high customised medical product manufacturing, *International Journal of Materials Processing Technology* 162-163 (2005) 156-162.
- [ADF+07] Ambrogio G., De Napoli L., Filice L., Muzzupappa M., Experimental evidences concerning geometrical accuracy after unclamping and trimming incrementally formed components, *Key Engineering Materials*, Vol. 344 (2007), 535-542.
- [AF04] Alberti, N. and Fratini, L., 2004, Innovative Sheet Metal Forming Processes: Numerical Simulations and Experimental Tests, *International Journal of Materials Processing Technology* 15, 2.
- [AFD+04] Ambrogio G., Filice L., De Napoli L., Muzzupappa M., A simple approach for reducing profile diverting in a single point incremental forming process, *Journal of Engineering Manufacture – Part B*, vol. 219, 2004, 823 – 830
- [AFF+03] Ambrogio G., Filice L., Fratini L., Micari F., “Some relevant considerations between the process parameters and process performance in incremental forming of metal sheet”, 6th Esaform Conference Proceedings, University of Salerno, Salerno, Italy, 2003, 175-178.
- [AFF04] Ambrogio, G. ; Filice, L. ; Fratini, L. ; Micari, F.: Process mechanics analysis in single point incremental forming. In: NUMIFORM 2004—Proceedings of the 8th International Conference on Numerical Methods in Industrial

-
- Forming Processes, American Institute of Physics, 2004, pp. 922–927
- [AFG+05] Ambrogio G., Filice L., Gagliardi F., Micari F., “Sheet thinning prediction in Single Point Incremental Forming”, *Advanced Material Research*, vol. 6-8, pp. 479-486.
- [AFG+05b] Ambrogio, G. ; Filice, L. ; Gagliardi, F. ; Micari, F. ; Umbrello, D.: Application of the neural network technique for reducing the springback in incremental forming processes. In: *ESAFORM 2005: Proceedings of the Eight ESAFORM Conference on Material Forming Vol. 2*. Cluj-Napoca, Romania: The Publishing House of the Romanian Academy, 2005. – ISBN 973–27–1174–4, pp. 699–702
- [AFG+04] Ambrogio G., Filice L., Gagliardi F., Micari F., *Advanced Material Research*, 6-8, 479-486 (2004)
- [AFG+05] Ambrogio G., Filice L., Gagliardi F., Micari F., Sheet Incremental Forming: a new process configuration allowing controlled flow of the sheet material under the blank-holder, *Proceeding of Advanced Technology of Plasticity – Proceedings of the 8th ICTP (2005)* 351-352.
- [AFM+07] Ambrogio G., Filice L., Manco G.L., Forcellese A., Simoncini M., “A FE approach to design warm deep drawing operations of magnesium alloys”, *Proc. 8th A.I.Te.M. Conference (2007)*, pp. 109-110.
- [AFM06] Ambrogio G., Filice L., Micari F., A force measuring based strategy for failure prevention in incremental forming, *Journal of Materials Processing Technology* 177 (2006) 413-416.
- [AFS+06] Ambrogio G., Filice L., Silvestri F., Micari F., “Rapid Prototyping through the application of AISF technique”, *9th Esaform Conference Proceedings*, University of Strathclyde, Glasgow, UK, 2006, 875-878.
- [AH02] Andersson A., Holmberg S., “Simulation and verification of different parameters effect on springback results” in *Numisheet Conference Proceedings*, Jeju Island, Korea, 2002 , pp. 201-206
- [AST07] Allwood, J.M. ; Shouler, D.R. ; Tekkaya, A.E.: The increased forming limits of incremental sheet forming processes. In: *SheMet '07, Proceedings of the 12th International Conference on Sheet Metal*, Apr 01.-04.2007,Palermo,Sicily, Italy, Trans Tech Publication Ltd., Switzerland, 2007. – ISBN 0–87849–437–5, pp. 621–628
- [Bam08] Bambach, M., 2008, *Process Strategies and Modelling Approaches for Asymmetric Incremental Sheet Forming*, *Umformtechnische Schriften* Band 139, Shaker Verlag, Aachen.
- [Bar06] Barrios E., BsMD: Bayesian Screening and Model Selection, R-package, URL: <http://cran-r-project.org/src/contrib/Descriptions/BsMD.html> (2006)

- [BEH+07] van Bael, A. ; Eyckens, P. ; He, S. ; Bouffioux, C. ; Henrard, C. ; Habraken, A.M. ; Duflou, J. ; Houtte, P. V.: Forming limit predictions for single-point incremental sheet metal forming. In: ESAFORM 2007: Proceedings of the 10th ESAFORM Conference on Material Forming, American Institute of Physics (AIP), 2007. – ISBN 973–27–1174–4, pp. 309–314
- [BHA04] Bambach M., Hirt G., Ames J., Modeling of optimization strategies in the incremental CNC sheet metal forming, Proc. of 8th NUMIFORM Conference, 2004, June 13-17, Columbus/Ohio (USA). Proceeding on a CD.
- [BHH05] Box G.E.P., Hunter W.G., Hunter J.S., Statistics for experimenters, 2nd ed., John Wiley, New York (2005).
- [BHJ03] Bambach, M. ; Hirt, G. ; Junk, S.: Modelling and experimental evaluation of the incremental CNC sheet metal forming process. In: Proceedings of the 7th International Conference on Computational Plasticity, CD-ROM, CIMNE, Barcelona, 2003, pp. 1–17
- [BL89] Barlat F., Lian, International journal of plasticity, 5, 51-66 (1989).
- [BM93] Box G.E.P., Meyer R.D., Finding the Active Factors in Fractionated Screening Experiments, Journal of Quality Technology, Vol. 25 (1993), 2, 94-105.
- [BTH07] Bambach M., Todorova M., Hirt G.: Experimental and numerical analysis of forming limits in CNC incremental sheet forming, Key Engineering Material Vol. 344 (2007), 511-518.
- [CCY+04] Chen H.S., Chao J., Yao H., Liu S.D., Kinsey B.: J. of Materials Processing Technology, vol. 151 (2004), pp. 133-140.
- [CH03] Chen F.-K., Huang T.-B., 2003, Formability of stamping magnesium-alloy AZ31 sheets, Journal of Materials Processing Technology 142, pp.643-647.
- [Cha00] Chakrabarty J., 2000, Applied Plasticity, Springer
- [EHB+07] Eyckens, P. ; He, S. ; Bael, A. V. ; Houtte, P. V. ; Duflou, J.: Forming limit prediction for the serrated strain paths in single point incremental sheet forming. In: AIP Conference Proceedings Volume 908, American Institute of Physics, 2007, pp. 141–146
- [ETP+98] El-Mahallawy N.A., Taha M.A., Pokora E., Klein F., On the influence of process variables on the thermal conditions and properties of high pressure die-cast magnesium alloys, J. Mater. Process. Technol. 73 (1998) 125–138.

- [FAM06] Filice L., Ambrogio G., Micari F., “On-Line Control of Single Point Incremental Forming Operations through Punch Force Monitoring”, *Annals of the CIRP*, vol. 55/1/2006, pp. 245-248.
- [FES+07] Forcellese A, El Mehtedi M., Simoncini M., Spigarelli S., 2007, Formability and microstructure of AZ31 magnesium alloy sheets, *Key Engineering Materials* 344, pp. 31-38.
- [FFG+98] Forcellese A., Fratini L., Gabrielli F., Micari F., The evaluation of springback in 3D and coining processes, *J. of Materials Processing Technology*, vol. 80-81, 1998, 108-112.
- [FFM02] Filice, L., Fratini, L., Micari, F., 2002, Analysis of material formability in incremental forming, *Annals of the CIRP*, 51/1:199-202.
- [Fil06] Filice L., “A Phenomenology Based Approach for Modelling Material Thinning and Formability in Incremental Forming of Cylindrical Parts”, *Journal of Engineering Manufacture Part B*, vol.220, pp. 1449-1455.
- [GV94] Geiger M., Vollertsen F., Mechanisms of laser forming, *Annals of the CIRP* 43/2 (1994) 563-570.
- [HAB+04] Hirt, G., Ames, J., Bambach, M., Kopp, R., 2004, Forming Strategies and Process Modelling for CNC incremental Sheet Forming, *Annals of the CIRP*, 52/1:203-2006.
- [HAB05] Hirt, G., Ames, J., Bambach, M., 2005, A New forming strategy to realise parts designed for deep drawing by incremental CNC sheet forming, *steel research*, 71/2: 160-166.
- [HBH07] Hadoush, A. ; van den Boogaard, A.H. ; Hu’etink, J.: Stable incremental deformation of a strip to high strain. In: *SheMet ’07, Proceedings of the 12th International Conference on Sheet Metal*, Apr 01.-04. 2007, Palermo, Sicily, Italy, Trans Tech Publication Ltd., Switzerland, 2007. – ISBN0–87849–437–5, pp. 615–620
- [HG07] Hussain G., Gao L., A novel method to test the thinning limits of sheet metals in negative incremental forming, *International Journal of machine Tools and Manufacturing*, 47 (2007) 419-435.
- [HHG08] Hussain G., Hayat N., Gao L., An experimental study on the effect of thinning band on the sheet formability in negative incremental forming, *International Journal of Machine Tool & Manufacture* 48 (2008) 1170-1178.
- [HJ07] Ham, M. ; Jeswiet, J.: Single point incremental forming limits using a Box-Behnken design of experiments. In: *SheMet ’07, Proceedings of the 12th International Conference on Sheet Metal*, Apr 01.-04. 2007, Palermo,

-
- Sicily, Italy, Trans Tech Publication Ltd., Switzerland, 2007. – ISBN 0–87849–437–5, pp. 629–636
- [Ise00] Iseki, H.: An experimental and theoretical study of a forming limit curve in incremental forming of sheet metal using a spherical roller. In: Metal Forming, Balkema, Rotterdam, 2000. – ISBN 90–5809–157–0, pp. 557–562
- [Ise01] H. Iseki, Flexible and incremental bulging of sheet metal using high-speed water jet, JSME International Journal 4 (2001) 486-493.
- [ITO+04] Iwanaga, K., Tashiro, H., Okamoto, H., Shimizu, K., 2004, Improvement of Formability from room temperature to warm temperature in AZ31 Magnesium Alloy, Journal of Materials Processing Technology, 155-156:1313-1316.
- [Jad04] Jadhav, S.: Basic investigation of the incremental sheet metal forming process on a CNC milling machine, Universität at Dortmund, Germany, Diss., 2004
- [JGH03] Jadhav, S. ; Goebel, R. ; Homberg, W. ; Kleiner, M.: Process optimization and control for incremental sheet metal forming. In: Proceedings of the Conference of the International Deep Drawing Research Group (IDDRG), Bled, Slovenien, 11.-014.5.2003, 2003, pp. 165–171
- [JMH+05] Jeswiet J., Micari F., Hirt G., Bramley A., Dufloy J., Allwood J., Asymmetric Single Point Incremental Forming of Sheet Metal, Annals of the CIRP, Vol. 54/2 (2005), 88-114.
- [Jun03] Junk, S.: Inkrementelle Blechumformung mit CNC Werkzeugmaschinen: Verfahrensgrenzen und Umformstrategien, Universität at des Saarlandes, Germany, Diss., 2003
- [JY05] Jeswiet, J. ; Young, D.: Forming limit diagrams for single-point incremental forming of aluminium sheet. In: Proc. IMechE Vol. 219 Part B: J. Engineering Manufacture (2005), pp. 359–364
- [KGK03] Kleiner, M., Geiger, M., Klaus A., 2003, Manufacturing of Lightweight Components by Metal Forming, Annals of the CIRP, 52/2: 521- 542.
- [KN99] Kitazawa K., Nakajima A., “Cylindrical incremental drawing of sheet metals by CNC incremental forming process”, Proc. of the 6th ICTP Conference, Nuremberg, 1999, pp. 1495-1500.
- [KOR+01] Kawka M., Olejnik L., Rosochowski A., Sunaga H., Makinouchi A., 2001, Simulation of wrinkling in sheet metal forming, Journal of Materials Processing Technology 109, pp.283-289.
- [KOS03] Kitazawa, K. ; Oka, T. ; Sato, Y.: Forming limit in incremental stretching

- of sheet metals. In: Proceedings of the 54th Japanese Joint Conference for the Technology of Plasticity, 6.-8.11.2003, Tokyo, Japan, 2003, pp. 421–422
- [KP02] Kim, Y.H. ; Park, J.J.: Effect of processing parameters on formability in incremental forming of sheet metal. In: Journal of Materials Processing Technology 130-131 (2002), pp. 42–46
- [KP03] Kim, Y.H. ; Park, J.J.: Fundamental studies on the incremental sheet metal forming technique. In: Journal of Materials Processing Technology 140 (2003), pp. 447–453
- [KS00] Kim Y., Son Y.: J. of Materials Processing Technology, vol. 97 (2000), pp. 88-94.
- [KS02] Kopp R., Schulz J., Flexible sheet forming technology by double-sided simultaneous shot peen forming, Annals of CIRP 51/1 (2002) 195-198.
- [Lan90] Lange, K., 1990, Umformtechnik. Handbuch für Industrie und Wissenschaft, Band 3: Blechbearbeitung, Springer-Verlag
- [Lee07] Lee, Y.S. et al., 2007, Experimental and analytical studies for forming limit of AZ31 alloy on warm sheet metal forming, Journal of Materials Processing Technology, 187-188: 103-107
- [MAF07] Micari F., Ambrogio G., Filice L., Shape and dimensional accuracy in Single Point Incremental Forming: state of the art and future trends, International Journal of Material Processing Technology, Vol.191 (2007), 390-395.
- [Mat94] Matsubara, S. Incremental Backward Bulge Forming of a Sheet Metal with a Hemispherical Tool. J. of the JSTP, vol. 35, pp. 1311-1316, 1994.
- [Mic04] Micari, F.: Single point incremental forming: recent results. In: Seminar on Incremental Forming, Cambridge University, CdRom, 2004
- [MKM97] Mwembela A., Konopleva E.B., McQueen H.J., Microstructural development in Mg alloy AZ31 during hot working, Scripta Mater. 37 (11) (1997) 1789–1795.
- [NAG+06] Neugebauer, R., Altan, T., Geiger, M., Kleiner, M., Sterzing, A., 2006, Sheet Metal Forming at elevated temperatures, Annals of the CIRP, 55/2:793-816.
- [NL99] Narasimhan N. Lovell M., Journal of Material Processing technology, 33,29-42 (1999)
- [PB46] Plackett R.L., Burman J.P., The Design of Optimum Multifactorial Experiments, Biometrika, Vol. 33 (1946), 305-325.

- [PK03] Park J.J., Kim Y.H., Fundamental studies on the incremental sheet metal forming technique, *J. of Materials Processing Technology*, vol. 140 (2003), 447-453.
- [PP74] Painter, M.J. ; Pearce, R.: Instability and fracture in sheet metal. In: *J. Phys. D: Appl. Phys.* 7 (1974), pp. 992–1002
- [Sch92] Schmoeckel D.: Developments in Automation, Flexibilization and Control of Forming Machinery. *Annals of CIRP* vol. 40/2/1992; 615.
- [SCR04] Strano, M. ; Carrino, L. ; Ruggiero, M.: Representation of forming limits for negative incremental forming of thin sheet metals. In: *IDDRG, Sindelfingen, 2004*, pp. 198–207
- [SEC+06] Spigarelli S., El Mehtedi M., Cabibbo M., Evangelista E., Kaneko J., Jäger A., Gartnerova V., 2006, Analysis of high-temperature deformation and microstructure of an AZ31 magnesium alloy, *Materials Science and Engineering*, in press.
- [SMS+99] Sakuda T., Matsabura S., Sakamoto M., Fukuhara G., Deformation analysis for stretching forming of sheet metal with CNC machine tools, *Proc. of the 6th ICTP Conference, Nuremberg, 1999*, pp. 1501-1504.
- [SP01] Shim, M.S. ; Park, J.J.: The formability of aluminium sheet in incremental forming. In: *Journal of Materials Processing Technology* 113 (2001), pp. 654–658
- [SR75] Stören, S. , Rice, J.R.: Localised necking in thin sheets. In: *J. Mech. and Phys. Solids* 23 (1975), pp. 421–441
- [Swi52] Swift, H.W.: Plastic instability under plane stress. In: *Journal of the Mechanics and Physics of Solids* 1 (1952), No. 1, pp. 1–18
- [TFH98] Takuda H., Fujimoto H., Hatta N, Modelling on flow stress of Mg–Al–Zn alloys at elevated temperatures, *J. Mater. Process. Technol.* 80–81 (1998) 513–516.
- [TYH99] Takuda H., Yoshii T., Hatta N., Finite-element analysis of the formability of a magnesium-based alloy AZ31 sheet, *J. Mater. Process. Technol.* 89–90 (1999) 135–140.
- [VDL07] Verbert, J. ; Dufloy, J. R. ; Lauwers, B.: Feature based approach for increasing the accuracy of the SPIF process. In: *SheMet '07, Proceedings of the 12th International Conference on Sheet Metal, Apr 01.-04. 2007, Palermo, Sicily, Italy, Trans Tech Publication Ltd., Switzerland, 2007.* – ISBN 0–87849–437–5, pp. 615–620
- [VMC97] Varady T., Martin R., Cox J., Reverse engineering of geometric models – an introduction”, *Computer-Aided Design*, Vol. 29/4 (1997), 255-268.

- [Wag02] Wagoner R.H., "Fundamental aspects of springback in sheet metal forming" in Proc of Numisheet Conf. Jeju Island, Korea 2002, pp. 13-24.
- [YJ04] Young D., Jesweit J., Wall thickness variation in single point incremental forming, *Journal of Engineering Manufacture - Part B* 218 (2004) 1453-1459.
- [YMN+04] Yoshihara S., MacDonald B.J., Nishimura H., Yamamoto H., Manabe K., 2004, Optimisation of magnesium alloy stamping with local heating and cooling using the finite element method, *International Journal of Materials Processing Technology* 153-154, 319.
- [YY03] Yoon S.J., Yang D.Y., Development of a highly flexible incremental roll forming process for the manufacture of a doubly curved sheet metal, *Annals of the CIRP*, Vol. 52/1 (2003), 201-204.
- [ZM98] Zeng X.M., Mahdavian S.M.: *J. of Material Processing Technology*, vol. 84 (1998), pp. 38-46.
- [ZRT+07] Zettler J., Rezai H., Taleb-Araghi B., Bambach M., Hirt G., Incremental sheet forming: process simulation with LS-DYNA, *Proceedings of the LS-Dyna Conference (2007) C-I-9, C-I-20*.
- [ZYW06] Zhang, K.F., Yin, D.L., Wu, D.Z., 2006, Formability of AZ31 magnesium alloy sheets at warm working conditions, *International Journal of Machine Tools & Manufacture*, 46:1276-1280.